2009

A System Dynamics Approach for the Development of a Patient-Specific Protocol for Radioiodine Treatment of Graves' Disease

Steven J. Merrill
University of Massachusetts Amherst, sjmerrill@gmail.com

Follow this and additional works at: http://scholarworks.umass.edu/theses

A SYSTEM DYNAMICS APPROACH FOR THE DEVELOPMENT OF A PATIENT-SPECIFIC PROTOCOL FOR RADIOIODINE TREATMENT OF GRAVES' DISEASE

A Thesis Presented

by

STEVEN J. MERRILL

Submitted to the Graduate School of the
University of Massachusetts Amherst in partial fulfillment
of the requirements for the degree of

MASTER OF SCIENCE IN MECHANICAL ENGINEERING

May 2009

Mechanical and Industrial Engineering

A SYSTEM DYNAMICS APPROACH FOR THE DEVELOPMENT OF A PATIENT-SPECIFIC PROTOCOL FOR RADIOIODINE TREATMENT OF GRAVES' DISEASE

A Thesis Presented

by

STEVEN J. MERRILL

Approved as to style and content by:

_____

Yossi Chait, Co-chair

_____

Christopher V. Hollot, Co-chair

_____

Stuart R. Chipkin, Member

_____

Joseph Horowitz, Member

_____

Kourosh Danai, Member

_____

Antonio C. Traino, Member

_____

Mario A. Rotea, Department Chair
Mechanical and Industrial Engineering

To my family and friends.

ACKNOWLEDGMENTS

I would like to thank my advisor Professor Yossi Chait, who has provided me the opportunity to perform research in the exciting field of systems biology. His enthusiasm, patience, and guidance have made the last two years both rewarding and enjoyable. I would also like to thank my co-advisor Professor Christopher V. Hollot for his input into the research as well as for his course on feedback control. As well as my co-advisor Professor Stuart R. Chipkin for his input into the clinical aspects of the research.

I would like to extent my gratitude to Professor Joseph Horowitz for the time and effort he has contributed to the uncertainty analysis portion of this research. I would also like to thank Dr. Antonio C. Traino for providing the clinical data we needed to make this research possible. As well as providing insight into the field of medical physics.

I would also like to thank Professor Kourosh Danai for serving on my thesis committee, Rajiv P. Shrestha for his friendship and help in and out of the lab, as well my family and friends for their support.

ABSTRACT

A SYSTEM DYNAMICS APPROACH FOR THE DEVELOPMENT OF A PATIENT-SPECIFIC PROTOCOL FOR RADIOIODINE TREATMENT OF GRAVES' DISEASE

MAY 2009

STEVEN J. MERRILL

B.S., UNIVERSITY OF MASSACHUSETTS AMHERST

M.S.M.E., UNIVERSITY OF MASSACHUSETTS AMHERST

Directed by: Professor Yossi Chait and Professor Christopher V. Hollot

The thyroid gland secretes hormones that help to govern metabolism and energy expenditure within the body [1]; these hormones also affect growth and development. As a result, the regulation of thyroid hormones is vital for maintaining an individual's well being. Graves' disease is an autoimmune disorder and is a major cause of hyperthyroidism or an overproduction of thyroid hormones. Radioactive iodine (RAI) therapy has become the preferred treatment with typical RAI protocols being based on the Marinelli-Quimby equation to compute the dose; however, up to 90% of subjects become hypothyroid within the first year after therapy. In this thesis we focus on the development of a new computational protocol for the calculation of RAI in the treatment of Graves' hyperthyroidism. The new protocol implements a two-compartment model to describe RAI kinetics in the body, which accounts for the conversion between different RAI isotopes used in diagnostic and therapeutic appli-

cations. Thus, by using the measured response of the subject's thyroid to a test dose of ^{123}I, the model predicts what amount of RAI (^{131}I) will be needed to reduce, through ablation, the functional, thyroid volume/mass to an amount that would result in a normal metabolic balance. A detailed uncertainty analysis was performed using both a standard propagation of error method as well as a simulation method. The simulation method consisted of both parametric and nonparametric bootstrapping techniques. Using clinical data consisting of activity kinetics and mass dynamics of 17 subjects and measured final mass values of 7 of the 17 subjects, we were able to validate the protocol as well as quantify the uncertainty analysis. This protocol is the basis of an ongoing pilot study in conjunction with Cooley Dickinson hospital, Northampton, MA.

TABLE OF CONTENTS

LIST OF TABLES

LIST OF FIGURES

CHAPTER 1
INTRODUCTION

The thyroid gland secretes hormones that help regulate metabolism and energy expenditure within the body [1]; these hormones also affect growth and development. As a result, the regulation of thyroid hormones is vital for maintaining an individual's well being. One form of thyroid dysfunction, which affects the secretion of hormones, is hyperthyroidism. Hyperthyroidism occurs when there is an overproduction of thyroid hormones due to a variety of reasons. It can lead to mild/moderate health risks, including nervousness, weight loss, sweating, tachycardia, and fatigue [1, 2, 3]. If left untreated, these symptoms can progress to more severe symptoms. For example, nervousness can progress into mental status changes and tachycardia can progress into arrhythmia.

When this overproduction of hormones is caused by thyroid stimulating anti-bodies, produced by the autoimmune system, it is known as Graves' Disease. Graves' disease is the most common form of hyperthyroidism and is more common in women than men [1, 2, 3]. Graves' disease occurs in 1-2 % of Americans and is approximately eight times more frequent in women than men [3]. As a result of the severity of the health risks mentioned above, a safe and effective treatment for Graves' disease is required. Currently, the three main forms of treatment are surgery, medication, and radioactive iodine (RAI) therapy [1, 2, 3]:

1. **Surgery.** The surgical treatment option usually involves subtotal thyroidectomy or the removal of most of the thyroid. While surgery is one of the oldest forms of therapy for hyperthyroidism caused by Graves' disease it is rarely used today [3]. Along with

1

complicati ons that accompany any surgery such as bleeding and infection, there can also be damage to the recurrent laryngeal nerve [3]. There is also debate on how much thyroid tissue to remove [1]. If not enough tissue is removed there is a chance of recurrent hyperthyroidism and if too much tissue is removed hypothyroidism (under active thyroid gland) will result. Therefore, surgery is usually performed on a limited number of cases involving children, pregnant women, and subjects with large goiters [3].

2. **Medication.** The two main antithyroid medications are methimazole, MMI, and propylthiouracil, PTU. The main action of MMI and PTU is to reduce thyroid hormone production by inhibiting iodine oxidization in the thyroid [1, 3]. PTU has the added effect of inhibiting conversion of the thyroid hormone Thyroxine, T_4, to the more potent thyroid hormone Triiodothyronine, T_3, in peripheral tissue [3]. Antithyroid drugs are usually associated with long-term treatment of Graves' hyperthyroidism with subjects being on antithyroid medication for 1-2 years [3]. It is reported in [1] that spontaneous remission is seen in only 20-40 % of subjects treated with antithyroid drugs. Along with the low remission rate, numerous side effects have been reported including fever, rash, and agranulocytosis or a reduction in the number of white blood cells [3]. If a patient is not euthyroid after 1-2 years, an alternative treatment is usually given because of the ongoing risk and seriousness of the side effects.

3. **Radioactive Iodine.** Radioactive iodine therapy has been administered to treat Graves' hyperthyroidism for over 50 years [4]. It is reported in [5] that RAI has become the primary treatment used by clinicians for the treatment of Graves' hyperthyroidism in the United States. RAI is administered orally in capsule form and is quickly concentrated in the thyroid. ^{131}I, the most common radioiodine isotope used in therapy, emits both beta and gamma radiation. However, it is only the beta radiation that

2

causes thyroid cell destruction [3]. The idea is that the thyroid will produce less hormones with fewer cells. Cell destruction is often referred to as mass destruction. RAI is relatively safe as side effects are uncommon with the exception of hypothyroidism [6]. Up to 90 % of subjects become hypothyroid within the first year after RAI therapy and about 2 % to 3 % become hypothyroid each year following the first [3].

In this thesis, we focus on RAI therapy. Currently, there is an ongoing debate on how much RAI activity needs to be administered. The three main protocols are to: 1) administer a fixed dose of RAI activity to all subjects, 2) administer a dose of RAI activity that was calculated using an absorbed dose that was fixed for all subject (i.e. the activity absorbed per unit mass in the target region), and 3) administer a dose of RAI activity based on an absorbed dose that has been calculated on a subject to subject basis. This debate will be discussed in detail in Chapter 2. We will follow the third protocol in this thesis. We will attempt to add rigor into the protocol by explicitly considering the underlying dynamics governed by the physics of radiation therapy.

1.1 Clinical Data

In order to test our protocol, we required clinical activity and mass data. Dr. Traino was generous enough to supply us with both clinical activity and mass data for 17 subjects; including mass values measured at one year for 7 of the 17 subjects. This data allowed us to both validate our new protocol and to quantify the uncertainty analysis. All of the data can be found in Appendix A.

1.2 Thesis Contributions

The contributions of this thesis are:

3

1. We present a new computational protocol for the calculation of RAI in the treatment of Graves' hyperthyroidism. This protocol was developed by utilizing a two-compartment model to describe the activity kinetics in the body and an improved method of estimating the mass dynamics required to calculate the absorbed dose. The activity kinetic model allows for the conversion between different RAI isotopes, which is a crucial step in our protocol.

2. A detailed uncertainty analysis was performed of the new protocol. The uncertainty analysis consisted of both a standard propagation of error method and a simulation based method. The ultimate goal of the uncertainty analysis was to estimate the uncertainty in the calculation of the final thyroid mass. The uncertainty analysis was also used to validate our new protocol. To our knowledge, this uncertainty analysis is the first of its kind.

CHAPTER 2

CURRENT PROTOCOLS FOR RAI DOSE COMPUTATION

Radioactive iodine has become the primary treatment for Graves' hyperthyroidism in the United States, however, there is not a consensus on how much RAI activity needs to be administered or if the desired outcome is a euthyroid or hypothyroid state. The three main protocols are to: 1) administer a fixed dose of RAI activity to all subjects, 2) administer a dose of RAI activity that was calculated using a fixed absorbed dose for all subjects using a version of the Marinelli-Quimby equation, and 3) administer a dose of RAI activity based on a subject-specific absorbed dose. Each of these protocols and their limitations will be discussed next.

2.1 Overview Of The Current Protocols

The protocol chosen by the clinician is often based on the desired outcome of the RAI therapy, euthyroidism or hypothyroidism [4]. It has been reported in [6] that hypothyroidism is an acceptable outcome of RAI therapy because it can be diagnosed at an early stage and easily treated with thyroid hormone replacement. As a result, some clinicians use a large fixed dose of RAI activity for all subjects in the hope of obtaining a hypothyroid state with a single round of treatment [4, 7, 8, 9]. The increase in cost due to extra measurements required for an optimized protocol also plays a role in the decision to use a fixed dose of RAI activity [4, 7]. A variation of this protocol is to administer a fixed dose of RAI activity per unit mass of the thyroid [4, 7]. However, these therapy protocols often result in the administration of higher levels of activities and absorbed doses than desired. This is due

5

to variability of intra-patient iodine metabolism kinetics [4, 7]. This over administration of activity has been one of the arguments in opposition of the fixed dose of RAI activity protocol [7].

One way clinicians try to overcome this problem is to explicitly account for the thyroid's iodine kinetics. This is often accomplished using empirical relations with the Marinelli-Quimby equation being the most famous [10]. This equation accounts for the approximated maximal iodine intake and effective half-life of iodine within the thyroid, the mass of the thyroid, and the estimated absorbed dose. The desired quantity of absorbed dose is usually chosen from a predetermined range based on the clinicians experience and judgment. This approach has been reported by many clinicians, e.g., [4, 7, 11, 12, 13, 14, 15]. It provides a patient-specific calculation of the dose of RAI activity to be administered and is preferred over the protocol that administers a fixed dose of RAI activity to all subjects [4, 7, 13].

However, there are two limitations to this approach as well: 1) in practice, not enough activity points are collected to accurately account for the kinetics and 2) the mass dynamics are ignored which results in the wrong absorbed dose being used. Clinicians often manage with only one RAI uptake measurement and assume that the maximum uptake of RAI by the thyroid occurs at 24 hours for each subject. The second limitation is assuming the effective half-life is 5 days for each subject. These assumptions allow for the clinician to take only one measurement at 24 hours for each subject. Furthermore, the Marinelli-Quimby equation assumes a fixed mass while RAI treatment always results in mass reduction. This assumption results in a larger dose of RAI than desired. This could be the reason [3] reports that currently up to 90 % of subjects become hypothyroid within 1 year after therapy. As a result, most clinicians aim for a hypothyroid state after RAI therapy because a euthyroid state is too hard to obtain.

To overcome the limitations associated with use of the Marinelli-Quimby equation, Traino et al have proposed a model for thyroidal mass reduction after RAI therapy [16, 17, 18,

6

19, 20]. The authors also report a protocol to calculate a subject specific absorbed dose. This absorbed dose can then be used to calculate an individualized dose of RAI activity to administer to a subject in the hopes of achieving a euthyroid state.

In this thesis, we will follow the work of Traino et al [16, 17, 18, 19, 20], however, we will utilize a two-compartment model to describe the activity kinetics in the body and an improved method of estimating the mass dynamics required to calculate the absorbed dose. Before we present a description of their work, a brief discussion of mass dynamics and its relation to the absorbed dose will be presented.

2.2   Medical Physics Background Of Radiation Effects On Cells

In [16], a new model was proposed to describe the reduction in the mass of the thyroid after RAI therapy. A brief description of mass reduction resulting from radiation will be discussed here in order to give some insight into the model.

In [21, 22] it has been reported that the number of cells that survive ionizing radiation therapy, N, can be described by a linear quadratic (LQ) model

$$N = N_0 e^{-(\alpha D_T + \beta D_T^2)}, \tag{2.1}$$

where N_0 is the number of cells before therapy, D_T (Gray, Gy) is the absorbed dose, and α (Gy^{-1}) and β (Gy^{-2}) are constants. An important assumption is this thesis is that α and β are the same for all subjects. Equation (2.1) describes cell death occurring due to two types of events at the chromosomal DNA level: a single double-hit event, or double single-hit events in the chromosomal DNA [21, 23, 24]. A single double-hit event occurs when a single ionizing track produces a lesion in both strands in chromosomal DNA [19, 22, 25]. A double single-hit event occurs when one ionizing track produces a lesion in one strand of the chromosomal DNA and a separate ionizing track produces a lesion in the other strand of the

7

chromosomal DNA [19, 22, 25]. In [26], these two types of events are referred to as Type A and Type B cell destruction, respectively. In (2.1), Type A cell destruction is represented by the term αD_T, while Type B cell destruction is represented by the term βD_T^2.

In certain situations, it is possible to simplify the LQ model. The simplification results from sub-lethal chromosomal DNA damage which is considered repairable with time [21, 25]. Sub-lethal damage can occur as a result of a few different causes. The first cause occurs when a single ionizing track produces a lesion in one strand of the chromosomal DNA [21]. Two other cases occur when the lesions in both strands of chromosomal DNA, resulting from either one or two tracks, are separated by greater than 3 base pairs [21]. In these three scenarios, a second ionizing track would be required to transform them into lethal chromosomal DNA damage. Therefore, the repair of sub-lethal damage is dependent on the frequency of the ionizing events near the chromosomal DNA [25]. As a result, Type B damage is also dependent on the frequency of the ionizing events because Type B damage is associated with more than one ionizing track [25]. The frequency of the ionizing events is directly related to the dose-rate or the rate at which the dose is absorbed by the cells [25]. Lower dose rates provide time for sub-lethal damage to repair itself before being hit by another ionizing track. For radiation therapy similar to RAI therapy which is administered in high doses but at low dose rates, the βD_T^2 term can be neglected [19, 25]. This results in

$$N = N_0 e^{-\alpha D_T}. \tag{2.2}$$

Following the hypothesis proposed in [19] that the mass of a tissue, m, is linearly related to N, (2.2) can be re-written to describe the ratio between the final mass $m(\infty)$ (grams, g) and the pre-treatment mass $m(0)$ by

$$\frac{m(\infty)}{m(0)} = e^{-\alpha D_T}. \tag{2.3}$$

8

The Medical Internal Radiation Dose committee (MIRD) [27, 28] defines D_T as

$$D_T = \sigma \int_0^\infty \frac{A(t)}{m(t)} \, dt, \tag{2.4}$$

where A denotes the activity kinetics in the target tissue (Becquerel, Bq), m denotes the mass dynamics [1] of the target tissue (grams, g), and σ is a constant dependent on the radioisotope. Both $A(t)$ and $m(t)$ will be discussed in detail, in Sections 2.3.1 and 2.3.2, respectively.

The above relations are general purpose concepts in internal radiation therapy. The mass dynamics can be specialized to RAI therapy for a patient with Graves' hyperthyroidism as proposed by Traino et al [16, 18]. It is reported that thyroid mass dynamics following Type A RAI destruction occurs in two distinct stages [18]. While [18] reports that the two stages are distinct we believe that the two stages could be coupled. However, because of the lack of evidence suggesting coupling we will assume that the two stages are distinct. The first stage is assumed to occur in the first 30-35 days (0- 840 hours) after RAI administration as a direct result of the activity of the RAI in the thyroid. The second stage is assumed to occur between 30-35 days to 1 year (840 - 8760 hours) as a result of irreparable damage of the thyroid cells caused by the RAI. Note that throughout this thesis we refer to these stages in units of hours. To clarify, (2.3) describes the mass dynamics of both stages. Next, all of the relations are specialized to RAI therapy for a patient with Graves' hyperthyroidism as proposed by Traino et al [16].

---

[1]This is sometimes referred to as mass destruction but, in this thesis, we will refer to cell destruction as mass dynamics.

2.3 Computational Protocol

The equations that relate the absorbed dose in terms of mass dynamics have been presented above in general terms. Traino et al have proposed mathematical models for both activity kinetics and mass dynamics specific for RAI therapy [16]. These relations will be presented next and will provide the basis for the protocol proposed in Chapter 3.

2.3.1 Activity Kinetic Model

The activity kinetics for RAI therapy for a patient with Graves' disease can be approximated to support two distinct phases: uptake and clearance [16]. The initial uptake phase is approximated to be linear, where the activity is 0 at the start of the application, $t = 0$, to where the activity is at a maximum value, A_{max}, at $t = T_{max}$ (usually within 12-36 hours). The clearance dynamics are modeled by a single exponential decay equation starting at T_{max} where $A(T_{max}) \triangleq A_{max}$. The overall activity kinetics is approximated in [16] by

$$A(t) = \begin{cases} A_{max} \frac{t}{T_{max}}, & t \in [0, T_{max}] \\ A_{max} e^{-\rho(t-T_{max})}, & t \geq T_{max} \end{cases} \tag{2.5}$$

where ρ is a patient-specific constant that depends on the physical half-life of the isotope and on the biological half-life of the isotope in the thyroid. The physical half-life is the time it takes the number of atoms to decay to half the original number. The biological half-life is the time it takes the thyroid to secrete half of its RAI atoms. In this thesis, we will drop this model of activity kinetics and use a two-compartment model to describe the activity kinetics.

2.3.2 Mass Dynamic Model

In [16] the following mass dynamics model was proposed

$$\dot{m}(t) = -k\frac{A(t)}{m(t)}, \tag{2.6}$$

where k $(\frac{g^2}{hrMBq})$ is a patient-specific constant. Equation (2.6) describes the mass dynamics that occur during the first stage and cannot be used to calculate the final mass $m(\infty)$ since the destruction continues even when $A(t) = 0$. Based on clinical observations, [16] assumed that $m(t) = m(0)$, $t \in [0, T_{max}]$, and used

$$A(t) = A_{max}e^{-\rho(t-T_{max})}$$

to solve (2.6) for $m(t)$:

$$m(t) = \left[2\left(\frac{kA_{max}}{\rho}e^{-\rho(t-T_{max})} - \frac{kA_{max}}{\rho} + \frac{m(0)^2}{2}\right)\right]^{\frac{1}{2}}. \tag{2.7}$$

The subject-specific constant k can be found by fitting (2.7) to clinical mass and activity data.

The key idea behind these relations is that, in theory, if a subjects' activity and mass parameters are known a priori, then one could compute the dose of RAI activity needed to achieve a desired final mass. In practice, however, the subjects' mass dynamics are not known a priori. As a result, [17] has proposed a procedure to calculate the constant k that does not require a priori knowledge of the subjects' mass dynamics. Specifically, [17] postulated that k is strongly correlated to key patient-specific data, $m(0)$ and A_{max}, so an estimate, referred to as k_{calc}, is given by

$$k = k_{calc} \triangleq \gamma_{calc}\frac{m(0)^2 A_d}{A_{max}}, \tag{2.8}$$

where γ_{calc} (hr^{-1}MBq^{-1}) is a fitting constant, and A_d is the initial ^{131}I dose of activity MBq.

11

2.3.3 Limitations Of The Computational Protocol That Are Addressed In This Thesis

The method of calculating a patient-specific absorbed dose for the treatment of Graves' hyperthyroidism, indicated above, improves on the previous protocols. However, even this method has limitations. It is common in the USA to use ^{123}I, a non-destructive isotope, as a diagnostic isotope [3]. To utilize data generated from a diagnostic procedure involving a different isotope requires a method to be able to convert ^{123}I activity data into the therapeutic isotope ^{131}I activity data. The activity kinetics proposed by [16] do not allow for this conversion. Another limitation is the absence of an uncertainty analysis reported for this method. Traino et al [16] report an uncertainty of 10% for activity measurements and 15%-20% for mass measurements. These values are rather large and should be propagated through to the calculation of the absorbed dose and the final mass.

CHAPTER 3

PROPOSED PROTOCOL FOR RAI DOSE COMPUTATION AND ADMINISTRATION

The computational approach described in Section 2.3 is the current state-of-the-art patient-specific approach for RAI dose calculation. We follow (2.3), however, we will remove the assumption of a linear uptake phase in the activity kinetics to provide a more accurate estimate of the activity in the thyroid. A computational approach to calculate the absorbed dose, based on new activity relations, and the approaches ability to predict the final mass will be discussed. Also, using this computational approach, we will show that a dose of RAI activity can be calculated to predict a desired final mass after therapy. In developing this protocol, the following tasks were addressed: the ability to convert between different RAI isotopes, the ability to estimate the activity parameters with a limited number of data points, the ability to estimate the mass dynamics during the first time frame, $t \in [0, 840]$, and the ability to estimate the constant α in (2.3).

3.1 Activity Kinetic Relations

A two-compartment model to describe the flow of iodine within the body was presented in [29]. We will adapt this model by explicitly including the physical decay constants. A schematic diagram of our new model can be found in Figure 3.1. This model is described by

$$
\begin{aligned}
\dot{x_1} &= \lambda_u x_2 - \lambda_s x_1 - \lambda_p x_1, & x_1(0) &= 0 \\
\dot{x_2} &= \lambda_s x_1 - \lambda_u x_2 - \lambda_c x_2 - \lambda_p x_2, & x_2(0) &= X_{Input}
\end{aligned}
\tag{3.1}
$$

13
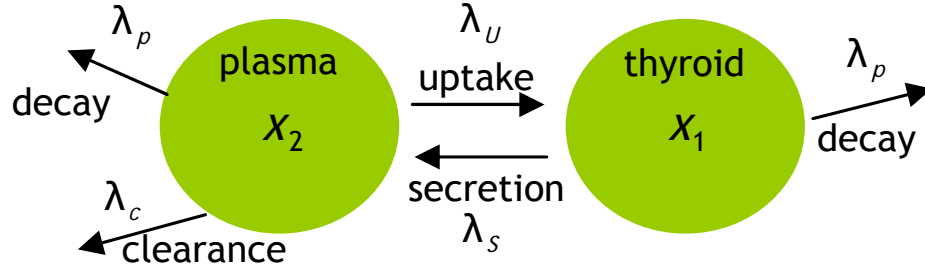
Figure 3.1. A two-compartment model of RAI flow within the body; λ_i represent rate constants $(\frac{1}{hr})$.

where x_1 is the amount of RAI in the thyroid (μg), x_2 is the amount of RAI in the plasma (μg), λ_u is the rate constant associated with thyroid iodine uptake, λ_s is the rate constant associated with thyroid iodine secretion, λ_c is the rate constant associated with urine iodine clearance, λ_p is the rate constant associated with the physical decay of RAI, and X_{Input} is the administered dose of RAI (μg). This model assumes that the appearance of administered RAI in the plasma is fast as can be noticed by the administration of the dose being modeled as an impulse. The solution of (3.1) can be derived analytically and is given by the form

$$x_1(t) = He^{-bt} - He^{-ct} \tag{3.2}$$

where,

$$H = \frac{\lambda_u X_{Input}}{(\lambda_u^2 + 2\lambda_u\lambda_c + 2\lambda_u\lambda_s - 2\lambda_c\lambda_s + \lambda_c^2 + \lambda_s^2)^{1/2}}$$
$$b = \frac{1}{2}(\lambda_u + \lambda_c + 2\lambda_p + \lambda_s) - \frac{1}{2}(\lambda_u^2 + 2\lambda_u\lambda_c + 2\lambda_u\lambda_s - 2\lambda_c\lambda_s + \lambda_c^2 + \lambda_s^2)^{\frac{1}{2}}$$
$$c = \frac{1}{2}(\lambda_u + \lambda_c + 2\lambda_p + \lambda_s) + \frac{1}{2}(\lambda_u^2 + 2\lambda_u\lambda_c + 2\lambda_u\lambda_s - 2\lambda_c\lambda_s + \lambda_c^2 + \lambda_s^2)^{\frac{1}{2}}.$$

Note that this model tracts the amount (μg) of RAI in the body and not the activity of RAI. However, the amount (μg) of RAI can be converted into activity (MBq) using

14

$$X_{Input} = \frac{1}{\delta_{conv}} \frac{1}{\lambda_p} A_d,$$

where A_d is the dose of RAI administered (MBq), and δ_{conv} can be found using the following conversion

$$\text{MBq} = \frac{\mu\text{g}}{\text{hr}} \cdot \frac{\text{nmol/hr}}{\mu\text{g/hr}} \frac{1}{0.127} \cdot \frac{\text{moles/hr}}{\text{nmol/hr}} 10^{-9} \cdot \frac{\text{moles/sec}}{\text{moles/hr}} \frac{1}{3600}$$
$$\cdot \frac{\text{disintegrations/sec}}{\text{moles}} 6.022 \cdot 10^{23} \cdot \frac{\text{MBq}}{\text{disintegrations/sec}} 10^6$$
$$= \delta_{conv} \frac{\mu\text{g}}{\text{hr}} = 1.317E18 \frac{\mu\text{g}}{\text{hr}}.$$

Using these conversions the activity found in the thyroid can be described by

$$A_1(t) = Y e^{-bt} - Y e^{-ct} \tag{3.3}$$

where,

$$Y = \frac{\lambda_u A_d}{(\lambda_u^2 + 2\lambda_u\lambda_c + 2\lambda_u\lambda_s - 2\lambda_c\lambda_s + \lambda_c^2 + \lambda_s^2)^{1/2}}$$
$$b = \frac{1}{2}(\lambda_u + \lambda_c + 2\lambda_p + \lambda_s) - \frac{1}{2}\left(\lambda_u^2 + 2\lambda_u\lambda_c + 2\lambda_u\lambda_s - 2\lambda_c\lambda_s + \lambda_c^2 + \lambda_s^2\right)^{\frac{1}{2}}$$
$$c = \frac{1}{2}(\lambda_u + \lambda_c + 2\lambda_p + \lambda_s) + \frac{1}{2}\left(\lambda_u^2 + 2\lambda_u\lambda_c + 2\lambda_u\lambda_s - 2\lambda_c\lambda_s + \lambda_c^2 + \lambda_s^2\right)^{\frac{1}{2}}.$$

This solution is described by two exponential terms which is notably different from Equation (2.5) which assumes a linear uptake and an exponential clearance phase. It should be of note that the two-compartment model has only been used in one protocol to calculate a dose of RAI activity for the treatment of Graves' hyperthyroidism [15]. And the model used in [15] did not explicitly account for the physical half-life of RAI.

There are a number of technical challenges related to the applicability of (3.3). One challenge was the conversion of diagnostic activity using ^{123}I to its corresponding therapeutic ^{131}I activity. [123]I only causes a minimal amount of mass dynamics and is therefore a desirable

diagnostic isotope [3]. Therefore, there exists a need to estimate ^{131}I activity dynamics from ^{123}I activity. A second challenge was how to identify the parameters of Equation (3.3) using a minimal number of data points. Constraints on both the subjects' time as well as the cost of the measurements have an effect on the number of measurements that can be taken. To simplify the presentation, here we will assume that there is no uncertainty associated with the activity measurements.

3.1.1 Converting Between Activities Of Different Isotopes

We can gain insight on how to convert between the different isotopes of RAI by investigating the closed form solution of the activity in the thyroid. It can be observed that the physical half-life, λ_p, can only be found in the two poles, b and c, in (3.3). In particular, λ_p is only found in the linear portion of the two pole equations. We make the reasonable assumption that the rate constants λ_u, λ_c, and λ_s will not change significantly between the different isotopes in comparison with the dynamics of the iodine present in the thyroid. The constant λ_p is known for each iodine isotope and can be assigned its value depending on the isotope of interest. Therefore, using activity data corresponding to ^{123}I, ^{131}I activity data can be estimated by switching λ_p of ^{123}I for λ_p of ^{131}I. An example will be shown to clarify this procedure.

Given ^{123}I activity data, non-linear regression of (3.3) will yield estimates of the parameters $\hat{Y}$, $\hat{b}$, and $\hat{c}$. The two estimates of the poles for ^{123}I activity data can be expressed as

$$\hat{b}_{123} = \frac{1}{2}\left(\lambda_u + \lambda_c + 2\lambda_{p123} + \lambda_s\right) - \frac{1}{2}\left(\lambda_u^2 + 2\lambda_u\lambda_c + 2\lambda_u\lambda_s - 2\lambda_c\lambda_s + \lambda_c^2 + \lambda_s^2\right)^{\frac{1}{2}}$$

$$\hat{c}_{123} = \frac{1}{2}\left(\lambda_u + \lambda_c + 2\lambda_{p123} + \lambda_s\right) + \frac{1}{2}\left(\lambda_u^2 + 2\lambda_u\lambda_c + 2\lambda_u\lambda_s - 2\lambda_c\lambda_s + \lambda_c^2 + \lambda_s^2\right)^{\frac{1}{2}},$$

where λ_{p123} is the rate constant associated with the physical decay of ^{123}I. These pole estimates can be converted to estimates of ^{131}I activity data by

16

$$\hat{b}_{131} = \hat{b}_{123} + \xi = \frac{1}{2} \left(\lambda_u + \lambda_c + 2\lambda_{p123} + \lambda_s \right) + \xi - \frac{1}{2} \left(\lambda_u^2 + 2\lambda_u\lambda_c + 2\lambda_u\lambda_s - 2\lambda_c\lambda_s + \lambda_c^2 + \lambda_s^2 \right)^{\frac{1}{2}}$$
$$\hat{c}_{131} = \hat{c}_{123} + \xi = \frac{1}{2} \left(\lambda_u + \lambda_c + 2\lambda_{p123} + \lambda_s \right) + \xi + \frac{1}{2} \left(\lambda_u^2 + 2\lambda_u\lambda_c + 2\lambda_u\lambda_s - 2\lambda_c\lambda_s + \lambda_c^2 + \lambda_s^2 \right)^{\frac{1}{2}},$$

where $\xi = \lambda_{p131} - \lambda_{p123}$. This results in estimates of the ^{131}I poles

$$\hat{b}_{131} = \frac{1}{2} \left(\lambda_u + \lambda_c + 2\lambda_{p131} + \lambda_s \right) - \frac{1}{2} \left(\lambda_u^2 + 2\lambda_u\lambda_c + 2\lambda_u\lambda_s - 2\lambda_c\lambda_s + \lambda_c^2 + \lambda_s^2 \right)^{\frac{1}{2}}$$
$$\hat{c}_{131} = \frac{1}{2} \left(\lambda_u + \lambda_c + 2\lambda_{p131} + \lambda_s \right) + \frac{1}{2} \left(\lambda_u^2 + 2\lambda_u\lambda_c + 2\lambda_u\lambda_s - 2\lambda_c\lambda_s + \lambda_c^2 + \lambda_s^2 \right)^{\frac{1}{2}}.$$

3.1.2   Estimating Activity Parameters With A Minimum Number Of Data Points

In an ideal case, many activity measurements would be made to aid in the identification of the activity parameters. However, only three measurement will be made when implementing our new protocol. The activity point $A(t = 0) = 0$ can be used as a fourth point. We used clinical activity data to test whether it is possible to accurately identify the activity parameters with a limited number of data points. Figure 3.2 shows the activity kinetics for subject 21. The solid line represents the activity kinetics found from non-linear regression of (3.3) and all of the measured activity data points. The dashed line represents the activity kinetics found from non-linear regression of (3.3) and a limited number of data points. Figure 3.2 shows that even with a limited number of data points the activity parameters can still be accurately identified. The times at which the limited number of activity points were chosen were $t_i = [0, 2, 70.5, 163.6]$ hours. These points are representative of the times at which the activity will be measured in our protocol. There is one measurement during the uptake phase and two measurements taken during the clearance phase. Before deciding to estimate the activity parameters using non-linear regression, we investigated calculating the activity parameter analytically. This analytical approach is discussed in Appendix B.
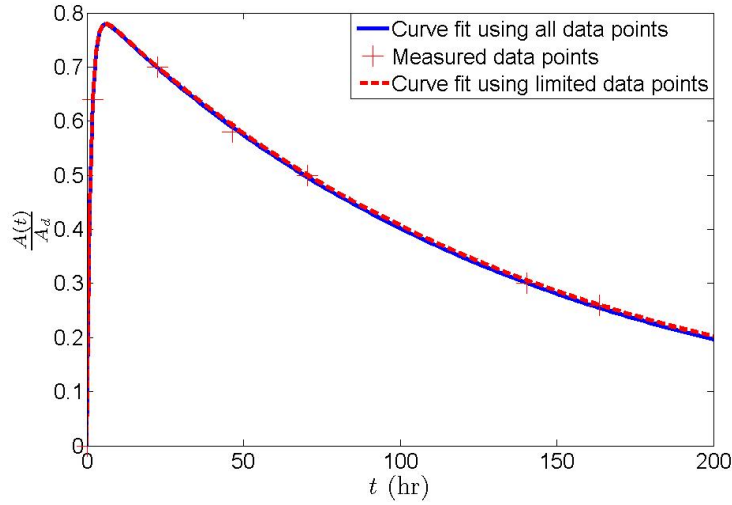
Figure 3.2. Activity kinetics for subject 21. The crosses represent measured activity data points. The solid line represents the activity kinetics fit using all measured data points. The dashed line represents the activity kinetics fit using a limited number of data points.

3.2 Calculation Of The Absorbed Dose

In computing the absorbed dose using (2.4), we follow (2.6) as the mass dynamics model

$$\dot{m}(t) = -k\frac{A(t)}{m}.$$

This equation is only valid while there is activity present in the thyroid. We make the assumption that $A(t) \approx 0$ at $t \geq 840$ from clinical data. As a result we can only directly calculate the mass until 840 hours, $m(840)$. Therefore, (2.6) describes the mass dynamics occurring in the first time frame, $t \in [0, 840]$. There is no available model for $m(t)$, $t \in [840, 8760]$. As a result we can only calculate the absorbed dose until $t = 840$ hours using

$$D_T \approx \sigma \int_0^{840} \frac{A(t)}{m(t)}\ dt,$$

where $\sigma = 0.1152\ \frac{Gy\ g}{MBqhr}$ [16]. We investigated computing D_T until other times around 840 hours, however, we found that there was negligible difference between D_T values when

18

calculated up to $t = 720$ hours or up to $t = 1080$ hours. These calculations can be found in Appendix C. This integral can be computed to produce the following closed form solution

$$D_T = \frac{\sigma}{k} \left(m(0) - m(840) \right), \tag{3.4}$$

where,

$$m(840) = \left[2 \left(\frac{Yk}{b} e^{-b\ 840} + \frac{Yk}{c} - \frac{Yk}{c} e^{-c\ 840} - \frac{Yk}{b} + \frac{m(0)^2}{2} \right) \right]^{\frac{1}{2}}. \tag{3.5}$$

As stated before, if the absorbed dose can be computed for a subject a priori, then one could compute the dose of RAI activity, A_d, that would achieve a desired final mass using (2.3) with an estimate of α. However, before this protocol can be used, a number of technical challenges need to be addressed. One challenge concerns the fact that a subject's mass dynamics during the first time frame, $t \in [0, 840]$ will not be known a priori. Therefore, a method to estimate $m(840)$ and therefore the parameter k is required. The second challenge involves the estimation of the constant α from (3.11). The protocol to calculate and administer A_d will be discussed in more detail later in the chapter; however, how to estimate the mass dynamics and α will be discussed next.

3.2.1 Estimating The Mass Dynamics During The First Time Frame, $t \in [0, 840]$

As a result of a subject's mass dynamics not being available before therapy, a method of estimating $m(840)$ is required to compute D_T. Traino et al, [17], proposed (2.8) to estimate the parameter k a priori. We propose a modification of this approach that utilizes all information that will be known a priori as well as accounts for the offset from linear regression to estimate the parameter k. Rearranging (3.5) yields

$$k_i = \frac{m_i^2(0)}{g_i} - \frac{m_i^2(840)}{g_i}, \tag{3.6}$$

19

where,

$$g_i = 2Y \left(\frac{1}{c} e^{-c\,840} - \frac{1}{b} e^{-b\,840} - \frac{1}{c} + \frac{1}{b} \right), \tag{3.7}$$

and i denotes the ith subject. The initial mass, $m_i(0)$, will be measured and g_i will be known once the activity parameters are obtained, however, $m_i(840)$ will not be known a priori but it can be estimated using two approaches: 1) by finding the average of measured $m(840)$ values $\left((\bar{m}(840))^2 \ or \ \overline{m^2(840)} \right)$ and 2) linear regression of

$$m_i^2(0) = k g_i + m^2(840),$$

to provide estimates of k and $m^2(840)$. The estimate of k will not be used but the estimate of $m^2(840)$ can be used in (3.6) as a common value for $m_i^2(840)$. However, both of these approaches to estimate $m^2(840)$ produced unreasonable results when used in (3.6) to calculate k_i. This is the result of the subject-specific nature of the mass dynamics.

To circumvent this technical limitation, we used an alternative approach. For the regression, k_i in (3.6) can be replaced by what [17] refers to as k_{fit}. k_{fit} can be found by fitting measured mass data to

$$m(t) = \left[2 \left(\frac{Yk}{b} e^{-bt} + \frac{Yk}{c} - \frac{Yk}{c} e^{-ct} - \frac{Yk}{b} + \frac{m(0)^2}{2} \right) \right]^{\frac{1}{2}} \tag{3.8}$$

using non-linear regression. Also, we will let the term $\frac{m_i^2(840)}{g_i}$, in (3.6), be defined as φ, and let the linear regression estimate it. Therefore, linear regression needs to be performed on

$$k_{fit_i} = \phi \frac{m_i^2(0)}{g_i} - \varphi,$$

to estimate ϕ and φ. After performing the linear regression, the following predictive equation for k, k_{pred} can be obtained:

$$k_{pred_i} = \phi \frac{m_i^2(0)}{g_i} - \varphi. \tag{3.9}$$

20

Equation (3.9) differs from (2.8) in that it takes advantage of all parameters that will be available before therapy as well accounts for the offset from the linear regression.

3.2.2 Estimating α

The constant α needs to be estimated before the dose of RAI activity can be computed. In this thesis we follow [16, 18] and assume α is a population constant. We used clinical data of 7 subjects to calculate α for each patient. Using measured activity data, the parameters Y, b, and c can be identified using non-linear regression of (3.3). Then using measured mass data, the parameter k can be identified using non-linear regression of (3.8). We decided to use the measured mass data in calculating k instead of using (3.16) because we wanted to take advantage of all data available to us. The absorbed dose can then be calculated using (3.4) and the identified parameters. α can be calculated by rearranging (3.11) to yield

$$\alpha = \frac{1}{D_T} \left(\ln \left(m(0) \right) - \ln \left(m(\infty) \right) \right). \tag{3.10}$$

Then a minimum variance estimate of α, $\hat{\alpha}_{mv}$, can be found by using

$$\hat{\alpha}_{mv} = \frac{\sum \frac{\alpha_i}{V(\alpha_i)}}{\sum \frac{1}{V(\alpha_i)}},$$

where

$$V(\hat{\alpha}_i) = \frac{0.015 + \alpha_i^2 \left(SE_{D_T} \right)^2}{D_T^2},$$

and where SE_{D_T} is the standard error of the absorbed dose, 0.015 corresponds to the assumed 15% multiplicative error in $m(0)$ and $m(\infty)$, and i denotes the ith subject. This expression was derived from the usual propagation of error formula [30, 31]. The 15% multiplicative

error assumption will be discussed in detail in Chapter 4. The variance of $\hat{\alpha}_{mv}$ can be calculated using

$$V(\hat{\alpha}_{mv}) = \frac{1}{\sum \frac{1}{V(\alpha_i)}}.$$

3.3   Proposed Protocol For Calculating And Administering A_d

The absorbed dose can be calculated with the estimate of $m(840)$. However, the dose of RAI activity, A_d, cannot be calculated without an estimate of $m(\infty)$ in (2.3). It is not feasible to estimate $m(\infty)$, therefore, using the assumption that the second time frame of the mass dynamics ends at 1 year, we will approximate $m(\infty)$ to be $m(8760)$. Note that from here on in this thesis $m(\infty)$ is defined as $m(8760)$. Rewriting (2.3) yields

$$m(\infty) \approx m(0)e^{-\alpha D_T}. \tag{3.11}$$

A method to estimate $m(\infty)$ is still required. A full-order mathematical model of the thyroid can be used to specify the desired $m(\infty)$ corresponding to a goal of becoming euthyroid [32]. The thyroid model is highly non-linear with an output of thyroid hormones in response to an input of thyroid stimulating hormone (TSH) and iodine. The model has been shown to match known thyroidal behavior such as the Wolff-Chaikoff block. Before the model can be used, it needs to be parameterized for a specific subject. The model can be parameterized using subject-specific measured values that will be known a priori, specifically, the initial mass and the measured activity values. The mass of the thyroid is often decreased until the thyroid hormone output of the model reaches a euthyroid state predetermined by an endocrinologist. The mass of the thyroid that results in the euthyroid state is the desired target $m(\infty)$.

22

With estimates of $m(840)$, $m(\infty)$, and $\hat{\alpha}$, we will be able to calculate a dose of RAI activity using (3.11). Equation (3.11) can be re-written as

$$\frac{m(\infty)}{m(0)} \approx e^{-\alpha A_d \tilde{D}_T}, \tag{3.12}$$

where

$$\tilde{D}_T = \frac{D_T}{A_d} = \sigma \int_0^{840} \frac{\tilde{A}(t)}{m(t)} dt,$$

and where

$$\tilde{A}(t) = \frac{A(t)}{A_d} = \tilde{Y}\left(e^{-bt} - e^{-ct}\right). \tag{3.13}$$

Solving (3.12) for A_d yields

$$A_d = -\frac{ln\left(\frac{m(\infty)}{m(0)}\right)}{\alpha \tilde{D}_T}. \tag{3.14}$$

The ability to calculate a dose of RAI activity that will achieve a desired final mass by using (3.14) has lead us to develop the following 3-step protocol for administering the dose A_d:

1. Measure the pre-therapy mass of the thyroid, $m(0)$.

2. Administer a tracer dose of ^{123}I. Measure the activity in the thyroid and convert the ^{123}I data into ^{131}I data. Compute k_{pred} using parameters found from the ^{131}I activity data.

3. Compute A_d in order to achieve the desired $m(\infty)$.

3.4   Validating The Protocol

The protocol was tested by using the clinical activity and mass data presented in Appendix A. The data was used to estimate the relevant parameters required to calculate D_T and $m(\infty)$. The calculated $m(\infty)$ values were compared to the measured $m(\infty)$ values for

23

each subject. As shown in Section 3.3, a normalized activity equation is required to calculate the initial dose A_d using (3.14). Therefore, activity data, normalized by A_d, was used with non-linear regression of (3.13) to estimate the activity parameters $\check{Y}$, b, and c. Inserting (3.13) into (2.6) yielded

$$\dot{m}(t) = -\check{k}\frac{\check{A}(t)}{m(t)},$$

where $\check{k} = A_d k$. Solving for $m(t)$ yielded

$$m(t) = \left(2 \left(\frac{\check{Y}\check{k}}{b}e^{-bt} + \frac{\check{Y}\check{k}}{c} - \frac{\check{Y}\check{k}}{c}e^{-ct} - \frac{\check{Y}\check{k}}{b} + \frac{m(0)^2}{2} \right) \right)^{\frac{1}{2}}. \tag{3.15}$$

$\check{k}$ was estimated by non-linear regression of (3.15) with mass data to yield $\check{k}_{fit}$ and also calculated using (3.9) as

$$\check{k}_{pred} = 0.5951\frac{m(0)^2}{\check{g}} - 0.0108, \tag{3.16}$$

where, $\check{g} = A_d g$. The calculation of the constants in (3.16) can be found in Appendix D.

Only the subjects with mass values measured at one year were used to test our protocol. The normalized activity data were used with non-linear regression to estimate the activity parameters of (3.13) and the parameters can be found in Table 3.1. Table 3.2 reports the mass parameter $\check{k}_{fit}$ found using non-linear regression of (3.15) using mass data.

Table 3.1. Activity parameters from (3.13) estimated using non-linear regression with normalized activity data.

Constants	# 12	# 13	# 19	# 21	# 28	# 30	# 43
$\check{Y}$	0.909	0.772	1.232	0.820	0.517	0.988	0.466
b (hr^{-1})	0.0059	0.0055	0.0054	0.0071	0.0059	0.0048	0.0047
c (hr^{-1})	0.523	0.112	0.082	0.792	0.159	1.271	0.282

24

Table 3.2. The mass parameter $\breve{k}$ from (3.15) estimated using non-linear regression with mass data.

Constants	# 12	# 13	# 19	# 21	# 28	# 30	# 43
$\breve{k}_{fit}$ $\left(\frac{g^2}{hr}\right)$	1.711	2.412	0.465	1.003	0.498	0.367	0.055

Using the estimated activity and mass parameters, α was found for each subject as described in Section 3.2.2. Table 3.3 contains α and its respective variance for each subject. Using these values, a minimum variance estimate of α was calculated to be $\hat{\alpha}_{mv}$=0.0031 Gy^{-1} with $V(\hat{\alpha}_{mv})$=1.30E-6 Gy^{-2}.

Table 3.3. α and its respective variance are reported for each subject. α and its variance were calculated as described in Section 3.2.2.

Constants	# 12	# 13	# 19	# 21	# 28	# 30	# 43
α (Gy^{-1})	0.0036	0.0037	0.0027	0.0037	0.0032	0.0023	0.0040
$V(\alpha)$ (Gy^{-2})	1.53E-5	2.90E-5	2.75E-5	3.76E-6	2.46E-5	3.62E-6	1.98E-5

Using $\hat{\alpha}_{mv}$ for all subjects, $m(\infty)$ was calculated using (3.11). D_T was calculated using three estimates of $\breve{k}$: 1) $\breve{k}_{fit}$ was estimated using non-linear regression of (3.15) with mass data 2) $\breve{k}_{pred}$ was calculated using (3.16) and 3) $\breve{k}_{calc}$ was calculated using (2.8). Table 3.4 contains estimates of $\breve{k}_{fit}$, D_T and $m(\infty)$.

Table 3.5 reports calculations of $\breve{k}_{pred}$, D_T, and $m(\infty)$. The parameter estimates are similar between Tables 3.5 and 3.4. This provides evidence that $\breve{k}_{pred}$ provides a reasonable estimate of $\breve{k}$ and can be used to accurately calculate $m(\infty)$.

Table 3.6 reports calculations of $\breve{k}_{calc}$, D_T, and $m(\infty)$. The parameter values from Table 3.6 are reasonably close to the parameter values in Tables 3.4 and 3.5.

To validate the protocol we compared the calculated $m(\infty)$ values to the measured values which are reported in Table 3.7. We minimized the error between the two $m(\infty)$ values by

25

Table 3.4. Calculated values of $\breve{k}_{fit}$, D_T, and $m(\infty)$. $\breve{k}$ was found using non-linear regression of (3.15).

Constants	# 12	# 13	# 19	# 21	# 28	# 30	# 43
$\breve{k}_{fit}$ $(\frac{g^2}{hr})$	1.71	2.41	0.47	1.00	0.50	0.37	0.06
D_T (Gy)	427	459	728	347	367	596	379
$m(\infty)$ (g)	8.2	6.2	2.0	5.9	4.9	2.4	2.7

Table 3.5. Calculated values of $\breve{k}_{pred}$, D_T, and $m(\infty)$. Each parameter's standard error values, found through Taylor series approximation, are reported.

Constants	# 12	# 13	# 19	# 21	# 28	# 30	# 43
$\breve{k}_{pred}$ $(\frac{g^2}{hr})$	2.00	1.64	0.62	0.84	0.90	0.37	0.24
D_T (Gy)	443	380	774	327	407	596	442
$m(\infty)$ (g)	7.7	8.0	1.8	6.3	4.3	2.4	2.2

Table 3.6. Calculated values of $\breve{k}_{calc}$, D_T, and $m(\infty)$. Each parameter's standard error values, found through Taylor series approximation, are reported.

Constants	# 12	# 13	# 19	# 21	# 28	# 30	# 43
$\breve{k}_{calc}$ $(\frac{g^2}{hr})$	1.80	1.74	0.70	0.62	0.88	0.40	0.28
D_T (Gy)	431	387	804	307	404	610	467
$m(\infty)$ (g)	8.0	7.8	1.6	6.7	4.4	2.3	2.0

26

taking the square root of the sum of the squares between the two values. The error between the $m(\infty)$ values calculated using $\breve{k}_{pred}$ and the measured $m(\infty)$ values was 3.96. The error between the $m(\infty)$ values calculated using $\breve{k}_{calc}$ and the measured $m(\infty)$ values was 4.12. This implies that $\breve{k}_{pred}$ provides a more accurate $m(\infty)$ than $\breve{k}_{calc}$.

Table 3.7. Mass values measured at one year.

Constants	# 12	# 13	# 19	# 21	# 28	# 30	# 43
$m(\infty)$ (g)	7	5	3	5	5	4	2

CHAPTER 4

UNCERTAINTY ANALYSIS - THEORETICAL AND COMPUTATIONAL CONSIDERATIONS

The central challenge in computing a subject-specific RAI dose to achieve a desired $m(\infty)$ relates to figuring out how measurement and parameter identification errors affect the prediction accuracy of the final result. This problem can be stated as follows.

Central Prediction Problem. Let the target subject mass $\underline{m}(\infty)$ be related to activity kinetics and mass dynamics by the following relations (see Chapter 3)

$$
\begin{aligned}
m(\infty) &= m(0)e^{-\alpha D_T} \\
D_T &= \frac{\sigma}{k}(m(0) - m(840)) \\
A(t) &= Y\left(e^{-bt} - e^{-ct}\right) \\
m(t) &= \left[2\left(\frac{Yk}{b}e^{-bt} + \frac{Yk}{c} - \frac{Yk}{c}e^{-ct} - \frac{Yk}{b} + \frac{m(0)^2}{2}\right)\right]^{\frac{1}{2}}, \quad t \in [0, \ 840]
\end{aligned}
$$

where all parameters in the above relations are unknown with the exception of σ. Given n_A activity measurements, $\tilde{A}(t_i)$, and n_m mass measurements, $\tilde{m}(t_i)$, estimate the true expected value of $m(\infty)$ in terms of its predicted value

$$
\overline{m}(\infty),
$$

and confidence interval

$$[m_L\left(\infty\right), m_H\left(\infty\right)].$$

Before the predicted value, $\overline{m}\left(\infty\right)$, and confidence interval, $[m_L\left(\infty\right), m_H\left(\infty\right)]$, can be obtained, the activity and mass parameters first need to be identified using non-linear regression and one should clarify which parameters are subject-specific and which can be considered population constants. Note that in this chapter we will write $\overline{m}\left(\infty\right)$ as $m\left(\infty\right)$ to simplify the notation. In this thesis we follow [16, 18] and assume α to be a population parameter, while all other parameters are evaluated as subject-specific values. All computations are based on clinical data consisting of activity and mass data sets of 17 subjects and mass values measured at one year for 7 of the 17 subjects [16].

The most common standard propagation of error used to quantify the confidence interval involves uncertainty propagation via the square root of the sum of squares method (RSS) [30, 31]. This method requires the standard error, SE, of each of the parameters. The standard errors can be obtained from non-linear regression and are estimates of the true standard error of the mean for each of the parameters. We pursued this route (see Section 4.6) but decided to discontinue due to unreasonably large standard errors in D_T and $m\left(\infty\right)$. Such large values might be due to the small sample size in the clinical data and/or a poor accuracy of the first-order expansion in the analytical derivations. *Our work, therefore, focuses on a simulation-based study which involves the generation of additional data* [33, 34]. As described in Section 2.3.3, Traino et al [16] reports the uncertainties for activity and mass measurements as percentages or relative errors. Relative errors correspond to multiplicative measurement errors, therefore, we assume a multiplicative measurement error model in the activity and mass models for an individual subject

29

$$\tilde{A}(t_i) = \left(Ye^{-bt_i} - Ye^{-ct_i}\right)(1 + \epsilon_{Ai}),$$

$$\tilde{m}(t_i) = \left(\left(2\left(\frac{Yk}{b}e^{-bt_i} + \frac{Yk}{c} - \frac{Yk}{c}e^{-ct_i} - \frac{Yk}{b} + \frac{m(0)^2}{2}\right)\right)^{\frac{1}{2}}\right)(1 + \epsilon_{m_i}),$$

where ϵ_{Ai} and ϵ_{mi} are independent random variables. The data can be simulated using two methods:

1. Parametric bootstrapping, and

2. Nonparametric bootstrapping,

which are described next.

4.1   Parametric Bootstrapping

Parametric bootstrapping can be used for generating additional data by assuming the measurement error associated with the data belongs to a known distribution with either specified or unspecified parameters [33, 34]. Therefore, this method can be used to simulate additional activity and mass data which can be used to obtain additional activity and mass parameters. This section focuses on the assumed distributions of the measurement error and the procedure used to simulate the additional data. Note that we assume the same error distribution for all subjects, which may be a limitation to the validity of the results. The results from this section can be found in Chapter 5. The additional parameters obtained from the simulated data can be used to estimate $m(\infty)$ as described in Section 4.3. Section 4.4 describes an alternative method to simulate the mass parameter k. Section 4.5 describes different ways to analyze the simulation results including how to estimate the confidence interval in the estimated $m(\infty)$ values, as well as, various tests that can be performed to determine the distribution of the measurement errors.

A method to estimate the original activity and mass parameters using non-linear regression of the measured activity and mass data is required before the simulations can be

www.manaraa.com

performed and will be described next. Again, by assuming a multiplicative measurement error, the measured activity in the thyroid is described by

$$\tilde{A}(t_i) = \left(Y e^{-bt_i} - Y e^{-ct_i} \right) (1 + \epsilon_{Ai}), \quad i = 1, \ldots, n_A, \tag{4.1}$$

where ϵ_{Ai} are independent, identically distributed random variables. However, (4.1) is not suitable for non-linear regression because the error term is not additive. An additive error model is obtained by taking the natural logarithm of (4.1)

$$\ln \left(\tilde{A}(t_i) \right) = \ln \left(Y \right) + \ln \left(e^{-bt_i} - e^{-ct_i} \right) + \ln \left(1 + \epsilon_{Ai} \right), \quad i = 1, \ldots, n_A. \tag{4.2}$$

The new error term in (4.2) has an expected value $E \left(\ln \left(1 + \epsilon_{Ai} \right) \right) = \mu_A$. Since non-linear regression requires the error term to have an expected value of zero, we re-write (4.2) as

$$\ln \left(\tilde{A}(t_i) \right) = \mu_A + \ln \left(Y \right) + \ln \left(e^{-bt_i} - e^{-ct_i} \right) + \eta_{Ai}, \quad i = 1, \ldots, n_A, \tag{4.3}$$

where $\eta_{Ai} \triangleq \ln \left(1 + \epsilon_{Ai} \right) - \mu_A$. The new error term η_{Ai} has an expected value $E \left(\eta_{Ai} \right) = 0$ and variance $V \left(\eta_{Ai} \right) = \sigma_{\eta_A}^2$. Note that μ_A and Y in (4.3) cannot be estimated separately. To circumvent this technical limitation, we can substitute a numerical value of μ_A into (4.3). Expected values of μ_A can be calculated by assuming a specific statistical distribution and will be described below.

Assuming a multiplicative measurement error and using the activity parameters estimated from the measured activity data, the measured mass is described by

$$\tilde{m}(t_i) = \left(\left(2 \left(\frac{\hat{Y}k}{\hat{b}} e^{-\hat{b}t_i} + \frac{\hat{Y}k}{\hat{c}_i} - \frac{\hat{Y}k}{\hat{c}} e^{-\hat{c}t} - \frac{\hat{Y}k}{\hat{b}} + \frac{m(0)^2}{2} \right) \right)^{\frac{1}{2}} \right) (1 + \epsilon_{mi}), \tag{4.4}$$

$$i = 1, \ldots, n_m,$$

31

where ϵ_{mi} are independent, identically distributed random variables. Following the same arguments used above, a mass model suitable for non-linear regression is obtained

$$\ln\left(\tilde{m}(t_i)\right) = \mu_m + \ln\left(\left(2\left(\frac{\hat{Y}k}{\hat{b}}e^{-\hat{b}t_i} + \frac{\hat{Y}k}{\hat{c}} - \frac{\hat{Y}k}{\hat{c}}e^{-\hat{c}t_i} - \frac{\hat{Y}k}{\hat{b}} + \frac{m(0)^2}{2}\right)\right)^{\frac{1}{2}}\right) + \eta_{mi}, \tag{4.5}$$

$$i = 1, \ldots, n_m,$$

where $\eta_{mi} \triangleq \ln\left(1 + \epsilon_{mi}\right) - \mu_m$. The error term η_{mi} has an expected value $E\left(\eta_{mi}\right) = 0$ and variance $V\left(\eta_{mi}\right) = \sigma_{\eta_m}^2$.

The measurement errors are used to simulate the additional data, however, very little is known about the statistical properties of these errors. As a result, we investigate the statistical properties of the measurement error using two approaches:

1. The errors are uniformly distributed, and

2. The errors are normally distributed.

We chose to model the errors to follow a uniform distribution based on the fact that Dr. Traino believes that the measurement errors are from a uniform distribution. We chose to model the errors to follow a normal distribution because this is the usual assumption for measurement errors. Both distributions will be discussed next. Note that we assume the same error distribution for all subjects.

4.1.1 Uniform Error Assumptions

The activity measurement errors, ϵ_{Ai}, are independent random errors and assumed to be Unif($-\zeta,\zeta$). Therefore, it follows that the term $(1 + \epsilon_{Ai})$ is Unif($1-\zeta$, $1+\zeta$), we chose $\zeta = 0.10$ for activity data based on the 10% error in the activity measurements reported in [16].

Expected values for μ_A and $\sigma^2_{\eta_A}$ following the uniform distribution, μ_{AU} and $\sigma^2_{\eta_A U}$, can be calculated as follows:

$$\mu_{AU} = E\left(ln\left(1 + \epsilon_{Ai}\right)\right) = \frac{1}{2\zeta} \int_{-\zeta}^{\zeta} ln\left(1 + \epsilon_{Ai}\right) d\epsilon_{Ai} = -0.00167,$$

and

$$\sigma^2_{\eta_A U} = \frac{1}{2\zeta} \int_{-\zeta}^{\zeta} \left(ln\left(1 + \epsilon_{Ai}\right) - \mu_{AU}\right)^2 d\epsilon_{Ai} = 0.00334,$$

where the subscript U refers to the uniform distribution.

The mass measurement errors, ϵ_{mi}, are independent random errors and assumed to be Unif($-\zeta, \zeta$). Therefore, it follows that the term $(1 + \epsilon_{mi})$ is Unif($1-\zeta$, $1+\zeta$), we chose $\zeta = 0.15$ for mass dynamics data based on the 15% error in the mass measurements reported in [16].

Expected values for μ_m and $\sigma^2_{\eta_m}$ following the uniform distribution, μ_{mU} and $\sigma^2_{\eta_m U}$, can be calculated as:

$$\mu_{mU} = E\left(\ln\left(1 + \epsilon_{mi}\right)\right) = \frac{1}{2\zeta} \int_{-\zeta}^{\zeta} ln\left(1 + \epsilon_{mi}\right) d\epsilon_{mi} = -0.00378,$$

and

$$\sigma^2_{\eta_m U} = \frac{1}{2\zeta} \int_{-\zeta}^{\zeta} \left(\ln\left(1 + \epsilon_{mi}\right) - \mu_{mU}\right)^2 d\epsilon_{mi} = 0.0076.$$

4.1.2 Normal Error Assumptions

Numerical values for μ_A and $\sigma^2_{\eta_A}$ can be calculated by assuming the activity measurement error, ϵ_{Ai}, are $N(0, \frac{\zeta^2}{9})$ ($\zeta = 0.10$). In order to get the activity measurements to fall within 3 standard deviations of the mean with a probability of 99.74%, the standard deviation, σ, is chosen to be $\frac{\zeta}{3}$ which yields a variance, σ^2, of $\frac{\zeta^2}{9}$. Hence, it follows that the term $(1 + \epsilon_{Ai})$ will be in the range of $1 \pm \zeta$ with the same probability. Expected values for μ_A and $\sigma^2_{\eta_A}$ following

the normal distribution, μ_{AN} and $\sigma^2_{\eta_A N}$ (the subscript N refers to the normal distribution), are more difficult to calculate because

$$P\left(-\infty \leq \epsilon_{Ai} \leq -1\right) = \int_{-\infty}^{-1} \frac{1}{SD\sqrt{2\pi}} e^{-\frac{\epsilon_{Ai}^2}{2SD^2}} d\epsilon_{Ai} = 4.9E - 198 \approx 0,$$

therefore, $\ln\left(1 + \epsilon_{Ai}\right)$ is undefined with probability ≈ 0. As a result, ϵ_{Ai} was considered to follow a truncated normal distribution confined to the interval (-1,1):

$$P\left(\epsilon_{Ai} \leq x \middle| -1 < \epsilon_{Ai} < 1\right) = \frac{P\left(\epsilon_{Ai} \leq x \bigcap -1 < \epsilon_{Ai} < 1\right)}{P\left(-1 < \epsilon_{Ai} < 1\right)} \approx P\left(\epsilon_{Ai} \leq x\right); \ |x| \leq 1.$$

Expected values of μ_{AN} and $\sigma^2_{\eta_A N}$ can be calculated as follows:

$$\mu_{AN} = E\left(ln\left(1 + \epsilon_{Ai}\right)\right) = \frac{3}{\sqrt{2\pi}(\zeta)} \int_{-1}^{1} ln\left(1 + \epsilon_{Ai}\right) e^{\frac{-9\epsilon_{Ai}^2}{2(\zeta)^2}} d\epsilon_{Ai} = -0.00056,$$

and

$$\sigma^2_{\eta_A N} = \frac{3}{\sqrt{2\pi}(\zeta)} \int_{-1}^{1} \left(ln\left(1 + \epsilon_{Ai}\right) - \mu_{AN}\right)^2 e^{\frac{-9\epsilon_{Ai}^2}{2(\zeta)^2}} d\epsilon_{Ai} = 0.00111.$$

Similarly, expected values for μ_m and $\sigma^2_{\eta_m}$ can be calculated by assuming a normal statistical distribution. ϵ_{mi} are assumed $N(0, \frac{\zeta^2}{9})$ ($\zeta = 0.15$) to again ensure that the mass data will fall within 3 standard deviations of the mean with a probability of 99.74%. Following the same argument proposed above, ϵ_{mi} are also considered to follow a truncated normal distribution confined to the interval (-1,1). μ_{mN} and $\sigma^2_{\eta_m N}$ can be calculated as follows:

$$\mu_{mN} = E\left(\ln\left(1 + \epsilon_{mi}\right)\right) = \frac{3}{\sqrt{2\pi}(\zeta)} \int_{-1}^{1} ln\left(1 + \epsilon_{mi}\right) e^{\frac{-9\epsilon_{mi}^2}{2(\zeta)^2}} d\epsilon_{mi} = -0.00125,$$

and

$$\sigma^2_{\eta_m U} = \frac{3}{\sqrt{2\pi}(\zeta)} \int_{-1}^{1} \left(ln\left(1 + \epsilon_{mi}\right) - \mu_{mN}\right)^2 e^{\frac{-9\epsilon_{mi}^2}{2(\zeta)^2}} d\epsilon_{mi} = 0.00252.$$

The activity and mass data can be simulated using both of these assumed distributions of the measurement error as will be described next. To aid in the procedure, consider that

34

subject ℓ has n_A^ℓ activity data points measured at times t_i. The superscript ℓ denotes the ℓth subject and $t_i \in \{t_A^\ell\}$ where $\{t_A^\ell\} = \{t_1^\ell, \ldots, t_{n_A^\ell}^\ell\}$. Also, subject ℓ has n_m^ℓ mass data points measured at times t_i. The superscript ℓ denotes the ℓth subject and $t_i \in \{t_m^\ell\}$ where $\{t_m^\ell\} = \{t_1^\ell, \ldots, t_{n_m^\ell}^\ell\}$. The procedure to simulate the activity and mass data is split into two sections for clarity.

4.1.3 Simulating Activity Kinetics

Non-linear regression of (4.3) using the measured activity data for subject ℓ yields estimates of the original activity parameters $\hat{Y}$, $\hat{b}$, and $\hat{c}$. Using these activity parameters, N simulated activity data sets can be created:

$$\tilde{A}_{sim}^j(t_i) = \hat{Y}\left(e^{-\hat{b}t_i} - e^{-\hat{c}t_i}\right)(1 + \epsilon_{Ai}^j), \qquad t_i \in \{t_A^\ell\},$$

where $j = 1, \ldots, N$ for patient ℓ. The error terms ϵ_{Ai} can be computed from either the $\text{Unif}(-\zeta, \zeta)$ or $\text{N}(0, \frac{\zeta^2}{9})$ distributions, with ζ=0.10. Figure 4.1 demonstrates the simulation of activity data for subject 12. At each time, t_i, there are N simulated data points. Each of the N simulated data sets can be put into the form of (4.3) and used in a non-linear regression routine to estimate the activity parameters for that set. For example, the jth set for subject ℓ will be

$$ln\left(\tilde{A}_{sim}^j(t_i)\right) = \mu_A + ln\left(Y\right) + ln\left(e^{-bt_i} - e^{-ct_i}\right) + \eta_{Ai}^j, \quad t_i \in \{t_A^\ell\},$$

Non-linear regression yields parameter estimates of $\hat{Y}^j$, $\hat{b}^j$, $\hat{c}^j$, and $\left(\hat{\sigma}_{\eta_A}^j\right)^2$ where $j = 1, \ldots, N$. These parameters can be studied using methods described in Section 4.5.

35
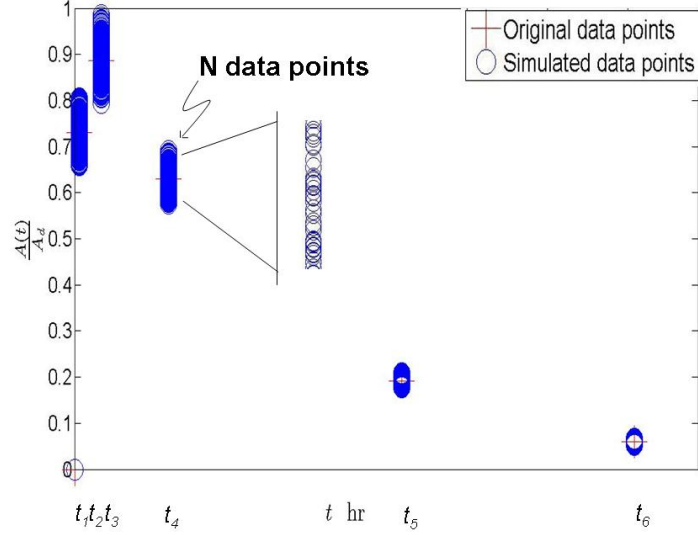
Figure 4.1. Activity kinetics for subject 12. The crosses represent the original measured activity data points. The circles represent the simulated activity data points. At each time, t_i, there are N simulated data points.

4.1.4 Simulating Mass Dynamics

The simulation of the mass dynamics were performed in a similar manner to the activity simulations. Non-linear regression of (4.5) using the measured mass data for subject ℓ yields estimates of the original mass parameters $\hat{\mu}_m$ and $\hat{k}$. Using these mass parameters and the N sets of activity parameters, N simulated mass data sets can be created:

$$
\tilde{m}_{sim}^{\jmath}(t_i) = \left(\left(2 \left(\frac{\hat{Y}^{\jmath}\hat{k}}{\hat{b}^{\jmath}} e^{-\hat{b}^{\jmath}t_i} + \frac{\hat{Y}^{\jmath}\hat{k}}{\hat{c}^{\jmath}} - \frac{\hat{Y}^{\jmath}\hat{k}}{\hat{c}^{\jmath}} e^{-\hat{c}^{\jmath}t_i} - \frac{\hat{Y}^{\jmath}\hat{k}}{\hat{b}^{\jmath}} + \frac{(m^{\jmath}(0))^2}{2} \right) \right)^{\frac{1}{2}} \right) (1 + \epsilon_{mi}^{\jmath}),
$$
$$
t_i \in \left\{ t_m^{\ell} \right\},
$$

where $\jmath = 1, \ldots, N$ for patient ℓ. The error term ϵ_{mi} can be computed from either the Unif($-\zeta, \zeta$) or N($0, \frac{\zeta^2}{9}$) distribution with $\zeta = 0.15$. The $m(0)$ term can also be simulated for each data set using the simulated $\epsilon_{mi\ell}$ error terms as

$$m^{\jmath}(0) = m(0) \left(1 + \epsilon_{m1}^1\right)$$

Each of the simulated data sets can be put into the form of (4.5) and used in a non-linear regression routine to estimate the mass parameter for that set. For example, the $\jmath^{th}$ set would be

$$\ln\left(\tilde{m}_{sim}^{\jmath}(t_i)\right) = \mu_m + \ln\left(\left(2\left(\frac{\hat{Y}^{\jmath}}{\hat{b}^{\jmath}}e^{-\hat{b}^{\jmath}t_i} + \frac{\hat{Y}^{\jmath}k}{\hat{c}^{\jmath}} - \frac{\hat{Y}^{\jmath}k}{\hat{c}^{\jmath}}e^{-\hat{c}^{\jmath}t_i} - \frac{\hat{Y}^{\jmath}k}{\hat{b}^{\jmath}} + \frac{(m^{\jmath}(0))^2}{2}\right)\right)^{\frac{1}{2}}\right) + \eta_{mi}^{\jmath},$$
$$t_i \in \left\{t_m^{\ell}\right\}.$$

Note that $\hat{Y}^{\jmath}$, $\hat{b}^{\jmath}$, and $\hat{c}^{\jmath}$ are as in Section 4.1.3. Non-linear regression will yield parameter estimates of $\hat{\mu}_m^{\jmath}$, $\hat{k}^{\jmath}$, and $\left(\hat{\sigma}_{\eta_m}^{\jmath}\right)$ where $\jmath = 1, \ldots, N$. These parameters can be studied using methods described in Section 4.5.

4.2 Nonparametric Bootstrapping

Nonparametric bootstrapping is used to study the distribution of the parameter estimators without an a priori statistical distribution assumption [33, 34]. Activity and mass data can be simulated by using the residuals obtained from regression of the measured activity and mass data and assuming that the residuals are independent and identically distributed [35]. An alternative form of (4.3) will be used to estimate the activity parameters because of the need to eliminate the assumptions associated with the numerical value of μ_A. This section describes how the activity and mass parameters are estimated, how the residuals are obtained from non-linear regression, and how the additional activity and mass data are simulated using these residuals. The results from this section can be found in Chapter 5. The simulated data are then used to estimate $m(\infty)$ as described in Section 4.3. Section 4.4 describes an alternative method to simulate the mass parameter k. Section 4.5 describes

different ways to analyze the simulation results including how to estimate the confidence interval in the estimated $m(\infty)$ values, as well as, various tests that can be performed to determine the distribution of the measurement errors.

4.2.1 Simulating The Activity Kinetics Using Residuals

As first described in Section 4.1, the expected value μ_A is required a priori in order to perform non-linear regression on (4.3). However, this forces a specific statistical distribution on ϵ_{Ai} and as a result proper analysis can not be conducted to verify the actual distribution of ϵ_{Ai}. To circumvent this technical limitation, (4.3) can be re-written as

$$\ln\left(\tilde{A}(t_i)\right) = z + \ln\left(e^{-bt_i} - e^{-ct_i}\right) + \eta_{Ai}, \tag{4.6}$$

where $z = \mu_A + \ln(Y)$. Non-linear regression of (4.6) using the original measured activity data yields predicted (or "fitted") values of activity given by

$$\ln\left(\hat{A}(t_i)\right) = \hat{z} + \ln\left(e^{-\hat{b}t_i} - e^{-\hat{c}t_i}\right). \tag{4.7}$$

The residuals were then calculated as the difference between the natural log of the original measured activity data points, $\ln\left(\tilde{A}(t_i)\right)$, used in the regression and the expected activity values calculated using (4.7). Mathematically the residuals can be written as

$$r_{Ai} = \ln\left(\tilde{A}(t_i)\right) - \ln\left(\hat{A}(t_i)\right).$$

The residuals for all subjects should be stored together yielding a bank of residuals which can be used to simulate the activity data. Note that this approach assumes that the error distributions are the same for all subjects.

38

Again, consider that subject ℓ has n_A^ℓ data points measured at times t_i. From this activity data set, estimates of the activity parameters $\hat{z}$, $\hat{b}$, and $\hat{c}$, are found for subject ℓ as described on the previous page. With these estimated activity parameters, N simulated activity data sets are created:

$$\ln\left(\tilde{A}_{sim}^\jmath(t_i)\right) = \hat{z} + \ln\left(e^{-\hat{b}t_i} - e^{-\hat{c}t_i}\right) + \eta_{Ai}^\jmath, \quad t_i \in \left\{t_A^\ell\right\}.$$

The error terms η_{Ai} are simulated using the residuals, that is the residuals r_{Ai} mimic η_{Ai}. The total number of residuals for all subjects was 43. However, bootstrap sampling is used to simulate a large number of sets of residuals [36, 37]. Therefore, even though the total number of residuals is small, bootstrap sampling can be used to simulate N sets of residuals and give the effect of a larger data set. Bootstrap sampling is the random sampling of a data set with replacement. A bootstrap sample of size w should be chosen for each of the N simulations, where w is the total number of residuals in the data set for all ℓ subjects. The bootstrap sampling should be repeated N times to yield N x w η_{Ai} values $\eta_{Ai}^\jmath$ where $\jmath = 1, \ldots, N$ and $i = 1, \ldots, w$. Simulations can be performed using each of the N sets of errors. The η_{Ai} values found in one of the N sets are to be used for all subjects. For example, the first n_{A1} values are used for subject 1 and the next n_{A2} values are used for subject 2. Where n_{A1} and n_{A2} are the number of measured data points for subjects 1 and 2 respectively. Each of the simulated data sets were used in a non-linear regression routine to estimate the activity parameters for that set. For example, the $\jmath^{th}$ set is

$$\ln\left(\tilde{A}_{sim}^\jmath(t_i)\right) = z + \ln\left(e^{-bt_i} - e^{-ct_i}\right) + \eta_{Ai}^\jmath, \quad t_i \in \left\{t_A^\ell\right\}.$$

Non-linear regression yields parameter estimates of $\hat{z}^\jmath$, $\hat{b}^\jmath$, $\hat{c}^\jmath$, and $\left(\hat{\sigma}_{\eta_A}^\jmath\right)^2$ where $\jmath = 1, \ldots, N$. These parameters can be studied using methods described in Section 4.5.

39

4.2.2 Simulating Mass Dynamics Using Residuals

Non-linear regression of (4.5) with the measured mass data yields estimates of the original mass parameters. The estimates of the activity parameters $\hat{z}$, $\hat{b}$, and $\hat{c}$ can be found using non-linear regression of the activity data as described in Section 4.2.1. $\hat{Y}$ is required for the estimation of the mass parameters and therefore needs to be calculated from the estimate of $\hat{z}$. Recalling, from Section 4.2.1, that

$$\hat{z} = \hat{\mu}_A + \ln\left(\hat{Y}\right), \tag{4.8}$$

an estimate of $\hat{\mu}_A$ is required to calculate $\hat{Y}$. To estimate $\hat{\mu}_A$, the error term

$$\eta_{Ai} = \ln\left(1 + \epsilon_{Ai}\right) - \mu_A$$

can be used. The residuals r_{Ai} are an approximation to the corresponding η_{Ai}

$$
\begin{aligned}
r_{Ai} &\approx \ln\left(1 + \epsilon_{Ai}\right) - \mu_A \\
&\therefore \\
e^{r_{Ai}} &\approx \left(1 + \epsilon_{Ai}\right) e^{-\mu_A}.
\end{aligned}
$$

Taking the average of both sides yields

$$\overline{e^r} \approx \left(1 + \bar{\epsilon}_A\right) e^{-\mu_A}.$$

Following the assumption that $\mathrm{E}(\epsilon_{Ai}) = 0$, it follows that $\bar{\epsilon}_A \approx 0$. As a result,

$$
\begin{aligned}
\overline{e^r} &\approx e^{-\mu_A} \\
&\therefore \\
\mu_A &\approx -\ln\left(\overline{e^r}\right).
\end{aligned}
$$

40

An estimate of $\hat{Y}$ to be used in the mass dynamics model can be calculated using (4.8) with the estimate $\hat{\mu}_A = -0.009$.

The parameters μ_m and k can be estimated using non-linear regression of (4.5) with measured mass data. The residuals can then be calculated as the difference between the natural logarithm of the actual measured mass data points, $\ln(\tilde{m}(t_i))$, used in the regression and the expected mass values calculated using (4.5). Mathematically this can be written as

$$r_{mi} = \ln(\tilde{m}(t_i)) - \ln(\hat{m}(t_i)).$$

Again, the residuals for all subjects should be stored together yielding a bank of residuals which can be used to simulate the mass data.

The simulation of the mass dynamics were performed in a similar manner to the activity kinetics simulations. Consider that subject ℓ has n_m^ℓ mass data points measured at times t_i. From this mass data set, estimates of the original mass parameters $\hat{\mu}_m$ and $\hat{k}$, are found for subject ℓ. Using these mass parameters, and the N sets of activity parameters, N simulated mass data sets can be created:

$$
\ln(\tilde{m}^{\jmath}_{sim}(t_i)) = \hat{\mu}_m
$$
$$
+ \ln\left(\left(\left(2\left(\frac{\hat{Y}^{\jmath}\hat{k}}{\hat{b}^{\jmath}}e^{-\hat{b}^{\jmath}t_i} + \frac{\hat{Y}^{\jmath}\hat{k}}{\hat{c}^{\jmath}} - \frac{\hat{Y}^{\jmath}\hat{k}}{\hat{c}^{\jmath}}e^{-\hat{c}^{\jmath}t_i} - \frac{\hat{Y}^{\jmath}\hat{k}}{\hat{b}^{\jmath}} + \frac{(m^{\jmath}(0))^2}{2}\right)\right)^{\frac{1}{2}}\right)\right) + \eta^{\jmath}_{mi},
$$
$$
t_i \in \left\{t_A^\ell\right\}.
$$

The error terms η_{mi} can be simulated using the mass residuals. The residuals r_{mi} mimic η_{mi}. A bootstrap sample of size w can be chosen for each of the N simulations, where w is the total number of residuals in the data set for all ℓ subjects. The bootstrap sampling can be repeated N times to yield w x N η_{mi} values $\eta^{\jmath}_{mi}$ where $\jmath = 1, \ldots, N$ and $i = 1, \ldots, w$. Simulations can be performed using each of the N sets of errors. The η_{mi} values found in

41

one of the N sets can be used for all subjects. For example, the first n_{m1} values can be used for subject 1 and the next n_{m2} values can be used for subject 2. Where n_{m1} and n_{m2} are the number of measured data points for subjects 1 and 2, respectively. The $m(0)$ term can also be simulated for each data set using the simulated η_m error terms by

$$m^j(0) = m(0)\left(1 + \epsilon_{mi}^1\right)$$

where $\epsilon_{mi} \approx e^{-\eta_{mi} + \mu_m} - 1$. μ_m was found using the same procedure to calculate μ_A as described above. The estimate of μ_m, $\hat{\mu}_m$, was calculated to be $\hat{\mu}_m = -0.0019$. Each of the simulated data sets can be used in a non-linear regression routine to estimate the mass parameter for that set. For example, the jth set will be

$$\ln\left(\tilde{m}_{sim}^j(t_i)\right) = \mu_m + \ln\left(\left(2\left(\frac{\hat{Y}^j k}{\hat{b}^j}e^{-\hat{b}^j t_i} + \frac{\hat{Y}^j k}{\hat{c}^j} - \frac{\hat{Y}^j k}{\hat{c}^j}e^{-\hat{c}^j t_i} - \frac{\hat{Y}^j k}{\hat{b}^j} + \frac{(m^j(0))^2}{2}\right)\right)^{\frac{1}{2}}\right) + \eta_{mi}^j,$$
$$t_i \in \left\{t_A^\ell\right\}.$$

Non-linear regression will yield parameter estimates of $\hat{\mu}_m^j$, $\hat{k}^j$, and $\left(\hat{\sigma}_{\eta_m}^j\right)^2$ $j = 1, \ldots, N$. These parameters can be studied using methods described in Section 4.5.

4.3   Predicting The Final Mass

Using the simulated activity and mass parameters obtained from either of the three approaches, $m(\infty)$ can be calculated using (3.11),

$$m(\infty) \approx m(0)e^{-\alpha D_T}.$$

The absorbed dose is expressed in the following closed form solution using (3.4)

$$D_T = \frac{\sigma}{k}\left(m(0) - m(840)\right), \tag{4.9}$$

where,

$$m(840) = \left(2\left(\frac{Yk}{b}e^{-b840} + \frac{Yk}{c} - \frac{Yk}{c}e^{-c840} - \frac{Yk}{b} + \frac{m(0)^2}{2}\right)\right)^{\frac{1}{2}}.$$

Using (4.9), the absorbed dose can be calculated for each of the N simulated data sets for subject ℓ:

$$\tilde{D}_{T\,sim}^{\jmath} = \frac{\sigma}{\hat{k}^{\jmath}}\left(m^{\jmath}(0) - \left(\left(2\left(\frac{\hat{Y}^{\jmath}\hat{k}^{\jmath}}{\hat{b}^{\jmath}}e^{-\hat{b}^{\jmath}840} + \frac{\hat{Y}^{\jmath}\hat{k}^{\jmath}}{\hat{c}^{\jmath}} - \frac{\hat{Y}^{\jmath}\hat{k}^{\jmath}}{\hat{c}^{\jmath}}e^{-\hat{c}^{\jmath}840} - \frac{\hat{Y}^{\jmath}\hat{k}^{\jmath}}{\hat{b}^{\jmath}} + \frac{(m^{\jmath}(0))^2}{2}\right)\right)^{\frac{1}{2}}\right)\right),$$

where $\jmath = 1, \ldots, N$ and $\hat{Y}^{\jmath}$, $\hat{b}^{\jmath}$, $\hat{c}^{\jmath}$, and $\hat{k}^{\jmath}$ were found using non-linear regression of the $\jmath^{\text{th}}$ simulated data set.

An α value is calculated using (3.10),

$$\alpha = \frac{1}{D_T}\left(\ln\left(m(0)\right) - \ln\left(m(\infty)\right)\right).$$

For subject ℓ, there are N simulated D_T and $m(0)$ values. By creating N more ϵ_{mi} error terms using one of the methods described in this chapter, N $m(\infty)$ values can be simulated from

$$m^{\jmath}(\infty) = m(\infty)\left(1 + \epsilon_{mi}^{\jmath}\right).$$

N α values can then be calculated for subject ℓ and an average $\bar{\alpha}_{subject}$,

$$\bar{\alpha}_{subject} = \sum_{1}^{N}\frac{\alpha^{\jmath}}{N},$$

as well as the standard deviation,

$$\sigma_\alpha = \left(\sum_{1}^{N}\frac{(\alpha^{\jmath} - \bar{\alpha}_{subject})^2}{N}\right)^{\frac{1}{2}},$$

43

of the N α values can be calculated. This procedure can be repeated for all subjects. Using the $\bar{\alpha}_{subject}$ values for each subject, a minimum variance estimate of α, $\hat{\alpha}_{mv}$, can be calculated

$$\hat{\alpha}_{mv} = \frac{\sum \frac{\bar{\alpha}_{subject}}{V(\bar{\alpha}_{subject})}}{\sum \frac{1}{V(\bar{\alpha}_{subject})}},$$

where $V(\bar{\alpha}_{subject}) = (\sigma(\bar{\alpha}_{subject}))^2$. The variance of $\hat{\alpha}_{mv}$ can be calculated using

$$V(\hat{\alpha}_{mv}) = \frac{1}{\sum \frac{1}{V(\bar{\alpha}_{subject})}}.$$

Inserting $\hat{\alpha}_{mv}$, into (3.11), the final mass can be calculated for each of the N simulated activity data sets for subject ℓ:

$$\tilde{m}^{\jmath}_{sim}(\infty) \approx m^{\jmath}(0)e^{-\hat{\alpha}_{mv}D^{\jmath}_T}$$

4.4   k$_{\text{pred}}$

Throughout this chapter we have estimated the mass parameter k using non-linear regression with mass data. However, the mass parameter k could have been estimated using (3.9) to yield k_{pred}. k_{pred} could be simulated N times using the simulated activity parameters as follows

$$\tilde{k}^{\jmath}_{pred,sim} = \phi \frac{(m^{\jmath}(0))^2}{\left(\frac{\hat{Y}^{\jmath}}{\hat{c}^{\jmath}}e^{-\hat{c}^{\jmath}840} - \frac{\hat{Y}^{\jmath}}{\hat{b}^{\jmath}}e^{-\hat{b}^{\jmath}840} - \frac{\hat{Y}^{\jmath}}{\hat{c}^{\jmath}} + \frac{\hat{Y}^{\jmath}}{\hat{b}^{\jmath}} \right)} - \varphi$$

where $\jmath = 1, \ldots, N$ and $\hat{Y}^{\jmath}$, $\hat{b}^{\jmath}$, and $\hat{c}^{\jmath}$ were found using non-linear regression of the $\jmath^{\text{th}}$ simulated activity kinetics data set. The $m(0)$ terms were simulated as described in Section 4.2.2. These simulated k_{pred} values could then be used to calculate D_T as described in Section 4.3.

44

4.5 Analysis

The simulations yield parameter estimates $\hat{Y}^{\jmath}$, $\hat{b}^{\jmath}$, $\hat{c}^{\jmath}$, $\hat{\mu}_m^{\jmath}$, $\hat{k}^{\jmath}$, $\hat{D}_T^{\jmath}$, and $\hat{m}^{\jmath}(\infty)$ where $\jmath = 1, \ldots, N$. The average parameter values can be calculated. For example, the average value of $\hat{Y}$ will be the average of $\hat{Y}^1, \ldots, \hat{Y}^N$. The standard deviation of these parameter estimates will be an approximation to the standard error of the estimator. The distribution of each of the parameters can be studied with the use of a histogram and normal probability plot. Also, the parameters estimated from the simulated data can be compared to parameters estimated from the measured data. For example, the average value of $\hat{Y}$ for patient ℓ estimated from the simulated data can be compared to $\hat{Y}$ estimated from regression of the measured data. Also, the standard deviation of the $\hat{Y}$ estimated from the simulated data can be compared to the standard error of $\hat{Y}$ estimated from the measured data. If the simulation results are reasonably close to the original regression results, then the simulations may not be required.

The N simulated $m(\infty)$ values can be used to estimate its confidence interval by finding the percentiles of the N values [38]. For example, if a 95% confidence level is desired, the 2.5% and 97.5% percentiles can be found from the N $m(\infty)$ values and the corresponding values at these percentiles will make up the uncertainty band or confidence interval.

4.5.1 Testing The Measurement Error Distribution Assumptions

Various methods exist to informally test which assumption about the statistical distributions of the activity and mass data are correct. One method is to compare the estimates of μ ($\mu = \mu_A$ or μ_m) and σ_η^2 ($\sigma_\eta^2 = \sigma_{\eta_A}^2$ or $\sigma_{\eta_m}^2$) found from the non-linear regression to their expected values. However, this method will not apply to the activity data because a numerical value of μ_A was inserted into (4.3). Non-linear regression of (4.5) provides estimates of the parameters $\hat{\mu}_m$, $\hat{k}$, and $\hat{\sigma}_{\eta_m}^2$. If $\hat{\mu}$ and $\hat{\sigma}_\eta^2$ are close to their expected values for a particular assumption, it will support that assumption. If the values are not close to the expected

values of either the uniform or normal distribution, then an alternative error distribution might need to be considered.

A second method is to investigate the residuals r_i ($r_i = r_{Ai}$ or r_{mi}) from the non-linear regression of Equations (4.3) and (4.5) while assuming either a uniform or normal error distribution. If the models were fit successfully, the residuals should mimic the η_i values

$$r_i \approx \eta_i = \ln(1 + \epsilon_i) - \mu,$$

where ($\epsilon_i = \epsilon_{Ai}$ or ϵ_{mi}). Therefore,

$$r_i + \mu \approx \ln(1 + \epsilon_i).$$

Solving for ϵ_i yields

$$\epsilon_i \approx e^{r_i + \mu} - 1.$$

The ϵ_i values should either be approximately Unif($-\zeta, \zeta$) or approximately N($0, \frac{\zeta^2}{9}$). These assumptions can be assessed by using histograms and normal probability plots of ϵ_i.

Various test can also be performed on the residuals themselves to try and gain insight into their statistical distribution. The tests include side by side box plots, normal probability plots, and histograms. The box plots are for each subject's residuals separately, while the normal probability plot and histogram are for all the residuals together. The box plots will provide evidence of whether each subject shares the same distribution and the normal probability plot and histogram will provide evidence of which distribution the subjects possibly share.

4.6 Standard Propagation of Error Method

The usual propagation of error formula to calculate the standard error of a variable, f, which is a function of variables, x and y, can be expressed as

46

$$SE_{f(x,y)} = \left[\left(\frac{\partial f(x,y)}{\partial x} SE_x \right)^2 + \left(\frac{\partial f(x,y)}{\partial y} SE_y \right)^2 \right]^{\frac{1}{2}}. \tag{4.10}$$

The uncertainty of the final result can be obtained by multiplying the standard error by a student t value [30, 31]. For example, the standard error of $m(\infty)$ will be computed using the standard errors of $m(0)$, α, and D_T. The method consists of calculating a Taylor series approximation about each of the parameters. The approximation of each parameter is then multiplied by its respective standard error, SE, and all the terms are combined taking the square root of the sum of the squares of the individual terms to provide the SE of the final answer. An example of the standard propagation of error method will now be shown. The final mass of the thyroid is defined as

$$m(\infty) \approx m(0)e^{-\alpha D_T}.$$

To emphasize the dependence on the individual parameters, the above equation is re-written as

$$m(\infty) \approx F\left(m(0), \alpha, D_T\left(m(0), k, m(840)\left(Y, b, c, m(0), k \right) \right) \right).$$

The Taylor series approximations were found by taking the partial derivatives of $m(\infty)$ with respect to α, $m(0)$, k, Y, b, and c. These partial derivatives were used to calculate the variance of $m(\infty)$ as follows

$$\begin{aligned}
SE(m(\infty)) = \Bigg[&\left(\frac{\partial m(\infty)}{\partial \alpha} SE_\alpha \right)^2 + \left(\frac{\partial m(\infty)}{\partial m(0)} SE_{m(0)} \right)^2 + \left(\frac{\partial m(\infty)}{\partial k} SE_k \right)^2 \\
&+ \left(\frac{\partial m(\infty)}{\partial Y} SE_Y \right)^2 + \left(\frac{\partial m(1\ year)}{\partial b} SE_b \right)^2 + \left(\frac{\partial m(\infty)}{\partial c} SE_c \right)^2 \\
&+ 2\frac{\partial m(\infty)}{\partial Y} \frac{\partial m(\infty)}{\partial b} COV(Y,b) + 2\frac{\partial m(\infty)}{\partial Y} \frac{\partial m(\infty)}{\partial c} COV(Y,c) \\
&+ 2\frac{\partial m(\infty)}{\partial b} \frac{\partial m(\infty)}{\partial c} COV(b,c) \Bigg]^{1/2}
\end{aligned}$$

The activity parameters, standard error, and covariance terms were estimated from the non-linear regression of the measured activity data. The uncertainty of $m(\infty)$ can be calculated using

$$\delta_m = SE\left(m(\infty)\right)t,$$

where t is a Student's t value.

CHAPTER 5

UNCERTAINTY ANALYSIS RESULTS AND DISCUSSION

This chapter will present and discuss the results of the uncertainty analysis discussed in Chapter 4. The uncertainty analysis was conducted as described in Chapter 4 with the exception that the activity data used to estimate the activity parameters was normalized by the initial dose, A_d. Normalized activity data was used because the activity data used in our new protocol will be normalized as described in Section 3.4. The fact that normalized activity data was used to estimate the activity parameters was omitted from Chapter 4 so the theory was not cluttered with extra notation. However, repeating what was presented in Section 3.4 to clarify the notation for this chapter, (3.3) was re-written as

$$\check{A}(t_i) = \check{Y} \left(e^{-bt_i} - e^{-ct_i} \right), \tag{5.1}$$

where $Y = A_d \check{Y}$. Inserting (5.1) into (2.6) yielded

$$\dot{m}(t) = -\check{k} \frac{\check{A}(t)}{m(t)},$$

where $\check{k} = A_d k$. Solving for $m(t)$ yielded

$$m(t) = \left(2 \left(\frac{\check{Y}\check{k}}{b} e^{-bt} + \frac{\check{Y}\check{k}}{c} - \frac{\check{Y}\check{k}}{c} e^{-ct} - \frac{\check{Y}\check{k}}{b} + \frac{m(0)^2}{2} \right) \right)^{\frac{1}{2}}. \tag{5.2}$$

49

$\breve{k}$ was estimated using non-linear regression to yield $\breve{k}_{fit}$ and using (3.16) to yield $\breve{k}_{pred}$

$$\breve{k}_{pred} = 0.5951\frac{m(0)^2}{\breve{g}} - 0.0108,$$

where, $\breve{g} = A_d g$.

This chapter is organized as follows. Section 5.1 is an overview of the results for the uncertainty analysis described in this chapter. Section 5.2 contains the results from the parametric bootstrap simulations. The results presented in this section will be of only the uniform distribution simulations. The normal distribution simulations resulted in confidence intervals for $m(\infty)$ that were much to narrow to be clinically useful and therefore will only be presented in Appendix E. Section 5.3 contains the results from the nonparametric bootstrap simulations. Section 5.4 contains the calculation of $m(\infty)$ using parameters estimated from data simulated from each of the methods. Finally, Section 5.5 contains the results from the standard propagation of error method.

5.1 Summary Of The Uncertainty Analysis Results

Our goal was to see how well we can predict $m(\infty)$ and to assess the uncertainty in the prediction. To do this we predict $m(\infty)$ in terms of its predicted value

$$\overline{m}\left(\infty\right),$$

and confidence interval

$$[m_L\left(\infty\right), m_H\left(\infty\right)].$$

To obtain the predicted value and the confidence interval, we used 2 methods: 1) A standard propagation of error method and 2) A bootstrap simulations method (parametric and

50

nonparametric). Note that in this chapter we will write $\overline{m}(\infty)$ as $m(\infty)$ to simplify the notation.

We first looked into the standard propagation of error method. The full results from this method can be found in Section 5.5. However, in following this method we obtained unreasonably large SE values for D_T and $m(\infty)$. Such large values might be due to the small sample size in the clinical data and/or a poor accuracy of the first-order expansion in the analytical derivations. The limited clinical data led us to simulate additional data. Note that we did not return to the standard propagation of error method after starting to investigate the bootstrap simulations.

We simulated data using the bootstrap techniques discussed in Chapter 4. When simulating data using the parametric bootstrap method, we assumed the measurement error follows a Unif$(-\zeta,\zeta)$ distribution. The full results from the parametric bootstrap method can be found in Section 5.2. As discussed in Chapter 4, we first estimated the activity and mass parameters using non-linear regression with the measured activity and mass data. The residuals obtained from regression of the measured activity data were used to estimate ϵ_{Ai} as described in Section 4.5.1. We could not conclude if the errors follow the Unif$(-\zeta,\zeta)$ or the $N(0,\frac{\zeta^2}{9})$ distribution or neither. The same is true for ϵ_{mi} estimated from the residuals of the regression of the measured mass data. As a result, we simulated activity and mass data using both distributions.

As described in Section 4.5, we compared the parameters and SE values estimated from the simulated data to the parameters and SE values estimated from the measured data. We can conclude that the parameters and SE values do not match well between the two methods of estimating the parameters, with the exception of the activity parameters and SE values estimated assuming the Unif$(-\zeta,\zeta)$ distribution. This implies that while investigating the uncertainty in $m(\infty)$, the simulated activity and mass data will be required to estimate the activity and mass parameters. The parameters estimated from the simulated data were also

used in histograms and normal probability plots to investigate their distributions as described in Section 4.5. However, conclusions could not be made from these plots. It should be noted that the parameters estimated from the data that was simulated assuming the $\text{Unif}(-\zeta,\zeta)$ distribution matched reasonably well with the parameters estimated from the data that was simulated assuming the $\text{N}(0,\frac{\varsigma^2}{9})$ distribution. However, the SE values estimated from data simulated assuming the $\text{N}(0,\frac{\varsigma^2}{9})$ distribution were on average smaller than the SE values estimated from the data simulated assuming the $\text{Unif}(-\zeta,\zeta)$ distribution. This was expected because the variance of the $\text{Unif}(-\zeta,\zeta)$ distribution is $\frac{\varsigma^2}{3}$, while the variance of the $\text{N}(0,\frac{\varsigma^2}{9})$ distribution is $\frac{\varsigma^2}{9}$.

The absorbed dose, D_T, α, and $m(\infty)$ were calculated using the parameters estimated from the data simulated assuming the $\text{Unif}(-\zeta,\zeta)$ distribution. To calculate D_T, we used 3 estimates of $\breve{k}$: 1) $\breve{k}_{fit}$ estimated from non-linear regression, 2) $\breve{k}_{pred}$ calculated using (3.16), and 3) $\breve{k}_{calc}$ calculated using (2.8). The 3 estimates of $\breve{k}$ were used to investigate the various ways to calculate D_T and their effect on the prediction of $m(\infty)$. The statistical properties of D_T and $m(\infty)$ were also studied with the use of histograms. However, a conclusion of what distribution these parameters follow could not be made from these plots alone. Here we will present the $m(\infty)$ values calculated using activity and mass parameters estimated from data simulated assuming the $\text{Unif}(-\zeta,\zeta)$ distribution and using $\breve{k}_{pred}$ to calculate D_T. The uncertainty in $m(\infty)$ will be presented in terms of the confidence interval of $m(\infty)$, $CI_{m(\infty)}$, as described in Section 4.5. Table 5.1 contains $m(\infty)$ values and its confidence interval corresponding to a 95% confidence level.

Table 5.1. $m(\infty)$ was calculated from parameters estimated from data simulated assuming the uniform distribution. The confidence interval of $m(\infty)$, $CI_{m(\infty)}$ was calculated as described in Section 4.5 assuming a 95% confidence level. Note that this table corresponds to Table 5.13.

Constants	# 12	# 13	# 19	# 21	# 28	# 43
$m(\infty)$ (g)	8.2	8.0	1.5	6.3	4.2	2.1
$CI_{m(\infty)}$	[5.5 11.4]	[5.5 10.6]	[0.8 2.4]	[4.4 8.1]	[2.8 5.6]	[1.5 3.0]

We also simulated data using the nonparametric bootstrapping techniques discussed in Section 4.2. Nonparametric bootstrapping is used to investigate data without assuming the data follows a specific distribution. Therefore, we had to use a new activity equation that does not assume a distribution as described in Section 4.2. The full results from the nonparametric bootstrapping can be found in Section 5.3. Again, we first estimated the activity and mass parameters using non-linear regression with the measured activity and mass data. The residuals obtained from the regression of the measured activity and mass data were used to simulate additional activity and mass data. We investigated these residuals with box and whisker plots, histograms, and normal probability plots. We could not conclude which distribution these residuals follow but we could conclude that the assumption that the residuals for all subjects follow the same distribution is a reasonable assumption from the box and whisker plot.

As described in Section 4.5, we compared the parameters and SE values estimated from the simulated data to the parameters and SE values estimated from the measured data. We can conclude that the parameters and SE values match well between the two methods of estimating the parameters. This implies that while investigating the uncertainty in the estimate of $m(\infty)$, the simulated activity and mass data may not be required because the regression of the measured data provides reasonable parameter estimates. The parameters

estimated from the simulated data were used in histograms and normal probability plots to investigate their distributions as described in Section 4.5. However, conclusions could not be made from these plots.

The absorbed dose, D_T, α, and $m(\infty)$ were calculated using the parameters estimated from the data simulated using the residuals. Similar to the parametric bootstrap method, we used the 3 estimates of $\breve{k}$ to calculate D_T. The statistical properties of D_T and $m(\infty)$ were also studied with the use of histograms. However, a conclusion of what distribution these parameters follow could not be made from these plots alone. The parameter estimates of D_T and $m(\infty)$ were not substantially different when calculated using either estimate of $\breve{k}$. Therefore, here we will present only the $m(\infty)$ values calculated using D_T which was calculated using $\breve{k}_{pred}$. The uncertainty in $m(\infty)$ will be presented in terms of the confidence interval of $m(\infty)$, $CI_{m(\infty)}$, as described in Section 4.5. Table 5.2 contains $m(\infty)$ values and its confidence interval corresponding to a 95% confidence level. The values in Table 5.2 match very closely with the values from Table 5.1.

Table 5.2. $m(\infty)$ was calculated from parameters estimated from data simulated using the residuals from the original regression. The confidence interval of $m(\infty)$, $CI_{m(\infty)}$ was calculated as described in Section 4.5 assuming a 95% confidence level. Note that this table corresponds to Table 5.17.

Constants	# 12	# 13	# 19	# 21	# 28	# 43
$m(\infty)$ (g)	8.3	7.6	1.9	7.7	4.3	1.8
$CI_{m(\infty)}$	[5.5 11.6]	[4.8 10.7]	[1.1 3.1]	[5.5 10.0]	[2.8 6.0]	[1.1 2.5]

5.2 Parametric Bootstrap Simulation Results

The results presented in this section are from the parametric bootstrap simulations. Section 5.2.1 will present the simulation results when the uniform distribution of the error

was assumed. This section will present both activity and mass parameters estimated from the original regression of the measured data and from the simulated data. The parameters obtained from the simulated data were used to calculate and investigate the error of $m(\infty)$. The results of these calculations are presented in Section 5.4.

5.2.1   Uniform Distribution Simulation Results

To simulate the activity and mass data using the parametric bootstrap method, a distribution needs to be assumed. In this section, the distribution was assumed Unif($-\zeta,\zeta$) as described in Section 4.1.1. The activity parameters estimated from the measured data and from the simulated data will be presented. Analysis of both methods will be presented along with a comparison of both methods. The same will be repeated for the mass parameters.

5.2.1.1   Activity Results For The Uniform Distribution

The original activity parameters were estimated using non-linear regression with the normalized measured activity data. The procedure discussed in Section 4.1 was still followed only a normalized version of (4.3),

$$\ln\left(\tilde{\breve{A}}(t_i)\right) = -0.00167 + \ln\left(\breve{Y}\right) + \ln\left(e^{-bt_i} - e^{-ct_i}\right) + \eta_{Ai}, \tag{5.3}$$

was used for the regression of the normalized measured activity data. μ_A was replaced by its expected value in (5.3) for the regression. Table 5.3 reports the original activity parameters and their respective standard errors (SE) found using non-linear regression of (5.3) with normalized measured activity data. Note that subject 30 does not have sufficient activity data for non-linear regression of (5.3) and was omitted from the simulations.

Table 5.3. The original activity parameters and their SE estimated using non-linear regression of (5.3) with normalized measured activity data. A uniform error distribution was assumed for the non-linear regression of (5.3).

Constants	# 12	# 13	# 19	# 21	# 28	# 43
$\ln\left(\check{Y}\right)$	0.017	-0.192	0.286	-0.169	-0.686	-0.737
$SE_{\check{Y}}$	0.047	0.106	0.049	0.028	0.039	0.041
$b\ (hr^{-1})$	0.0071	0.0060	0.0052	0.0075	0.0057	0.0049
SE_b	0.0002	0.0004	0.0001	0.0001	0.0002	0.0002
$c\ (hr^{-1})$	0.410	0.104	0.037	0.744	0.195	0.272
SE_c	0.057	0.024	0.003	0.235	0.016	0.028
$\sigma^2_{\eta_A}$	0.064	0.004	0.089	0.001	0.009	0.004

As a result of the uniform error distribution being assumed while estimating the activity parameters, μ_A and $\sigma^2_{\eta_A}$ could not be compared to their expected values in order to gain insight of the distribution of ϵ_{Ai} as described in Section 4.5.1. However, a histogram and normal probability plot of ϵ_{Ai} was used instead which was also described in Section 4.5.1. Figure 5.1 contains a histogram and a normal probability plot of ϵ_{Ai} for all subjects. The purpose of these plots was to determine if ϵ_{Ai} follows either the Unif(-ζ,ζ) or N(0,$\frac{\zeta^2}{9}$) distributions ($\zeta = 0.10$). By inspection, the histogram suggests normality as compared with uniformity. The normal probability plot does not provide much more information. Although the middle of the data appears to follow a linear trend, the tails of the data depart from linearity. However, the departure from linearity in the tails, in not uncommon for small sample sizes. This suggests that $N\left(0, \frac{\zeta^2}{9}\right)$ might be reasonable for the errors and could be used in the simulations.
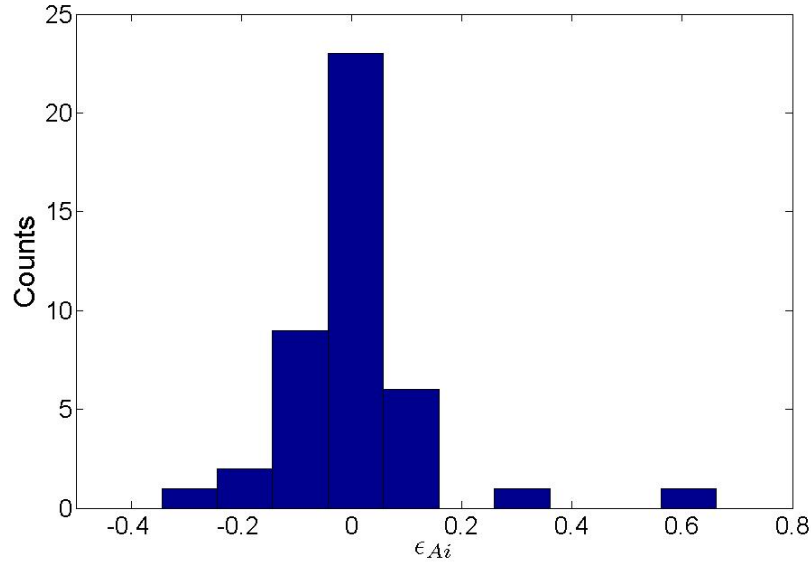
(a) Histogram of ϵ_{Ai} for all subjects.
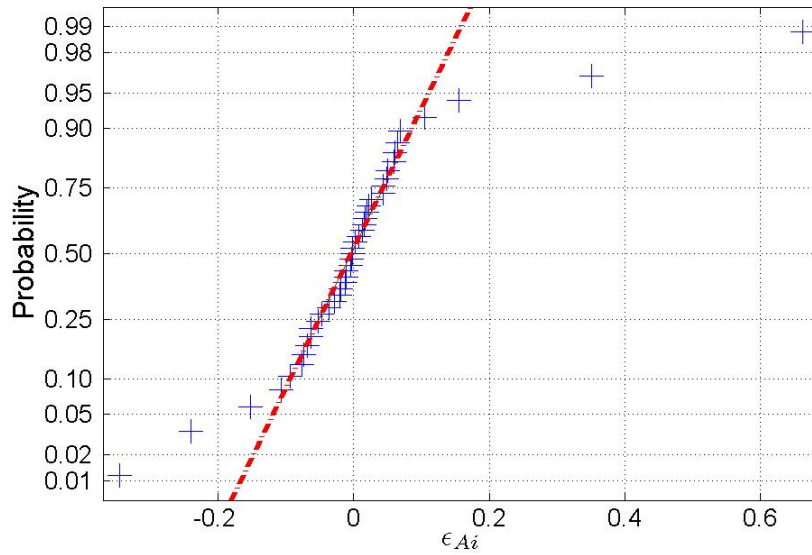
(b) Normal probability plot of ϵ_{Ai} for all subjects.

Figure 5.1. Histogram and normal probability plot of ϵ_{Ai} for all subjects assuming a uniform error distribution. The crosses represent the ϵ_{Ai} data points and the dotted line is used to help evaluate the linearity of the data.

57

The activity parameters were also estimated from the simulated activity data sets following the method described in Section 4.1.3. Section 4.5 describes how an average estimate and standard deviation of each activity parameter can be obtained from the $N = 500$ sets of simulated activity parameters. Similar to the measured data, the simulated data was also normalized by A_d, and therefore (5.3) was used again to estimate the activity parameters. Table 5.4 contains the estimated activity parameters and their standard deviations (SD).

The activity parameters estimated from the simulated data were used to check the accuracy of the parameters estimated from the measured activity data as described in Section 4.5. The estimated activity parameter values in Table 5.4 were compared to their respective estimated values from Table 5.3. By inspection, all parameter estimates and standard error values match reasonably well between the two tables. For example, $\ln\left(\check{Y}\right) = 0.019$, -0.192, and 0.290 for subjects 12, 13, and 19 respectively. These values were estimated from the simulated data. For the same subjects, $\ln\left(\check{Y}\right) = 0.017$, -0.192, and 0.286 estimated from the measured data. The values are identical for subject 13 and within 10% for subjects 12 and 19. The parameter estimates from the simulated data support the parameter estimates from the measured data which suggests that the parameter estimates from the measured data may be sufficient to investigate the uncertainty in $m(\infty)$.

Table 5.4. Activity parameters from (5.3) and their standard deviations estimated from the simulations which assumed a uniform distribution.

Constants	# 12	# 13	# 19	# 21	# 28	# 43
$\ln\left(\check{Y}\right)$	0.019	-0.192	0.290	-0.168	-0.687	-0.739
$SD_{\check{Y}}$	0.043	0.060	0.050	0.034	0.033	0.032
$b\ (hr^{-1})$	0.0071	0.0060	0.0052	0.0075	0.0057	0.0049
SD_b	0.0002	0.0002	0.0001	0.0001	0.0001	0.0001
$c\ (hr^{-1})$	0.417	0.105	0.037	0.765	0.167	0.272
SD_c	0.067	0.012	0.002	0.120	0.015	0.021
$\sigma_{\eta_A}^2$	0.0036	0.0111	0.0036	0.0024	0.0042	0.0052

The activity parameters estimated from the simulated data can also be used to study their distribution as described in Section 4.5. Figures 5.2(a)-5.2(c) are histograms for the estimated activity parameters for subject 21. We have assumed that the error distribution is the same for all subjects and therefore the results from subject 21 are representative of all the subjects. As a result, only subject 21 will be used to provide examples for all of the simulations. Figures 5.2(a) and 5.2(b) are histograms of $\ln\left(\check{Y}\right)$ and b respectively. By inspection, the figures appear to possibly follow a normal distribution. However, Figure 5.2(c) is a histogram of c and by inspection does not appear to follow a normal distribution. Figures 5.3(a)-5.3(c) are normal probability plots for each of the estimated activity parameters. Figures 5.3(a) and 5.3(b) are normal probability plots of $\ln\left(\check{Y}\right)$ and b respectively. These figures provide more evidence that $\ln\left(\check{Y}\right)$ and b may follow a normal distribution. All of the data in Figure 5.3(a) appears to follow a linear trend, however, only the middle of the data in Figure 5.3(b) follows a linear trend. Figure 5.3(c) is a normal probability plot of c and
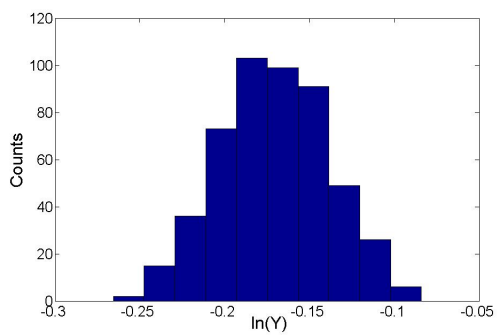
(a) Histogram of $\ln\left(\check{Y}\right)$ for subject 21.
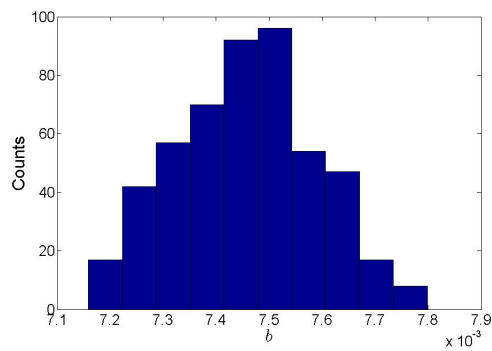
(b) Histogram of b for subject 21.
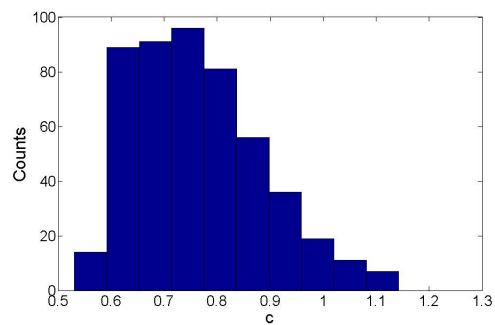
(c) Histogram of c for subject 21.

Figure 5.2. Histograms of the activity parameters from (5.3) assuming a uniform error distribution for subject 21.

does not provide definitive evidence that c does or does not follow a normal distribution. However, a conclusion of which statistical distribution the activity parameters follow could not be made from these plots alone.
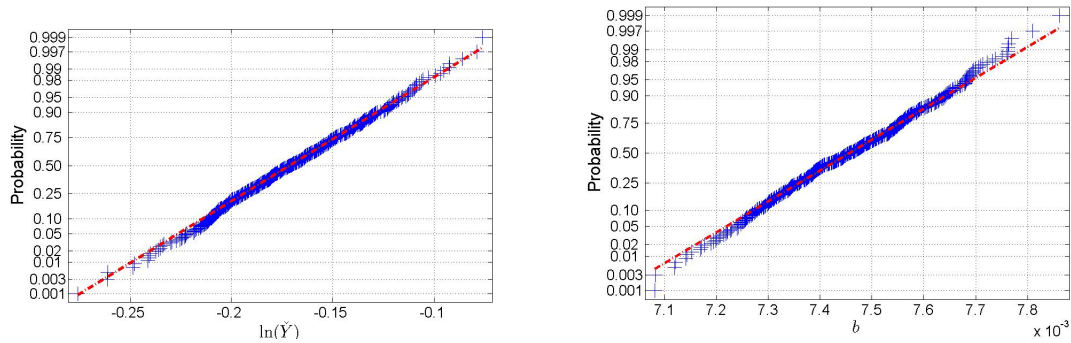
(a) Normal probability plot of $\ln\left(\check{Y}\right)$ for subject 21.

(b) Normal probability plot of b for subject 21.
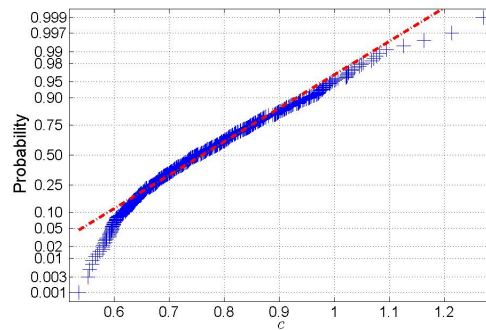
(c) Normal probability plot of c for subject 21.

Figure 5.3. Normal probability plots of the activity parameters from (5.3) assuming a uniform error distribution for subject 21. The crosses represent the data points and the dotted line is used to help evaluate the linearity of the data.

5.2.1.2 Mass Results For The Uniform Distribution

The original mass parameters were estimated using the method described in Section 4.1. Equation (4.5) was re-written to incorporate the normalized activity parameters which yielded

$$\ln\left(\tilde{m}(t_i)\right) = \mu_m + \ln\left(\left(2\left(\frac{\hat{\check{Y}}\check{k}}{\hat{b}}e^{-\hat{b}t_i} + \frac{\hat{\check{Y}}\check{k}}{\hat{c}} - \frac{\hat{\check{Y}}\check{k}}{\hat{c}}e^{-\hat{c}t_i} - \frac{\hat{\check{Y}}\check{k}}{\hat{b}} + \frac{m(0)^2}{2}\right)\right)^{\frac{1}{2}}\right) + \eta_{mi}. \quad (5.4)$$

Equation (5.4) was used for the initial regression of the measured mass data. Table 5.5 reports the mass parameters and their respective standard errors found using non-linear regression of (5.4) with measured mass data. Note that the symbol "-" was used in the table when a parameter could not be estimated because of a lack of mass data. Specifically, data for subjects 12 and 13 consists of two measured points. This leads to a problem of estimating the standard errors of the mass parameters because the degrees of freedom becomes zero as a result of the regression estimating two parameters.

Table 5.5. Mass parameters from (5.4) and their standard errors estimated using non-linear regression with measured mass data. Note that the symbol "-" was used in the table when a parameter could not be estimated because of a lack of mass data.

Constants	# 12	# 13	# 19	# 21	# 28	# 43
$\check{k}_{fit}\ \left(\frac{g^2}{hr}\right)$	1.94	2.49	0.48	1.18	0.69	0.04
$SE_{\check{k}_{fit}}$	-	-	0.04	0.07	0.09	0.06
μ_m	0.039	0.040	0.018	0.165	0.077	-0.015
SE_{μ_m}	-	-	0.028	0.087	0.036	0.054
$\sigma^2_{\eta_m}$	-	-	0.0016	0.0164	0.0022	0.0043

The estimated μ_m and $\sigma^2_{\eta_m}$ values were compared to their expected values calculated assuming either a uniform or a normal distribution of ϵ_{mi} as described in Section 4.5.1. The estimated μ_m values from the regression are positive for all subjects with the exception of subject 43. The estimated μ_m values could not support either a Unif(-ζ, ζ) or N(0,$\frac{\zeta^2}{9}$) distribution of ϵ_{mi} ($\zeta = 0.15$) because both expected μ_m values are negative. $\mu_{mU} = $ -0.00378 and $\mu_{mN} = $ -0.00125. This can be explained by the fact that the error model is

correct, however there is an upward bias or that the error model is wrong. The estimated $\sigma_{\eta_m}^2$ values did not support either distribution. The expected $\sigma_{\eta_m}^2$ values are 0.0076 and 0.0025 for the uniform and normal distribution respectively. While on the same order of magnitude, definite support for either distribution could not be concluded.

As with the activity parameters, a histogram and normal probability plot of ϵ_{mi} was used to investigate the error distribution as described in Section 4.5.1. Figure 5.4 contains a histogram and normal probability plot of ϵ_{mi}. By inspection, the histogram of ϵ_{mi} neither supports the Unif($-\zeta, \zeta$) nor the N($0, \frac{\zeta^2}{9}$) distribution. The normal probability plot of ϵ_{mi} does not provide evidence that the sample does or does not follow a normal distribution. A section of the data appears to follow a linear trend, however, the tails depart from linearity.

The mass parameters were also estimated from the simulated mass data sets following the method described in Section 4.1.4. Section 4.5 describes how an average estimate and standard deviation of each mass parameter can be obtained from the $N = 500$ sets of simulated mass parameters. However, similar to the estimation of the mass parameters from the measured data, (5.4) was used to incorporate the normalized activity parameters and estimate the mass parameter from the simulated data. Table 5.6 contains the estimated mass parameters and their standard deviations (SD).

The mass parameters estimated from the simulated data were also compared to the mass parameters estimated from the measured mass data as described in Section 4.5. The estimated mass parameters in Table 5.6 were compared to their respective estimated values from Table 5.5. The mass parameter $\breve{k}_{fit}$ matched reasonable well between the two tables. For example, $\breve{k}_{fit} = 0.49 \frac{\mathrm{g}2}{\mathrm{hr}}$ and $1.18 \frac{\mathrm{g}2}{\mathrm{hr}}$ for subjects 19 and 21 respectively. These values were obtained from the simulated data. For the same subjects, $\breve{k}_{fit} = 0.48 \frac{\mathrm{g}2}{\mathrm{hr}}$ and 1.18 $\frac{\mathrm{g}2}{\mathrm{hr}}$ estimated from the measured data. The values match exactly for subject 21 and only differ by 2% for subject 19. However, the standard deviations of $\breve{k}_{fit}$ are on an order of magnitude larger than the standard errors of $\breve{k}_{fit}$. For example, $SE_{\breve{k}_{fit}} = 0.04 \frac{\mathrm{g}2}{\mathrm{hr}}$ and 0.07

63
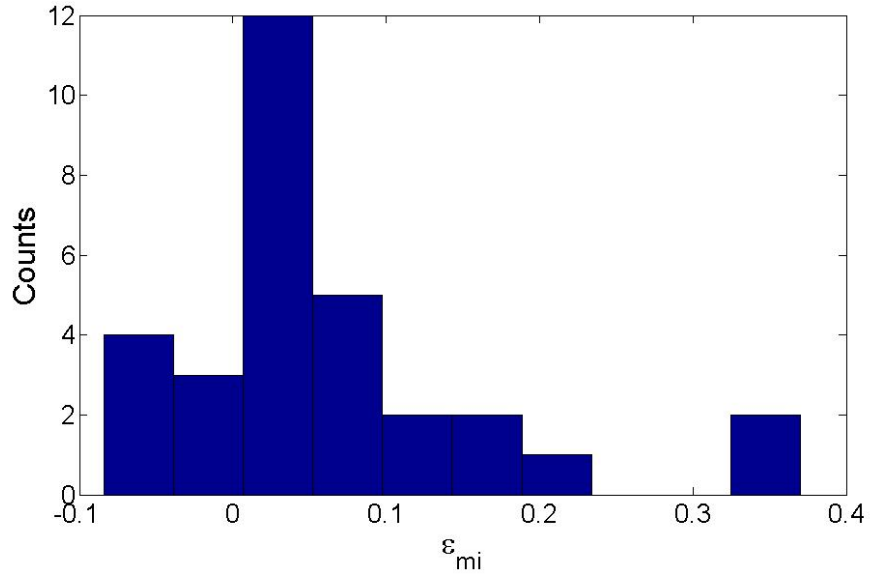
(a) Histogram of ϵ_{mi} for all subjects.
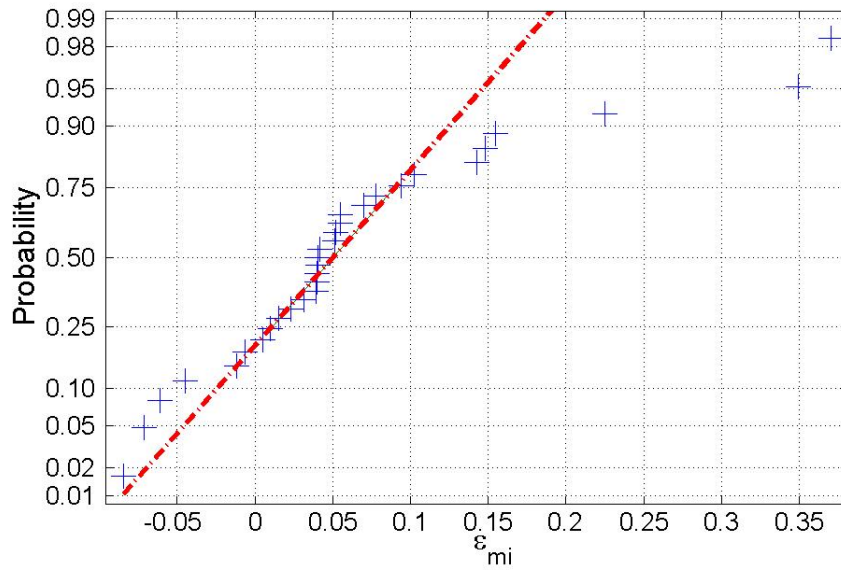
(b) Normal probability plot of ϵ_{mi} for all subjects.

Figure 5.4. Histogram and normal probability plot of ϵ_{mi} for all subjects. The crosses represent the ϵ_{mi} data points and the dotted line is used to help evaluate the linearity of the data.

64

$\frac{\text{g}^2}{\text{hr}}$ for subjects 19 and 21, while $SD_{\breve{k}_{fit}} = 0.16 \ \frac{\text{g}^2}{\text{hr}}$ and 0.24 $\frac{\text{g}^2}{\text{hr}}$ for the same subjects. The estimated μ_m values from the simulated data were all negative, μ_m = -0.0029 and -0.00003 for subjects 19 and 21, while the μ_m values estimated from the measured data were all positive, $\mu_m = 0.018$ and 0.165 for subjects 19 and 21, with the exception of subject 43, μ_m = -0.015. However, the standard errors of μ_m, $SE_{\mu_m} = 0.028$ for subject 19, and standard deviations of μ_m, $SE_{\mu_m} = 0.064$ for subject 19, match well. Also, the estimated $\sigma^2_{\eta_m}$ values match well between the two tables. The fact that all of the parameters do not match well between the two tables suggests that the simulated data are required for estimating the mass parameters while assuming a uniform distribution of ϵ_{mi}.

Table 5.6. Mass parameters from (5.4) and their standard deviations estimated from the simulations which assumed a uniform distribution.

Constants	# 12	# 13	# 19	# 21	# 28	# 43
$\breve{k}_{fit}$ $(\frac{g^2}{hr})$	1.94	2.52	0.49	1.18	0.69	0.048
$SD_{\breve{k}_{fit}}$	0.77	0.51	0.16	0.24	0.26	0.08
μ_m	-0.0014	-0.0002	-0.0029	-0.00003	-0.0053	-0.0006
SD_{μ_m}	0.0107	0.0022	0.0635	0.0673	0.0626	0.0549
$\sigma^2_{\eta_m}$	-	-	0.0075	0.0079	0.0076	0.0074

Figures 5.5(a) and 5.5(b) are histograms of $\breve{k}_{fit}$ and μ_m, respectively. Not much can be concluded from these plots by inspection. Another approach to gain insight into the distributions of these parameters is to investigate the normal probability plots in Figures 5.6(a) and 5.6(b). Figures 5.6(a) and 5.6(b) are normal probability plots of $\breve{k}_{fit}$ and μ_m respectively. In both plots, the tails of the data deviate from linearity, which does not imply whether these parameters follow a normal distribution or not.

65
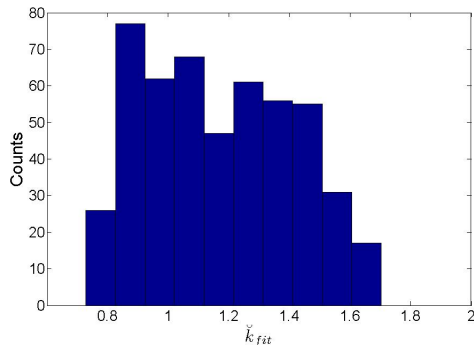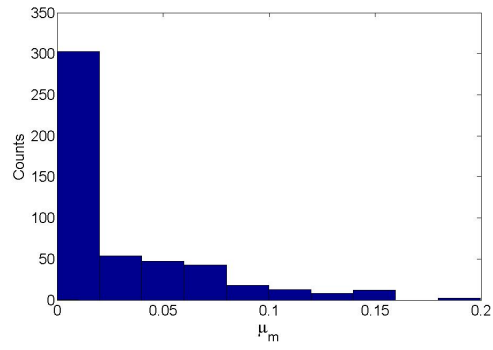
(a) Histogram of $\breve{k}_{fit}$ for subject 21.   (b) Histogram of μ_m for subject 21.

Figure 5.5. Histograms of the mass parameters from (5.4) assuming a uniform error distribution for subject 21.
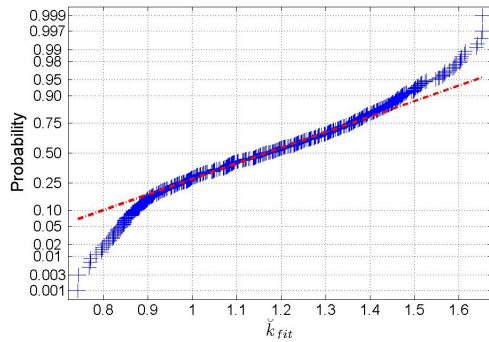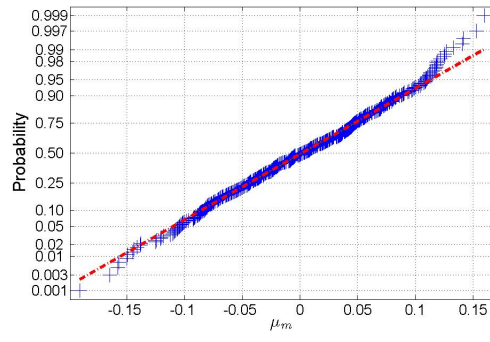
(a) Normal probability plot of $\breve{k}_{fit}$ for subject 21. (b) Normal probability plot of μ_m for subject 21.

Figure 5.6. Normal probability plots of the mass parameters from (5.4) assuming a uniform error distribution for subject 21. The crosses represent the data points and the dotted line is used to help evaluate the linearity of the data.

5.3 Nonparametric Bootstrap Simulation Results

The results presented in this section are from the nonparametric simulations. The simulations can be performed by using the residuals from the non-linear regression of the measured activity and mass data as the error terms. Section 5.3.1 will present how the activity residuals are obtained and used to simulate the activity data. Section 5.3.2 will present how the mass residuals are obtained and used to simulate the mass data. The parameters estimated from the simulated data were used to calculate and investigate the error of $m(\infty)$. The results of these calculations are presented in Section 5.4.

5.3.1 Results From Simulating The Activity Kinetics Using Residuals

The original activity parameters were estimated using non-linear regression with the normalized measured activity data. The procedure discussed in Section 4.2.1 was still followed only a normalized version of (4.6),

$$\ln\left(\tilde{\check{A}}(t_i)\right) = \check{z} + \ln\left(e^{-bt_i} - e^{-ct_i}\right) + \eta_{Ai}, \tag{5.5}$$

was used to estimate the activity parameters. $\check{z} = \mu_A + \ln\left(\check{Y}\right)$. Table 5.7 reports the original activity parameters and their respective standard errors (SE) found using non-linear regression of (5.5) with the normalized measured activity data.

The residuals from the regression will be used to simulate the activity data as described in Section 4.2.1. The residuals were investigated using the usual histogram and normal probability plot as well as a box and whisker plot as described in Section 4.5.1. Figures 5.7(a)-5.7(c) are of a histogram, a normal probability plot, and a box and whisker plot, respectively, of the activity residuals r_{Ai} for all subjects. By inspection, the histogram appears to possibly follow a normal distribution. The tails of the data depart from linearity on the normal probability plot, which does not imply whether r_{Ai} follows a normal distribution or

67

Table 5.7. The original activity parameters from (5.5) and their SE estimated using non-linear regression with the normalized measured activity data.

Constants	# 12	# 13	# 19	# 21	# 28	# 43
$\check{z}$	0.015	-0.195	0.284	-0.171	-0.687	-0.739
$SE_{\check{z}}$	0.199	0.065	0.248	0.015	0.057	0.035
$\check{Y}$	1.024	0.830	1.341	0.850	0.508	0.482
$SE_{\check{Y}}$	-	-	-	-	-	-
$b\ (hr^{-1})$	0.0070	0.0060	0.0052	0.0075	0.0057	0.0049
SE_b	0.0008	0.0002	0.0006	0.0001	0.0002	0.0001
$c\ (hr^{-1})$	0.411	0.104	0.037	0.745	0.165	0.272
SE_c	0.271	0.013	0.012	0.050	0.024	0.022
$\sigma_{\eta_A}^2$	0.0641	0.0039	0.0894	0.0007	0.0092	0.0038

not. By inspection, the box and whisker plot provides evidence that all subjects possibly share the same statistical distribution. The median and quartile values for each subject are within reason of each other implying that their respective distributions share the same characteristics.

(a) Histogram of r_{Ai} for the activity data.

(b) Normal probability plot of r_{Ai} for the activity data.

(c) Box and whisker plot of r_{Ai} for the activity data.

Figure 5.7. Analysis of the activity residuals consisted of a box and whisker plot, a normal probability plot and a histogram.

The activity parameters were also estimated from the simulated activity data sets following the method described in Section 4.2.1. Section 4.5 describes how an average estimate and standard deviation of each activity parameter can be obtained from the $N = 500$ sets of simulated activity parameters. However, similar to estimating the activity parameters from the measured data (5.5) was use to estimate the activity parameters from the simulated data.

69

Note that we had to put bounds on the activity parameters while performing non-linear regression on (5.5). This was due to the residuals. One of the residuals was relatively large (r_{Ai}=0.5) and when it was added to a subjects initial activity data point it would make this point the largest for that subject. If the initial data point is the largest value, then the data would resemble a straight line making the estimation of the activity parameters impossible. We used the following bounds: $-3 \leq z \leq 1$, $0 \leq b \leq 0.01$, and $0 \leq c \leq 2$. Table 5.8 contains the estimated activity parameters and their standard deviations (SD).

The activity parameters estimated from the simulated data were used to check the accuracy of the results from the original regression of the measured activity data. The estimated activity parameter values in Table 5.8 were compared to their respective estimated values from Table 5.7. All parameter estimates and standard error values match reasonable well between the two tables. For example, $\check{Y} = 0.920$ and 0.842 for subjects 12 and 13 estimated from the simulated data. For the same subjects, $\check{Y} = 1.024$ and 0.830 estimated from the measured data.

Figures 5.8(a) - 5.8(c) are histograms of $\check{z}$, b and c respectively. By inspection, the Figures 5.8(a) and 5.8(c) do not appear to follow a normal distribution however Figure 5.8(b) does appear to possibly follow a normal distribution.

Table 5.8. Activity parameters from (5.5) and their standard deviations estimated from the simulations performed using the residuals.

Constants	# 12	# 13	# 19	# 21	# 28	# 43
$\check{z}$	-0.097	-0.192	-0.194	-0.169	-0.691	-0.735
$SE_{\check{z}}$	0.098	0.140	0.091	0.072	0.080	0.077
$\check{Y}$	0.920	0.842	0.835	0.854	0.507	0.485
$SE_{\check{Y}}$	0.092	0.127	0.078	0.062	0.042	0.038
b (hr^{-1})	0.0067	0.0060	0.0042	0.0075	0.0057	0.0049
SE_b	0.0004	0.0005	0.0002	0.0003	0.0003	0.0003
c (hr^{-1})	0.681	0.111	0.060	0.803	0.171	0.272
SE_c	0.468	0.043	0.011	0.305	0.041	0.048
$\sigma^2_{\eta_A}$	0.0188	0.0157	0.0172	0.0188	0.0168	0.0178

71
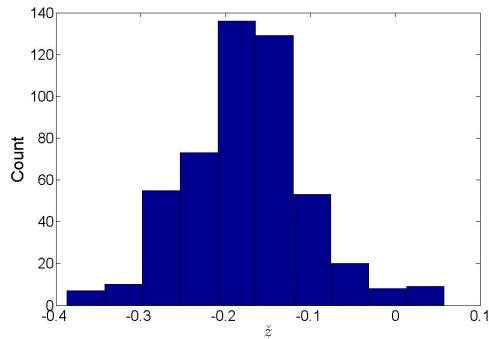
(a) Histogram of $\check{z}$ for subject 21.
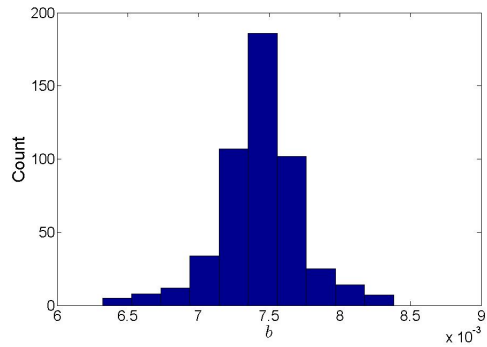
(b) Histogram of b for subject 21.
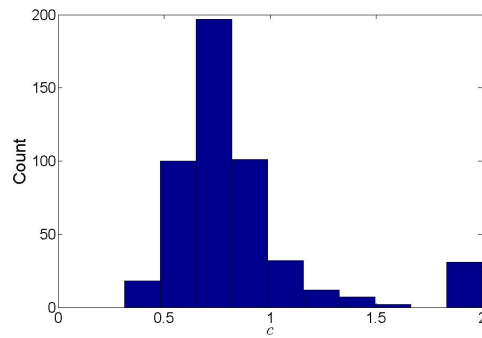
(c) Histogram of c for subject 21.

Figure 5.8. Histograms of the activity parameters from (5.5) for subject 21.

Figures 5.9(a) - 5.9(c) are normal probability plots of $\check{z}$, b, and c respectively. The figures do not provide evidence that the activity parameters do or do not follow a normal distribution as a result of the tails of the data departing from linearity on each plot. A conclusion could not be made from these plots alone.
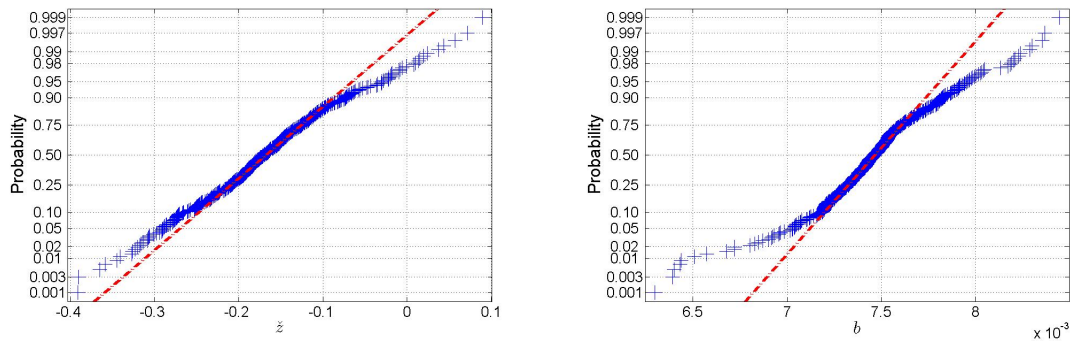
(a) Normal probability plot of $\check{z}$ for subject 21.   (b) Normal probability plot of b for subject 21.
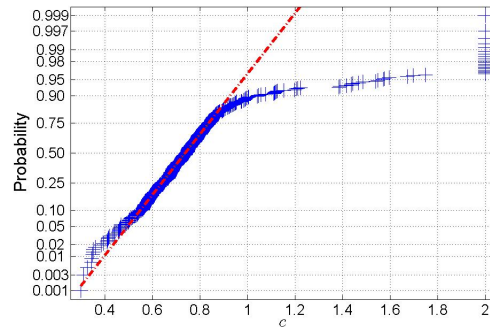
(c) Normal probability plot of c for subject 21.

Figure 5.9. Normal probability plots of the activity parameters from (5.5) for subject 21. The crosses represent the data points and the dotted line is used to help evaluate the linearity of the data.

5.3.2   Results From Simulating The Mass Dynamics Using Residuals

The original mass parameters were estimated using the method described in Section 4.2.2. Equation (5.4) was used to incorporate the normalized activity parameters and estimate the mass parameters from the measured mass data. Table 5.9 reports the mass parameters and their respective standard errors found using non-linear regression of (5.4) with measured mass data.

The estimated μ_m and $\sigma^2_{\eta_m}$ values were compared to their expected values calculated assuming either a uniform or a normal distribution of ϵ_{mi} as described in Section 4.5.1. The estimated μ_m values from the regression are positive for all subjects with the exception of sub-

Table 5.9. The original mass parameters from (5.4) and their SE estimated using non-linear regression with measured mass data.

Constants	# 12	# 13	# 19	# 21	# 28	# 43
$\breve{k}_{fit}$ $(\frac{g^2}{hr})$	1.93	2.48	0.48	1.17	0.69	0.04
$SE_{\breve{k}_{fit}}$	-	-	0.04	0.07	0.09	0.06
μ_m	0.039	0.040	0.018	0.165	0.077	-0.015
SE_{μ_m}	-	-	0.028	0.087	0.036	0.054
$\sigma^2_{\eta_m}$	-	-	0.0016	0.0164	0.0022	0.0043

ject 43. The estimated μ_m values could not support either a U($-\zeta, \zeta$) or N($0, \frac{\zeta^2}{9}$) distribution of ϵ_{mi} ($\zeta = 0.15$) because both expected μ_m values (μ_{mU}=-0.00378 and μ_{mN}=-0.00125) are negative. The estimated $\sigma^2_{\eta_m}$ values did not support either distribution. The expected $\sigma^2_{\eta_m}$ values are 0.0076 and 0.0025 for the uniform and normal distribution respectively. While on the same order of magnitude, definite support for either distribution could not be concluded.

Similar to the activity residuals, the mass residuals were investigated with the use of a histogram, normal probability plot, and a box and whisker plot as described in Section 4.5.1. Figures 5.10(a)-5.10(c) are a histogram, a normal probability plot, and a box and whisker plot, respectively, of the mass residuals r_{mi} for all subjects. By inspection, a conclusion about the distribution of the histogram cannot be made. The tails of the data depart from linearity on the normal probability plot, which does not imply whether r_{mi} follows a normal distribution or not. By inspection, the box and whisker plot provides evidence that all subjects possibly share the same statistical distribution. The median and quartile values for each subject are within reason of each other implying that their respective distributions share the same characteristics.
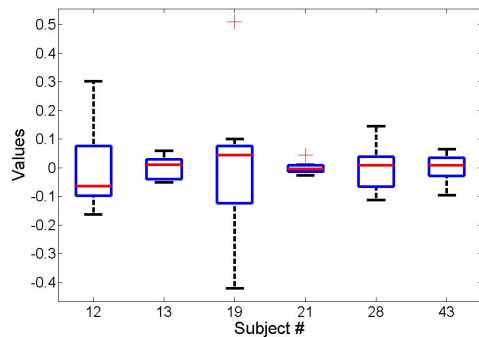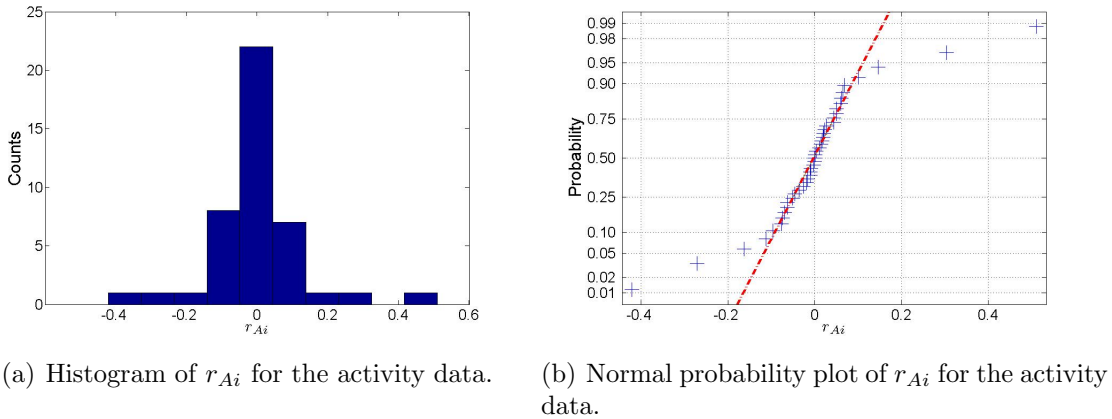
74
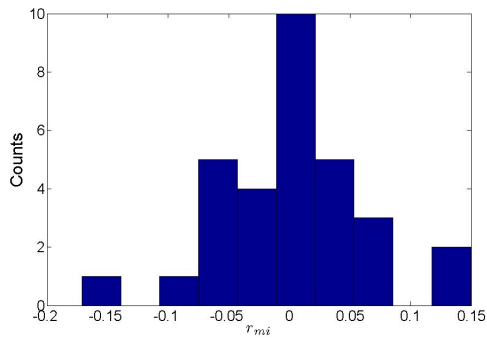
(a) Histogram of r_{mi} for the mass data.
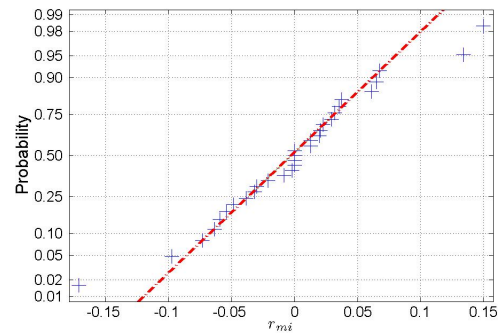
(b) Normal probability plot of r_{mi} for the mass data.
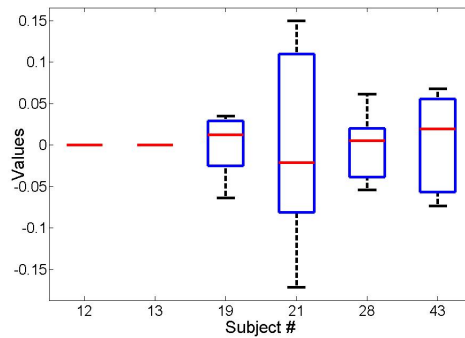
(c) Box and whisker plot of r_{mi} for the mass data.

Figure 5.10. Analysis of the mass residuals consisted of a box and whisker plot, a normal probability plot and a histogram.

The mass parameters were also estimated from the simulated mass data sets following the method described in Section 4.2.2. Section 4.5 describes how an average estimate and standard deviation of each mass parameter can be obtained from the $N = 500$ sets of simulated mass parameters. However, similar to the estimation of the measured mass parameters, (5.4) was used to incorporate the normalized activity parameters and estimate the mass parameters using the simulated data. Table 5.10 contains the estimated mass parameters and their standard deviations (SD).

The mass parameters estimated from the simulated data were also compared to the mass parameters estimated from the measured data. The estimated mass parameters in Table 5.10 were compared to their respective estimated values from Table 5.9. All parameters except μ_m match reasonable well between the two tables. For example, $\breve{k}_{fit} = 2.16 \; \frac{\text{g2}}{\text{hr}}$ and $2.60 \; \frac{\text{g2}}{\text{hr}}$ for subjects 19 and 21 respectively. These values were obtained from the simulated data. For the same subjects, $\breve{k}_{fit} = 1.93 \; \frac{\text{g2}}{\text{hr}}$ and $2.48 \; \frac{\text{g2}}{\text{hr}}$ estimated from the measured data. With the exception of subjects 28 and 43, all of the estimated μ_m values from the simulated data were negative while the μ_m values estimated from the measured data were all positive with the exception of subject 43. These results suggest that the simulated mass data are required for estimating the mass parameters.

Figures 5.11(a) and 5.11(b) are histograms of $\breve{k}_{fit}$ and μ_m, respectively. The histograms appear to follow a normal distribution. Another approach to gain insight into the distributions of these parameters is to investigate the normal probability plots in Figures 5.12(a) and 5.12(b). Figures 5.12(a) and 5.12(b) are normal probability plots of $\breve{k}_{fit}$ and μ_m, respectively, and do not provide evidence that the mass parameters do or do not belong to a normal distribution because the tails of the data depart from linearity on each plot. A conclusion could not be made from these plots alone.

Table 5.10. Mass parameters from (5.4) and their standard deviations estimated from the simulations performed using the residuals.

| Constants	# 12	# 13	# 19	# 21	# 28	# 43
$\breve{k}_{fit}$ $(\frac{g^2}{hr})$	2.16	2.60	0.59	1.59	0.78	0.06
$SE_{\breve{k}_{fit}}$	0.64	0.42	0.15	0.22	0.23	0.06
μ_m	-0.0006	-0.0003	-0.0004	-0.0055	0.0009	0.0001
SE_{μ_m}	0.0076	0.0036	0.0439	0.0747	0.0460	0.0448
$\sigma^2_{\eta_m}$	-	-	0.0038	0.0040	0.0042	0.0040
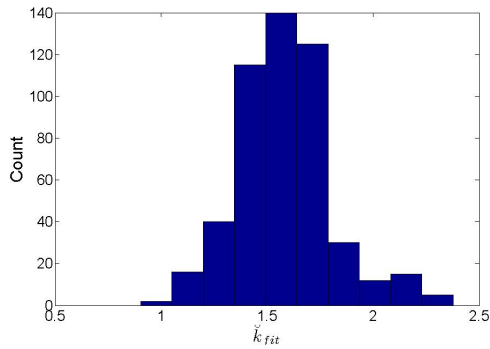
(a) Histogram of $\breve{k}_{fit}$ for subject 21.
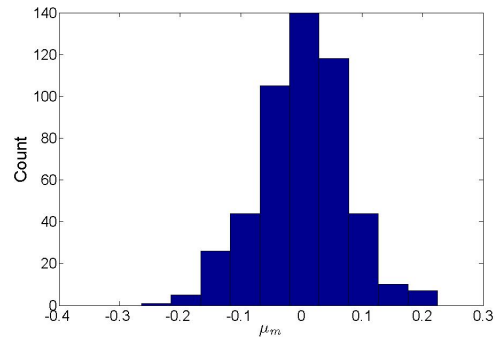
(b) Histogram of μ_m for subject 21.

Figure 5.11. Histogram of the mass parameters from (5.4) for subject 21.
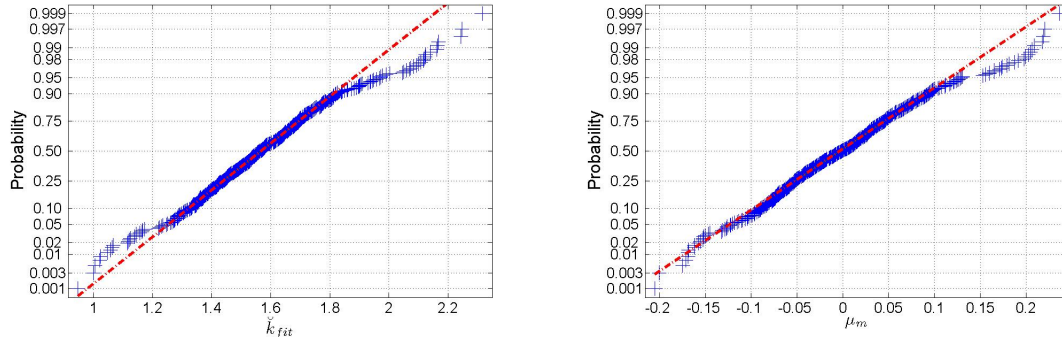
(a) Normal probability plot of $\breve{k}_{fit}$ for subject 21. (b) Normal probability plot of μ_m for subject 21.

Figure 5.12. Normal probability plots of the mass parameters from (5.4) for subject 21. The crosses represent the data points and the dotted line is used to help evaluate the linearity of the data.

5.4 $\mathrm{m}(\infty)$ Calculation Results

This section presents the results of the calculation of $m(\infty)$ as described in Section 4.3. Section 5.4.1 presents the calculation of $m(\infty)$ using parameters estimated from the uniformly distributed data. Finally, Section 5.4.2 presents the calculation of $m(\infty)$ using parameters estimated from the nonparametric bootstrap simulations. In each section, $m(\infty)$ will be calculated using 3 estimates of the mass parameter $\breve{k}$: 1) $\breve{k}$ found using non-linear regression of mass data, $\breve{k}_{fit}$, 2) $\breve{k}$ calculated using (3.16), $\breve{k}_{pred}$, and 3) $\breve{k}$ calculated using (2.8), $\breve{k}_{calc}$. The 3 estimates of $\breve{k}$ are used to investigate the error in our new protocol when using a predictive equation to calculate $\breve{k}$.

5.4.1 $\mathrm{m}(\infty)$ Calculated Using Parameters Estimated From Simulations Of The Uniform Distribution

Using the activity and mass parameters estimated from the data simulated assuming the Unif(-ζ,ζ) distribution, D_T was calculated as described in Section 4.3. Here, $\breve{k}_{fit}$ was used to calculate D_T. With an estimate of D_T, $\bar{\alpha}_{subject}$ was found as also described in Section 4.3. Table 5.11 contains $\bar{\alpha}_{subject}$ and its respective variance for each subject. Using these

78

values, a minimum variance estimate of α was calculated to be $\hat{\alpha}_{mv}$=0.0033 Gy^{-1}. Also, $V(\hat{\alpha}_{mv})$=3.35E-8 Gy^{-2}.

Table 5.11. For each subject an average α, $\bar{\alpha}_{subject}$ was calculated along with the variance in $\bar{\alpha}_{subject}$ as described in Section 4.3.

Constants	# 12	# 13	# 19	# 21	# 28	# 43
$\bar{\alpha}_{subject}$ (Gy^{-1})	0.0038	0.0037	0.0026	0.0035	0.0031	0.0041
$V(\bar{\alpha}_{subject})$ (Gy^{-2})	1.66E-7	2.10E-7	1.06E-7	3.53E-7	2.79E-7	3.15E-7

Using $\hat{\alpha}_{mv}$ for all subjects, $m(\infty)$ could be calculated as described in Section 4.3. To calculate $m(\infty)$, D_T and thus an estimate of $\breve{k}$ is required. Again, here we used $\breve{k}_{fit}$ to calculate D_T and $m(\infty)$. Table 5.12 contains estimates of $\breve{k}_{fit}$, D_T and $m(\infty)$. Each parameters standard error was also found from the simulated data. The confidence interval of $m(\infty)$, $CI_{m(\infty)}$, was calculated as described in Section 4.5 assuming a 95% confidence level.

The statistical distributions of D_T and $m(\infty)$ were investigated with the use of histograms as described in Section 4.5. Normal probability plots were not used because the distribution of D_T and $m(\infty)$ are not expected to be normal. Figure 5.13(a) is the histogram of D_T for subject 21 and Figure 5.13(b) is the histogram of $m(\infty)$ for subject 21. By inspection, a conclusion of the distribution of these parameters could not be made from the histograms. The histograms are only reported for D_T and $m(\infty)$ which were calculated using $\breve{k}_{fit}$. Histograms of D_T and $m(\infty)$ calculated using $\breve{k}_{pred}$ and $\breve{k}_{calc}$ were very similar.

Table 5.13 reports estimates of $\breve{k}_{pred}$, D_T, and $m(\infty)$ which were calculated from parameters estimated from data that was simulated assuming the uniform distribution. Table 5.14 reports estimates of $\breve{k}_{calc}$, D_T, and $m(\infty)$.

79

Table 5.12. $\breve{k}_{fit}$, D_T, and $m(\infty)$ were calculated from parameters estimated from data simulated assuming the uniform distribution. The standard deviation of the parameters were found as described in Section 4.5. The confidence interval of $m(\infty)$, $CI_{m(\infty)}$, was calculated as described in Section 4.5 assuming a 95% confidence level.

Constants	# 12	# 13	# 19	# 21	# 28	# 43
$\breve{k}_{fit}$ $(\frac{g^2}{hr})$	1.92	2.53	0.49	1.19	0.69	0.05
$SD_{\breve{k}_{fit}}$	0.76	0.51	0.15	0.23	0.26	0.08
D_T (Gy)	405	454	770	372	391	370
SD_{D_T}	27.4	34.1	58.6	29.0	29.0	26.6
$m(\infty)$ (g)	8.4	6.1	1.7	5.4	4.4	2.7
$SD_{m(\infty)}$	1.4	1.2	0.5	0.9	0.8	0.4
$CI_{m(\infty)}$	[6.1 11.0]	[4.3 8.0]	[1.0 2.6]	[3.8 7.0]	[3.2 5.8]	[1.9 3.4]
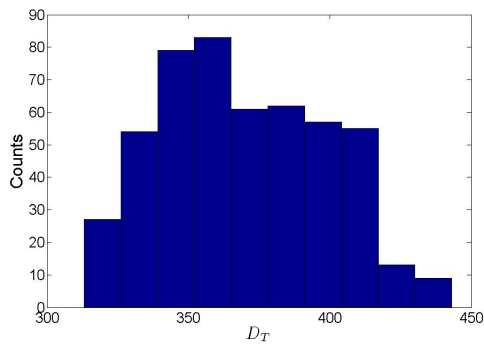
(a) Histogram of D_T for subject 21.
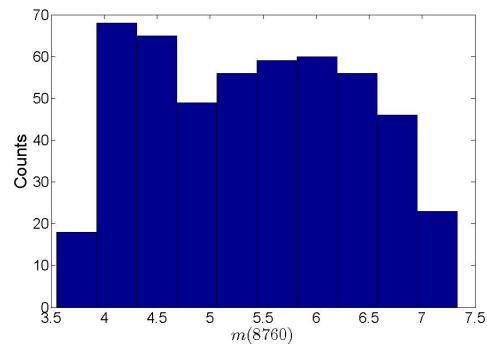
(b) Histogram of $m(\infty)$ for subject 21.

Figure 5.13. Histograms of the D_T and $m(\infty)$ for subject 21.

Table 5.13. $\breve{k}_{pred}$, D_T, and $m(\infty)$ were calculated from parameters estimated from data simulated assuming the uniform distribution. The standard deviation of the parameters were found as described in Section 4.5. The confidence interval of $m(\infty)$, $CI_{m(\infty)}$ was calculated as described in Section 4.5 assuming a 95% confidence level.

Constants	# 12	# 13	# 19	# 21	# 28	# 43
$\breve{k}_{pred}$ ($\frac{g^2}{hr}$)	2.15	1.69	0.60	0.87	0.90	0.24
$SD_{k_{pred}}$	0.37	0.31	0.12	0.15	0.16	0.04
D_T (Gy)	417	375	805	323	414	440
SD_{D_T}	37.0	35.7	72.0	28.2	37.3	37.6
$m(\infty)$ (g)	8.2	8.0	1.5	6.3	4.2	2.1
$SD_{m(\infty)}$	1.7	1.6	0.48	1.1	0.9	0.4
$CI_{m(\infty)}$	[5.5 11.4]	[5.5 10.6]	[0.8 2.4]	[4.4 8.1]	[2.8 5.6]	[1.5 3.0]

Table 5.14. $\breve{k}_{calc}$, D_T, and $m(\infty)$ were calculated from parameters estimated from data simulated assuming the uniform distribution. The standard deviation of the parameters were found as described in Section 4.5. The confidence interval of $m(\infty)$, $CI_{m(\infty)}$ was calculated as described in Section 4.5 assuming a 95% confidence level.

Constants	# 12	# 13	# 19	# 21	# 28	# 43
$\breve{k}_{calc}$ ($\frac{g^2}{hr}$)	1.65	1.69	0.79	0.62	0.91	0.28
$SD_{\breve{k}_{calc}}$	0.29	0.29	0.14	0.10	0.15	0.05
D_T (Gy)	395	374	918	302	411	458
SD_{D_T}	36.0	33.4	85.7	27.3	36.1	42.1
$m(\infty)$ (g)	8.8	7.8	1.1	6.8	4.2	2.0
$SD_{m(\infty)}$	1.7	1.5	0.4	1.2	0.8	0.4
$CI_{m(\infty)}$	[6.1 12.1]	[5.4 10.7]	[0.5 1.8]	[4.8 8.6]	[2.8 5.7]	[1.3 2.8]

81

The parameter estimates and their standard deviations are very similar between Tables 5.13, 5.14, and 5.12. For example, $m(\infty)$ =8.2, 8.0, and 1.5 grams for subjects 12, 13, and 19 from Table 5.13. For the same subjects, $m(\infty)$ =8.4, 6.1, and 1.7 grams from Table 5.12 and $m(\infty)$ =8.8, 7.8, and 1.1 grams from Table 5.14. The $m(\infty)$ values for a particular subject are within 1.9 grams of each other between the three tables. This provides evidence that $\breve{k}_{pred}$ and $\breve{k}_{calc}$ provide a reasonable estimate of $\breve{k}_{fit}$ and can be used to accurately calculate $m(\infty)$.

5.4.2   m(∞) Calculated Using Parameters Estimated From The Nonparametric Bootstrap Simulations

Using the activity and mass parameters estimated from the data simulated assuming the residuals, D_T was calculated as described in Section 4.3. Here, $\breve{k}_{fit}$ was used to calculate D_T. With an estimate of D_T, $\bar{\alpha}_{subject}$ was found as described in Section 4.3. Table 5.15 contains $\bar{\alpha}_{subject}$ and its respective variance for each subject. Using these values, a minimum variance estimate of α was calculated to be $\hat{\alpha}_{mv}$=0.0034 Gy^{-1} with $V(\hat{\alpha}_{mv})$=2.64E-8 Gy^{-2}. Using

Table 5.15. For each subject an average α, $\bar{\alpha}_{subject}$ was calculated along with the variance in $\bar{\alpha}_{subject}$ as described in Section 4.3.

| Constants	# 12	# 13	# 19	# 21	# 28	# 43
$\bar{\alpha}_{subject}$ (Gy^{-1})	0.0042	0.0040	0.0031	0.0042	0.0033	0.0038
$V(\bar{\alpha}_{subject})$ (Gy^{-2})	1.68E-7	1.75E-7	8.87E-8	2.70E-7	1.70E-7	1.88E-7

$\hat{\alpha}_{mv}$ for all subjects, $m(\infty)$ could be calculated as described in Section 4.3. To calculate $m(\infty)$, D_T and thus an estimate of $\breve{k}$ is required. Again, here we used $\breve{k}_{fit}$ to calculate D_T and $m(\infty)$. Table 5.16 contains estimates of $\breve{k}_{fit}$, D_T and $m(\infty)$.

Table 5.16. $\breve{k}_{fit}$, D_T, and $m(\infty)$ were calculated from parameters estimated from data simulated using the residuals. The standard deviation of the parameters were found as described in Section 4.5. The confidence interval of $m(\infty)$, $CI_{m(\infty)}$, was calculated as described in Section 4.5 assuming a 95% confidence level.

Constants	# 12	# 13	# 19	# 21	# 28	# 43
$\breve{k}_{fit}$ $(\frac{g^2}{hr})$	2.14	2.58	0.60	1.58	0.77	0.05
$SD_{\breve{k}_{fit}}$	0.61	0.4391	0.15	0.23	0.21	0.06
D_T (Gy)	367	428	619	310	360	376
SD_{D_T}	29.2	37.4	43.0	25.6	25.0	26.6
$m(\infty)$ (g)	8.7	5.9	2.2	6.9	4.6	2.3
$SD_{m(\infty)}$	1.3	1.0	0.5	1.0	0.6	0.3
$CI_{m(\infty)}$	[6.1 11.4]	[4.1 8.3]	[1.5 3.5]	[4.7 9.2]	[3.5 6.4]	[1.7 3.1]

The statistical distributions of D_T and $m(\infty)$ were investigated with the use of histograms as described in Section 4.5. Figures 5.14(a) and 5.14(b) are histograms of D_T and $m(\infty)$, respectively, for subject 21. By inspection, the histograms appear to follow a normal distribution.

Table 5.17 reports estimates of $\breve{k}_{pred}$, D_T, and $m(\infty)$. Table 5.18 reports estimates of $\breve{k}_{calc}$, D_T, and $m(\infty)$. The parameter estimates and their standard errors are very similar between Tables 5.17, 5.18, and 5.16. For example, $m(\infty)$ = 8.3, 7.6, and 1.9 grams for subjects 12, 13, and 19 from Table 5.17. For the same subjects, $m(\infty)$ = 8.7, 5.9, and 2.2 grams from Table 5.16 and $m(\infty)$ = 8.9, 7.5, and 1.3 grams from Table 5.18. The $m(\infty)$ values for a particular subject are within 1.7 grams of each other between the three tables. This provides evidence that $\breve{k}_{pred}$ and $\breve{k}_{calc}$ provide a reasonable estimate of $\breve{k}$ and can be used to accurately calculate $m(\infty)$.
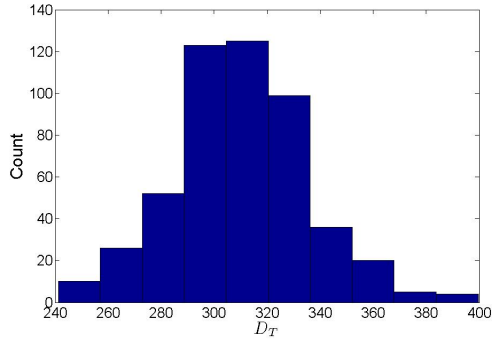
(a) Histogram of D_T for subject 21.
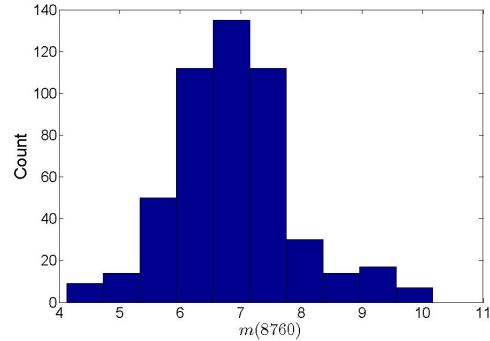
(b) Histogram of $m(\infty)$ for subject 21.

Figure 5.14. Histograms of the D_T and $m(\infty)$ for subject 21.

Table 5.17. $\breve{k}_{pred}$, D_T, and $m(\infty)$ were calculated from parameters estimated from data simulated using the residuals. The standard deviation of the parameters were found as described in Section 4.5. The confidence interval of $m(\infty)$, $CI_{m(\infty)}$ was calculated as described in Section 4.5 assuming a 95% confidence level.

Constants	# 12	# 13	# 19	# 21	# 28	# 43
$\breve{k}_{pred}$ $\left(\frac{g^2}{hr}\right)$	2.50	1.8	0.74	1.19	1.05	0.24
$SD_{\breve{k}_{pred}}$	0.37	0.25	0.11	0.16	0.14	0.04
D_T (Gy)	382	359	660	278	382	438
SD_{D_T}	37.0	30.6	55.3	22.5	29.5	34.1
$m(\infty)$ (g)	8.3	7.6	1.9	7.7	4.3	1.8
$SD_{m(\infty)}$	1.5	1.2	0.5	1.1	0.7	0.3
$CI_{m(\infty)}$	[5.5 11.6]	[4.8 10.7]	[1.1 3.1]	[5.5 10.0]	[2.8 6.0]	[1.1 2.5]

84

Table 5.18. $\breve{k}_{calc}$, D_T, and $m(\infty)$ were calculated from parameters estimated from data simulated using the residuals. The standard deviation of the parameters were found as described in Section 4.5. The confidence interval of $m(\infty)$, $CI_{m(\infty)}$, was calculated as described in Section 4.5 assuming a 95% confidence level.

Constants	# 12	# 13	# 19	# 21	# 28	# 43
$\breve{k}_{calc}$ $(\frac{g^2}{hr})$	1.94	1.82	1.10	0.85	1.04	0.28
$SD_{\breve{k}_{calc}}$	0.28	0.28	0.14	0.13	0.15	0.04
D_T (Gy)	363	363	780	257	386	460
SD_{D_T}	33.5	35.4	61.1	20.9	32.8	36.9
$m(\infty)$ (g)	8.9	7.5	1.3	8.3	4.3	1.7
$SD_{m(\infty)}$	1.4	1.3	0.3	1.1	0.7	0.3
$CI_{m(\infty)}$	[6.2 10.2]	[5.0 10.1]	[0.61 2.3]	[6.0 10.9]	[2.8 6.0]	[1.2 2.5]

5.5 Standard Propagation Of Error Method Results

The first step in performing the standard propagation of error method was to estimate the relevant parameter values. Table 5.19 reports the activity parameters and their respective SE values found using non-linear regression of (5.1) with normalized activity data. Table 5.20 reports the mass parameters and their respective SE values found using non-linear regression of (5.2) using mass data.

Using the estimated activity and mass parameters, α was found for each subject as described in Section 3.2.2. Table 5.21 contains α and its respective variance for each subject. Using these values, a minimum variance estimate of α was calculated to be $\hat{\alpha}_{mv}=0.0031\ Gy^{-1}$ with $V(\hat{\alpha}_{mv})=1.30$E-6 Gy^{-2}.

85

Table 5.19. Activity parameters from (5.1) and their SE estimated using non-linear regression with normalized activity data.

Constants	# 12	# 13	# 19	# 21	# 28	# 30	# 43
$\check{Y}$	0.909	0.772	1.232	0.820	0.517	0.988	0.466
$SE_{\check{Y}}$	0.035	0.026	0.137	0.006	0.031	0.021	0.014
b (hr^{-1})	0.0059	0.0055	0.0054	0.0071	0.0059	0.0048	0.0047
SE_b	0.0005	0.0003	0.0009	0.0001	0.0007	0.0002	0.0003
c (hr^{-1})	0.523	0.112	0.082	0.792	0.159	1.271	0.282
SE_c	0.076	0.008	0.024	0.021	0.029	0.666	0.041

Table 5.20. The mass parameter $\check{k}_{fit}$ from (5.2) and its SE estimated using non-linear regression with mass data.

Constants	# 12	# 13	# 19	# 21	# 28	# 30	# 43
$\check{k}_{fit}$ $(\frac{g^2}{hr})$	1.7	2.4	0.5	1.0	0.5	0.4	0.06
$SE_{\check{k}_{fit}}$	5.8E-14	1.8E-15	0.0283	0.0855	0.0857	0.1256	0.0228

Table 5.21. α and its respective variance are reported for each subject. α and its variance were calculated as described in Section 3.2.2.

Constants	# 12	# 13	# 19	# 21	# 28	# 30	# 43
α (Gy^{-1})	0.0036	0.0037	0.0027	0.0037	0.0032	0.0023	0.0040
$V(\alpha)$ (Gy^{-2})	1.53E-5	2.90E-5	2.75E-5	3.76E-6	2.46E-5	3.62E-6	1.98E-5

Using $\hat{\alpha}_{mv}$ for all subjects, $m(\infty)$ was calculated. To calculate $m(\infty)$, D_T and thus an estimate of $\breve{k}$ is required. Here we used $\breve{k}_{fit}$ to calculate D_T and $m(\infty)$. Table 5.22 contains estimates of $\breve{k}_{fit}$, D_T and $m(\infty)$. Each parameters standard error was calculated using the analytical approximation method.

Table 5.22. Calculated values of $\breve{k}_{fit}$, D_T, and $m(\infty)$. Each parameter's standard error values were found using the standard propagation of error method.

Constants	# 12	# 13	# 19	# 21	# 28	# 30	# 43
$\breve{k}_{fit}$ $(\frac{g^2}{hr})$	1.71	2.41	0.47	1.00	0.50	0.37	0.06
$SE_{\breve{k}_{fit}}$	5.8E-14	1.8E-15	0.03	0.09	0.09	0.13	0.023
D_T (Gy)	427	459	728	347	367	596	379
SE_{D_T}	463	668	1413	179	568	490	421
$m(\infty)$ (g)	8.2	6.2	2.0	5.9	4.9	2.4	2.7
$SE_{m(\infty)}$	11.4	12.8	9.1	2.3	8.7	3.3	3.4

Table 5.23 reports calculations of $\breve{k}_{pred}$, D_T, and $m(\infty)$. Table 5.24 reports calculations of $\breve{k}_{calc}$, D_T, and $m(\infty)$. The parameter estimates and their standard errors are very similar between Tables 5.23, 5.24, and 5.22. For example, $m(\infty) = 7.7$, 8.0, and 1.8 grams for subjects 12, 13, and 19 from Table 5.23. For the same subjects, $m(\infty) = 8.2$, 6.2, and 2.0 grams from Table 5.22 and $m(\infty) = 8.0$, 7.8, and 1.6 grams from Table 5.24. The $m(\infty)$ values for a particular subject are within 1.8 grams of each other between the three tables. This provides evidence that $\breve{k}_{pred}$ and $\breve{k}_{calc}$ provide a reasonable estimate of $\breve{k}$ and can be used to accurately calculate $m(\infty)$.

The standard errors for D_T and $m(\infty)$ are unreasonably large and therefore the uncertainties were not calculated. The standard errors calculated from the standard propagation

Table 5.23. Calculated values of $\breve{k}_{pred}$, D_T, and $m(\infty)$. Each parameter's standard error values were found using the standard propagation of error method.

Constants	# 12	# 13	# 19	# 21	# 28	# 30	# 43
$\breve{k}_{pred}$ $\left(\frac{g^2}{hr}\right)$	2.00	1.64	0.62	0.84	0.90	0.37	0.24
$SE_{\breve{k}_{pred}}$	2.25	1.85	1.29	0.39	1.54	0.31	0.32
D_T (Gy)	443	380	774	327	407	596	442
SE_{D_T}	499	431	1589	158	690	490	557
$m(\infty)$ (g)	7.7	8.0	1.8	6.3	4.3	2.4	2.2
$SE_{m(\infty)}$	11.7	10.4	8.8	2.0	9.4	3.4	3.7

Table 5.24. Calculated values of $\breve{k}_{calc}$, D_T, and $m(\infty)$. Each parameter's standard error values were found using the standard propagation of error method.

Constants	# 12	# 13	# 19	# 21	# 28	# 30	# 43
$\breve{k}_{calc}$ $\left(\frac{g^2}{hr}\right)$	1.80	1.74	0.70	0.62	0.88	0.40	0.28
$SE_{\breve{k}_{calc}}$	0.33	0.78	0.73	0.09	0.52	0.05	0.08
D_T (Gy)	431	387	804	307	404	610	467
SE_{D_T}	532	472	1708	160	744	574	683
$m(\infty)$ (g)	8.0	7.8	1.6	6.7	4.4	2.3	2.0
$SE_{m(\infty)}$	13.0	11.2	8.6	2.3	10.2	3.9	4.3

of error method can be compared with the standard deviations calculated from the simulated data. The estimates of D_T and $m(\infty)$ are similar between the three methods of estimating $\breve{k}$ and therefore only the values calculated using $\breve{k}_{pred}$ will be used to compare the standard propagation of error and simulation methods. Comparing the parameter estimates from Table 5.13 with the parameters estimates from Table 5.23 shows that the simulation results are very different from the standard propagation of error method results. While the parameter estimates of $\breve{k}_{pred}$, D_T, and $m(\infty)$ are close between the two tables, each parameter's standard error is considerably different. The standard errors from the standard propagation of error method ($SE_{m(\infty)} = 13.0$ grams and 11.2 grams for subjects 12 and 13) are much larger than the standard deviations from the simulated data ($SD_{m(\infty)} = 1.4$ grams and 1.2 grams for subjects 12 and 13). The standard deviations calculated from the simulated data are an order of magnitude smaller than the standard errors calculated from the standard propagation of error method. This implies that the standard propagation of error method does not provide reasonable estimates of the standard errors and provides evidence that the simulated data are required for the uncertainty analysis of our new protocol.

CHAPTER 6

CONCLUSIONS AND FUTURE WORK

In this thesis we presented a new computational protocol for the calculation of RAI in the treatment of Graves' hyperthyroidism. The new protocol implemented a two-compartment model to describe RAI kinetics in the body which allows for the conversion between different RAI isotopes used in diagnostic and therapeutic applications. The protocol allows for the prediction of the final thyroid mass from the absorbed dose which is calculated using the new activity kinetics and an improved method to predict the thyroid mass dynamics directly related to the activity in the thyroid. Using clinical data consisting of activity kinetics and mass dynamics of 17 subjects and measured final mass values of 7 of the 17 subjects, we were able to show that our new protocol can accurately predict the measured final thyroid mass values. Uncertainty analysis of the protocol was performed using an standard propagation of error method, however, this yielded large standard error values in the absorbed dose and final mass. The unreasonable results could be due to the small sample size of the clinical data. As a result, we simulated additional data using parametric and nonparametric bootstrap methods. Conclusions could not be made of the statistical distributions of the activity and mass data, however we were able to obtain a 95 % confidence interval: $0.53\overline{m}(\infty) < \overline{m}(\infty) < 1.38\overline{m}(\infty)$. The uncertainty was calculated using the bootstrap methods with a 95% confidence level.

There is an open question, namely, whether this confidence interval is clinically useful, because, if a subject were at one of the extremes of the confidence interval, it may not correspond to a euthyroid state.

90

There are also some open problems that still remain. One problem would be to identify an error distribution pertaining to all subjects. The proper way to identify this error distribution would be through the use of non-linear mixed-effects (NLME) models.

Another problem would be to investigate the quality of the activity parameters estimated from three activity measurements. We have touched on this briefly in this thesis, however, a detailed investigation is required. The identification of the activity parameters based on three measurements is at the heart of our protocol and needs to be formally addressed.

Finally, the constant α in (3.11) needs to be further investigated. Much of the uncertainty in the final mass estimate is a result from the uncertainty in α. Therefore, if we can find a better estimate of α, then we can reduce the uncertainty in the calculation of the final mass. This can be accomplished by either finding a better method of calculating the variance of α, $V(\hat{\alpha})$, or by using the data of more subjects to estimate α.

APPENDIX A

CLINICAL DATA

Dr. Traino provided us with detailed activity and mass data of 7 Graves' subjects who underwent RAI therapy. The data consists of pre-therapy mass $m(0)$ and therapeutic activity A_d in Table A.1, measured mass dynamics in Table A.2, and measured, normalized activity kinetics $\frac{A(t)}{A_d}$ in Table A.3.

Table A.1. The measured pre-therapeutic mass and the therapeutic activity A_d.

Subject #	12	13	19	21	28	30	43
$m(0)$ (g)	32	27	21	18	16	16	9
A_d (MBq)	666	555	555	370	555	339	296

Table A.2. Measured mass dynamics data.

Time (days)	RAI therapy mass dynamics $m(t)$						
	# 12	# 13	# 19	# 21	# 28	# 30	# 43
Pre-therapy	32	27	21	18	16	16	9
3 days	-	-	21	18	17	-	9
7 days	-	-	18	16	15	-	8
14 days	-	-	17	9	13	15	8
21 days	23	-	15	11	13	-	9
28 days	-	-	16	9	13	-	9
30 days	-	10	-	-	-	8	-
35 days	-	-	16	9	-	-	8
1 year	7	5	3	5	5	4	2

Table A.3. Measured, normalized activity kinetics data.

# 12		# 13		# 19		# 21	
Time(hr)	$A(t)/A_d$	Time(hr)	$A(t)/A_d$	Time(hr)	$A(t)/A_d$	Time(hr)	$A(t)/A_d$
0	0	0	0	0	0	0	0
3.3	0.73	6	0.36	2.3	0.06	2	0.64
19.3	0.82	23	0.61	21.5	0.97	22.6	0.70
68.0	0.59	95.0	0.47	45.1	0.88	46.5	0.58
236.2	0.26	263.0	0.18	69.3	0.88	70.5	0.50
404.0	0.05	430.0	0.06	141.4	0.48	140.4	0.30
-	-	-	-	165.1	0.52	163.6	0.26
-	-	-	-	333.2	0.25	332.4	0.07
-	-	-	-	526.5	0.09	500.3	0.02
-	-	-	-	670.3	0.04	-	-

# 28		# 30		# 43	
Time(hr)	$A(t)/A_d$	Time(hr)	$A(t)/A_d$	Time(hr)	$A(t)/A_d$
0	0	0	0	0	0
3.5	0.21	3.5	0.96	1.2	0.13
22.6	0.44	22.8	0.87	20.2	0.44
46.3	0.36	70.3	0.73	44.1	0.35
70.0	0.39	239.5	0.30	67.4	0.35
141.7	0.20	407.5	0.14	139.1	0.24
166.0	0.20	-	-	163.3	0.23
333.8	0.07	-	-	331.2	0.10
501.5	0.03	-	-	499.4	0.04

Dr. Traino also provided the normalized activity kinetics data and mass dynamics data of the additional ten subjects [16]. The initial administered RAI dose and initial measured mass can be found in Table A.4. The activity kinetics data is in Table A.5 and the mass dynamics data is in Table A.6.

Table A.4. The measured pre-therapeutic mass and the therapeutic activity A_d.

Subject #	1	2	3	4	5	6	7	8	9	10
$m(0)$ (g)	64	54	43	40	26	18	16	14	13	13
A_d (MBq)	592	666	555	555	629	518	518	518	518	444

<div align="center">

Table A.5. Measured, normalized activity kinetics data.

</div>

#1		# 2		#3		# 4	
Time(hr)	$A(t)/A_d$	**Time(hr)**	$A(t)/A_d$	**Time(hr)**	$A(t)/A_d$	**Time(hr)**	$A(t)/A_d$
0	0	0	0	0	0	0	0
2	0.52	2	0.10	2	0.49	2	0.35
24	0.46	24	0.44	3	0.44	24	0.52
72	0.32	72	0.39	24	0.34	48	0.62
120	0.26	120	0.31	72	0.38	168	0.38
144	0.23	168	0.26	120	0.26	336	0.13
168	0.19	336	0.12	240	0.13	840	0.02
336	0.1	504	0.05	288	0.11	-	-
-	-	-	-	480	0.04	-	-
-	-	-	-	576	0.02	-	-

# 5		# 6		# 7		# 8	
Time(hr)	$A(t)/A_d$	**Time(hr)**	$A(t)/A_d$	**Time(hr)**	$A(t)/A_d$	**Time(hr)**	$A(t)/A_d$
0	0	0	0	0	0	0	0
24	0.43	2	0.34	8	0.20	2	0.17
48	0.46	72	0.47	24	0.41	24	0.38
72	0.41	168	0.24	72	0.28	48	0.29
120	0.38	312	0.10	120	0.23	120	0.21
168	0.30	144	0.21	144	0.21	144	0.21
336	0.11	480	0.047	168	0.16	168	0.21
600	0.03	-	-	336	0.07	336	0.08
-	-	-	-	504	0.02	480	0.04

# 9		# 10	
Time(hr)	$A(t)/A_d$	**Time(hr)**	$A(t)/A_d$
0	0	0	0
2	0.22	2	0.31
24	0.63	24	0.53
72	0.41	72	0.50
120	0.34	120	0.44
144	0.32	144	0.39
168	0.30	168	0.35
312	0.12	336	0.17
480	0.06	504	0.06

Table A.6. Measured mass dynamics data.

Time (days)	RAI therapy mass dynamics $m(t)$									
	# 1	# 2	# 3	# 4	# 5	# 6	# 7	# 8	# 9	# 10
Pre-therapy	64	54	43	40	26	18	16	14	13	13
3 days	56	42	41	39	24	15	15	16	10	-
7 days	58	47	34	36	23	17	16	14	14	12
14 days	-	33	33	29	23	7	12	14	10	6
21 days	43	39	32	17	21	-	12	11	12	6
30 days	-	25	27	10	20	9	-	7	9	9

APPENDIX B

CALCULATING THE ACTIVITY PARAMETERS ANALYTICALLY WITH LIMITED DATA

Before deciding to use non-linear regression to estimate the activity parameters Y, b, and c with 3 measured data points, we looked into calculating these parameters analytically. Below is our attempt at finding an analytical solution to this problem.

Original Question. Given a function of the form

$$A(t) = Y \left(e^{-bt} - e^{-ct} \right),$$

where $b < c$ and $t \geq 0$, is it possible to determine Y, b, and c on the basis of 3 observations a times $t_1 < t_2 < t_3$?

Answer. Let $c = b + \delta$ $(\delta > 0)$, so

$$A(t) = Y \left(e^{-bt} - e^{-bt-\delta t} \right)$$
$$= Y e^{-bt} \left(1 - e^{-\delta t} \right),$$

and let

$$a_i = A(t_i) = Y e^{-bt_i} \left(1 - e^{-\delta t_i} \right).$$

Also, denote

$$\eta_{12} = \frac{a_1}{a_2} = e^{-b(t_1 - t_2)} \frac{1 - e^{-\delta t_1}}{1 - e^{-\delta t_2}}, \tag{B.1}$$

$$\eta_{13} = \frac{a_1}{a_3} = e^{-b(t_1 - t_3)} \frac{1 - e^{-\delta t_1}}{1 - e^{-\delta t_3}}, \tag{B.2}$$

$$\Delta_{12} = t_1 - t_2, \tag{B.3}$$

and

$$\Delta_{13} = t_1 - t_3. \tag{B.4}$$

Equation (B.1) can be re-written using (B.3) to yield

$$e^{b\Delta_{12}} = \frac{1}{\eta_{12}} \frac{1 - e^{-\delta t_1}}{1 - e^{-\delta t_2}}, \tag{B.5}$$

also, (B.2) can be re-written using (B.4) to yield

$$e^{b\Delta_{13}} = \left(e^{b\Delta_{12}}\right)^P, \tag{B.6}$$

where $P = \frac{\Delta_{13}}{\Delta_{12}} > 1$. Combining (B.5) and (B.6) yields

$$\left(\frac{1}{\eta_{12}} \frac{1 - e^{-\delta t_1}}{1 - e^{-\delta t_2}}\right)^P = e^{b\Delta_{13}}$$
$$= \frac{1}{\eta_{13}} \frac{1 - e^{-\delta t_1}}{1 - e^{-\delta t_3}},$$

which reduces to

$$\left(\frac{1 - e^{-\delta t_1}}{1 - e^{-\delta t_2}}\right)^P \frac{1 - e^{-\delta t_3}}{1 - e^{-\delta t_1}} = \frac{\eta_{12}^P}{\eta_{13}}. \tag{B.7}$$

The parameters η_{12} and η_{13} are known from observations, if (B.7) can be solved for δ, then b can be calculated from (B.5) and Y can be calculated from

$$a_1 = Y e^{-bt_1} \left(1 - e^{-\delta t_1}\right). \tag{B.8}$$

97

Denote the left side of (B.7) by $f(\delta)$ where δ is the only unknown parameter in (B.7). The question is whether there exists a $\delta > 0$ such that

$$f(\delta) = \frac{\eta_{12}^P}{\eta_{13}}.$$

Note that

$$f(0+) = \lim_{\delta \downarrow 0} f(\delta) = \left(\frac{t_1}{t_2}\right)^P \frac{t_3}{t_1}$$

$$f(\infty) = 1.$$

Let $u = e^{-\delta t_1}$, so as δ goes from 0 to ∞, u goes from 1 to 0. Now

$$e^{-\delta t_2} = \left(e^{-\delta t_1}\right)^{\frac{t_2}{t_1}} = u^{\frac{t_2}{t_1}} = u^{\tau_{21}}$$

$$e^{-\delta t_3} = u^{\frac{t_3}{t_1}} = u^{\tau_{31}},$$

where $\tau_{21} = \frac{t_2}{t_1}$, $\tau_{31} = \frac{t_3}{t_1}$, and $\tau_{21}, \tau_{31} > 1$. This results in

$$f(\delta) = \left(\frac{1-u}{1-u^{\tau_{21}}}\right)^P \frac{1 - u^{\tau_{31}}}{1-u}$$

$$= h(u).$$

This can be further explored through an example.

Example. Let P=2, τ_{21}=2, and τ_{31}=3. Using these values in the equation for $h(u)$ yields

$$h(u) = \left(\frac{1-u}{1-u^2}\right)^2 \frac{1-u^3}{1-u}$$

$$= \frac{u^2 + u + 1}{(1+u)^2}.$$

98

Taking the derivative of this equation with respect to u results in

$$h'(u) = \frac{u^2 - 1}{(u+1)^4},$$

where $0 < u < 1$. If we denote the numerator of $h'(u)$ to be $\Theta(u)$, then $\Theta(0) = -1$ and $\Theta(1)=0$. Taking the derivative of $\Theta(u)$ with respect to u results in

$$\Theta'(u) = 2u.$$

The term $\Theta'(u) \geq 0$ for $0 \leq u \leq 1$ and hence $\Theta(u)$ is monotone increasing on $0 \leq u \leq 1$. Therefore, $\Theta(u) \leq 0$ and $h'(u) \leq 0$ for $0 \leq u \leq 1$. It follows that $h(u)$ is a monotone decreasing function. Thus the values of $h(u)$ all lie between $h(0)=1$ and $h(1)=0.75$ and the values of $f(\delta)$ lie between 0.75 and 1. Therefore, (B.7) will have a solution δ if and only if $0.75 \leq \frac{\eta_{12}^P}{\eta_{13}} \leq 1$.

General conditions could probably be found that would guarantee a solution to (B.7), however, we did not pursue this further. We used non-linear regression to estimate the activity parameters Y, b, and c throughout this thesis.

APPENDIX C

INVESTIGATING D_T

The absorbed dose can be expressed as

$$D_T = \sigma \int_0^\infty \frac{A(x)}{m(x)} \, dx.$$

As described in Section 3.2, we can only directly calculate the mass dynamics, $m(t)$, during the first time frame. The first time frame, as described in Section 2.2, is assumed to occur during the first 30-35 days (720-840 hours) after administration of RAI. Throughout this thesis we have calculated the mass dynamics, $m(t)$, until $t = 840$ hours, $m(840)$. As a result, we only calculated the absorbed dose integral to $t = 840$ hours. Although we cannot prove that the first time frame does occur during the first 840 hours after RAI administration, we can prove that the absorbed dose will be not change significantly when calculated up $t = 720$ hours or up to $t = 1080$ hours (45 days). To investigate this conjecture, we can re-write the absorbed dose integral as

$$D_T = \sigma \int_0^t \frac{A(t)}{m(t)} \, dt.$$

We set the upper limit of the integral to the time variable, t, because we want to evaluate this integral at various times. The following closed from solution of this integral can be found

$$D_T = \frac{\sigma}{k} \left(m(0) - m(t) \right), \tag{C.1}$$

where,

$$m(t) = \left[2 \left(\frac{Yk}{b} e^{-b\,t} + \frac{Yk}{c} - \frac{Yk}{c} e^{-c\,t} - \frac{Yk}{b} + \frac{m(0)^2}{2} \right) \right]^{\frac{1}{2}}.$$

100

We calculated the absorbed dose using (C.1) evaluated at times $t=$ 720, 840, and 1080 hours. The absorbed dose values can be found in Table C.1. As can be seen from Table C.1, D_T does not change significantly when calculated using these three times. While any of these time values would result in a reasonable D_T, we chose to calculate D_T up to $t = 840$ hours.

Table C.1. D_T values calculated using (C.1) evaluated at times $t = 720$, $t = 840$, and $t = 1080$. $D_{T_{720}}$ denotes the absorbed dose evaluated up to time $t = 720$. $D_{T_{840}}$ denotes the absorbed dose evaluated up to time $t = 840$. $D_{T_{1080}}$ denotes the absorbed dose evaluated up to time $t = 1080$.

Constants	# 12	# 13	# 19	# 21	# 28	# 30	# 43
$D_{T_{720}}$ Gy	423	451	719	346	364	585	373
$D_{T_{840}}$ Gy	427	459	728	347	367	596	379
$D_{T_{1080}}$ Gy	429	466	735	348	369	605	384

101

APPENDIX D

CALCULATING K$_{\textbf{PRED}}$

The general procedure to calculate k_{pred} is described in Section 3.2.1. k_{pred} can be expressed using (3.9)

$$k_{pred_i} = \phi \frac{m_i^2(0)}{g_i} - \varphi,$$

where

$$g_i = 2Y \left(\frac{1}{c} e^{-c\ 840} - \frac{1}{b} e^{-b\ 840} - \frac{1}{c} + \frac{1}{b} \right),$$

and i denotes the ith subject. As described in Section 3.4, an estimate of $\breve{k}_{pred}$ is desired. The mass constant $\breve{k}_{pred}$ can be expressed as

$$\breve{k}_{pred_i} = \breve{\phi} \frac{m_i^2(0)}{\breve{g}_i} - \breve{\varphi}, \tag{D.1}$$

where

$$\breve{g}_i = 2\breve{Y} \left(\frac{1}{c} e^{-c\ 840} - \frac{1}{b} e^{-b\ 840} - \frac{1}{c} + \frac{1}{b} \right).$$

We will describe the procedure to estimate the constants $\breve{\phi}$ and $\breve{\varphi}$. We used the data for all 17 subjects to calculate these constants because $\breve{k}_{pred}$ is used to estimate the mass dynamics during the first time frame for which we had data from all subjects. Using the normalized activity data, the activity parameters $\breve{Y}$, b, and c were estimated using non-linear regression

of (3.13). With these activity parameters, $\breve{g}$ was calculated for each subject. These values were stored together in a vector as

$$\breve{g}_i = [193\ 222\ 177\ 292\ 228\ 225\ 141\ 163\ 246\ 296\ 283\ 257\ 433\ 224\ 169\ 401\ 190],$$

where $i = [\text{1-10,12,13,19,21,28,30,43}]$. The activity parameters were also used in (3.15) to estimate $\breve{k}_{fit}$ for each subject. These values were also stored together in a vector as

$$\breve{k}_{fit_i} = [12\ 9\ 5\ 5\ 1\ 1\ 1\ 1\ 0.3\ 0.4\ 2\ 2\ 0.5\ 1\ 1\ 0.4\ 0.06],$$

where $i = [\text{1-10,12,13,19,21,28,30,43}]$. Using the measured initial mass, $m(0)$, values

$$m_i(0) = [64\ 54\ 43\ 40\ 26\ 18\ 16\ 14\ 13\ 13\ 32\ 27\ 21\ 18\ 16\ 16\ 9],$$

the term $\frac{m_i^2(0)}{\breve{g}_i}$ was calculated. These values were also stored in a vector as

$$\frac{m_i^2(0)}{\breve{g}_i} = [21\ 13\ 10\ 5\ 3\ 1\ 2\ 1\ 1\ 1\ 4\ 3\ 1\ 1\ 2\ 1\ 0.4].$$

Using linear algebra, (D.1) can be expressed as

$$\breve{k}_{pred_i} = \begin{bmatrix} \dfrac{m_i^2(0)}{\breve{g}_i} & 1 \end{bmatrix} \begin{bmatrix} \breve{\phi} & -\breve{\varphi} \end{bmatrix}^T, \tag{D.2}$$

where T denotes transpose. Following the argument in Section 3.2.1, $\breve{k}_{fit}$ can replace $\breve{k}_{pred}$ in (D.2) which yields

$$\breve{k}_{fit_i} = \begin{bmatrix} \dfrac{m_i^2(0)}{\breve{g}_i} & 1 \end{bmatrix} \begin{bmatrix} \breve{\phi} & -\breve{\varphi} \end{bmatrix}^T. \tag{D.3}$$

103

Linear regression on (D.3) yields the estimates of $\breve{\phi} = 0.5951$ and $\breve{\varphi} = 0.0108$. Plugging these estimates into (D.1) yields

$$\breve{k}_{pred_i} = 0.5951 \frac{m_i^2(0)}{\breve{g}_i} - 0.0108,$$

which can be used to estimate the mass dynamics during the first time frame.

PARAMETRIC BOOTSTRAPPING RESULTS ASSUMING A NORMAL DISTRIBUTION

The results presented in this appendix are from the parametric bootstrap simulations when the normal distribution of the error was assumed. This appendix will present both activity and mass parameters estimated from the original regression of the measured data and from the simulated data. The parameters obtained from the simulated data were used to calculate and investigate the error of $m(\infty)$. The results of these calculations are presented in this appendix.

Normal Distribution Simulation Results

In this section, the measurement error distribution was assumed $N(0, \frac{\zeta^2}{9})(\zeta = 0.10)$ as described in Section 4.1.2. The activity parameters estimated from the measured activity data and from the simulated data will be presented. Analysis of both methods will be presented along with a comparison of both methods. The same will be repeated for the mass parameters.

Activity Results For The Normal Distribution

The original activity parameters were estimated using non-linear regression with the normalized measured activity data. The procedure discussed in Section 4.1 was still followed only a normalized version of (4.3),

$$\ln\left(\tilde{A}(t_i)\right) = -0.00056 + \ln\left(\check{Y}\right) + \ln\left(e^{-bt_i} - e^{-ct_i}\right) + \eta_{Ai}, \tag{E.1}$$

105

was used for the regression of the normalized measured activity data. μ_A was replaced with its expected value in (E.1) for the regression. Table E.1 reports the original activity parameters and their respective standard errors found using non-linear regression of (E.1) with normalized measured activity data.

Table E.1. The original activity parameters from (E.1) and their SE estimated using non-linear regression with normalized measured activity data.

Constants	# 12	# 13	# 19	# 21	# 28	# 43
$\ln\left(\check{Y}\right)$	0.016	-0.193	0.285	-0.171	-0.687	-0.738
$SE_{\check{Y}}$	0.008	0.014	0.008	0.006	0.007	0.003
b (hr^{-1})	0.0071	0.0060	0.0052	0.0075	0.0057	0.0049
SE_b	0.00004	0.00005	0.00002	0.00003	0.00003	0.00001
c (hr^{-1})	0.410	0.104	0.037	0.744	0.165	0.272
SE_c	0.011	0.003	0.0004	0.021	0.003	0.002
$\sigma^2_{\eta_A}$	0.064	0.004	0.089	0.001	0.009	0.004

The normal error distribution was assumed while estimating the activity parameters from the measured data and therefore μ_A and $\sigma^2_{\eta_A}$ could not be compared to their expected values in order to gain insight of their distributions as described in Section 4.5.1. However, as described in Section 4.5.1, a histogram and normal probability plot of ϵ_{Ai} was used instead. The histogram and normal probability plot for ϵ_{Ai} found assuming the normal error distribution were almost identical to Figure 5.1 and therefore were not included in this thesis.

The activity parameters were also estimated from the simulated activity data sets following the method described in Section 4.1.3. Section 4.5 describes how an average estimate and standard deviation of each activity parameter can be obtained from the $N = 500$ sets of

simulated activity parameters. The simulated data was also normalized by A_d, and therefore (E.1) was used to again estimate the activity parameters. Table E.2 contains the activity parameters and their standard deviations (SD) estimated from the simulated data.

The activity parameters estimated from the simulated data were used to check the accuracy of the results from the original regression of the measured activity data. The estimated activity parameter values in Table E.2 were compared to their respective estimated values from Table E.1. All parameter estimates and standard error values match reasonably well between the two tables except for $\sigma_{\eta_A}^2$. The variance $\sigma_{\eta_A}^2$ estimated from the measured data is much larger than its respective value from the simulated data. For example, $\sigma_{\eta_A}^2 = 0.00008$ and 0.00009 for subjects 12 and 13, estimated from the simulated data. For the same subjects, $\sigma_{\eta_A}^2 = 0.064$ and 0.004 estimated from the measured data. Because of the discrepancy between the $\sigma_{\eta_A}^2$ values, the simulations of the activity data assuming a normal distribution appear to be required to accurately estimate the parameters.

Table E.2. Activity parameters from (E.1) and their standard deviations estimated from the simulations which assumed a normal distribution.

Constants	# 12	# 13	# 19	# 21	# 28	# 43
$\ln\left(\check{Y}\right)$	0.033	-0.178	0.302	-0.154	-0.670	-0.721
$SD_{\check{Y}}$	0.008	0.010	0.008	0.006	0.006	0.005
$b\ (hr^{-1})$	0.0070	0.0060	0.0052	0.0075	0.0057	0.0049
SD_b	0.00003	0.00004	0.00002	0.00002	0.00002	0.00002
$c\ (hr^{-1})$	0.411	0.104	0.037	0.745	0.165	0.271
SD_c	0.010	0.002	0.0004	0.018	0.002	0.004
$\sigma_{\eta_A}^2$	0.00008	0.00009	0.00009	0.00008	0.00009	0.00009

107

The activity parameters estimated from the simulated data can also be used to study their distributions through the use of histograms and normal probability plots as described in Section 4.5. Figures E.1(a) - E.1(c) are histograms of $\ln\left(\check{Y}\right)$, b and c respectively. By inspection, the figures appear to possibly follow a normal distribution. Figures E.2(a)-E.2(c) are normal probability plots for each of the activity parameters estimated from the simulated data. Figures E.2(a) - E.2(c) are normal probability plots of $\ln\left(\check{Y}\right)$, b, and c respectively. Although the tails of the data depart from linearity, the plots suggest that normality could be approximately correct. However, a conclusion could not be made from these plots alone.
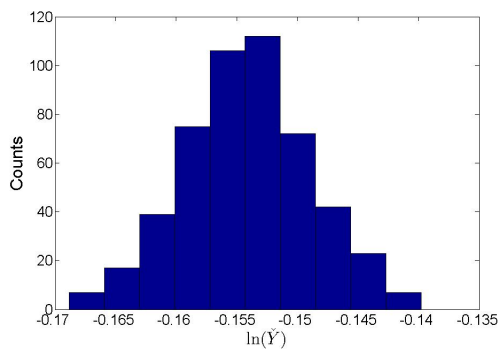
(a) Histogram of $\ln\left(\check{Y}\right)$ for subject 21.
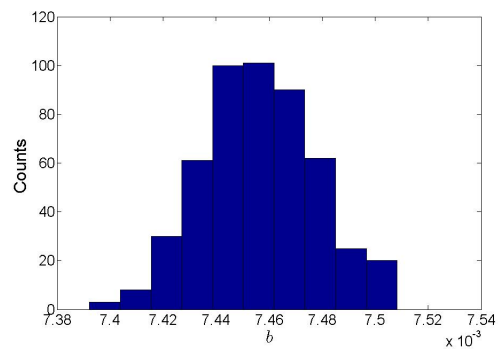
(b) Histogram of b for subject 21.
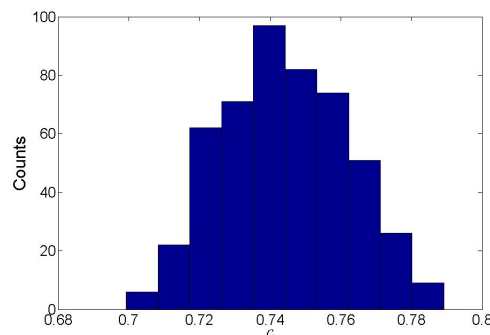
(c) Histogram of c for subject 21.

Figure E.1. Histograms of the activity parameters from (E.1) assuming a normal error distribution for subject 21.
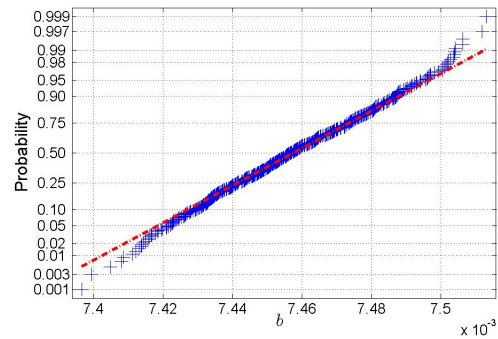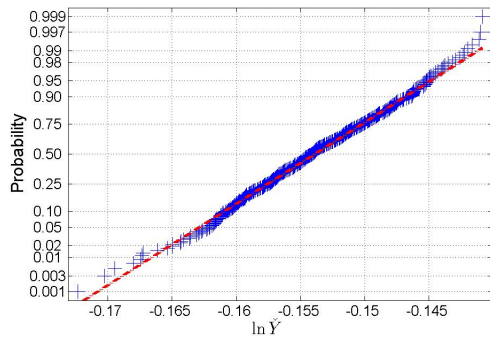
(a) Normal probability plot of $\ln\left(\check{Y}\right)$ for subject 21.

(b) Normal probability plot of b for subject 21.
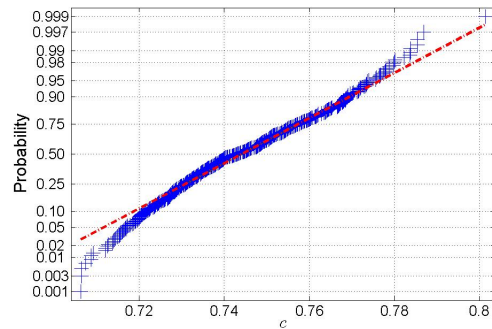
(c) Normal probability plot of c for subject 21.

Figure E.2. Normal probability plots of the activity parameters from (E.1) assuming a normal error distribution for subject 21. The crosses represent the data points and the dotted line is used to help evaluate the linearity of the data.

109

Mass Results For The Normal Distribution

The original mass parameters were estimated using the method described in Section 4.1. Equation (5.4) was used to incorporate the normalized activity parameters. Table E.3 reports the mass parameters and their respective standard errors found using non-linear regression of (5.4) with measured mass data.

Table E.3. The original mass parameters from (5.4) and their SE estimated using non-linear regression with measured mass data.

Constants	# 12	# 13	# 19	# 21	# 28	# 43
$\breve{k}_{fit}\ (\frac{g^2}{hr})$	1.95	2.50	0.48	1.18	0.69	0.04
$SE_{\breve{k}_{fit}}$	-	-	0.04	0.07	0.09	0.06
μ_m	0.039	0.040	0.018	0.165	0.077	-0.014
SE_{μ_m}	-	-	0.028	0.087	0.036	0.054
$\sigma^2_{\eta_m}$	-	-	0.0016	0.0164	0.0022	0.0043

The estimated μ_m and $\sigma^2_{\eta_m}$ values were compared to their respective expected values calculated assuming both a uniform and normal distribution of ϵ_{mi} as described in Section 4.5.1. The estimated μ_m values from the regression are positive for all subjects with the exception of subject 43. The estimated μ_m values could not support either a U($-\zeta, \zeta$) or N($0, \frac{\zeta^2}{9}$) distribution of ϵ_{mi} ($\zeta = 0.15$) because both expected μ_m values (μ_{mU}=-0.00378 and μ_{mN}=-0.00125) are negative. This can be explained by the fact that the error model is correct, however there is an upward bias or that the error model is wrong. The estimated $\sigma^2_{\eta_m}$ values did not support either distribution. The expected $\sigma^2_{\eta_m}$ values are 0.0076 and 0.0025 for the uniform and normal distribution respectively. While on the same order of magnitude, definite support for either distribution could not be concluded.

As with the activity kinetics, a histogram and normal probability plot of ϵ_{mi} was used to investigate the error distribution as described in Section 4.5.1. The histogram and normal probability plot for ϵ_{mi} found assuming the normal error distribution were almost identical to Figure 5.4 and therefore were not included in this thesis.

The mass parameters were also estimated from the simulated mass data sets following the method described in Section 4.1.4. Section 4.5 describes how an average estimate and standard deviation of each mass parameter can be obtained from the $N = 500$ sets of simulated mass parameters. However, similar to estimating the parameters from the measured mass data, (5.4) was used to incorporate the normalized activity parameters and estimate the mass parameters from the simulated data. Table E.4 contains the estimated mass parameters and their standard deviations (SD).

The mass parameters estimated from the simulated data were also compared to the mass parameters estimated from the measured data. The estimated mass parameters in Table E.4 were compared to their respective estimated values from Table E.3. $\breve{k}_{fit}$ matched reasonably well between the two tables. For example, $\breve{k}_{fit} = 0.50 \, \frac{\text{g}^2}{\text{hr}}$ and $1.22 \, \frac{\text{g}^2}{\text{hr}}$ for subjects 19 and 21 respectively. These values were obtained from the simulated data. For the same subjects, $\breve{k}_{fit} = 0.48 \, \frac{\text{g}^2}{\text{hr}}$ and $1.18 \, \frac{\text{g}^2}{\text{hr}}$ estimated from the measured data. With the exception of subject 19, all of the estimated μ_m values from the simulated data were negative while the μ_m values estimated from the measured data were all positive with the exception of subject 43. However, the standard errors of μ_m and $\breve{k}_{fit}$ match well between the two tables. For example, $SE_{\breve{k}_{fit}} = 0.04 \, \frac{\text{g}^2}{\text{hr}}$ and $0.07 \, \frac{\text{g}^2}{\text{hr}}$ and $SD_{\breve{k}_{fit}} = 0.03 \, \frac{\text{g}^2}{\text{hr}}$ and $0.04 \, \frac{\text{g}^2}{\text{hr}}$ for subjects 19 and 21. Also, $SE_{\mu_m} = 0.028$ and 0.087 and $SD_{\mu_m} = 0.01$ and 0.01 for subjects 19 and 21. $\sigma^2_{\eta_m}$ is on an order of magnitude smaller when estimated from the simulated data $\left(\sigma^2_{\eta_m} = 0.0002 \text{ for subject 19}\right)$ than from the measured data $\left(\sigma^2_{\eta_m} = 0.0016 \text{for subject 19 }\right)$. The fact that the parameter values do not match well between the two tables suggests that

111

the simulated data are required for estimating the mass parameters while assuming a normal distribution of ϵ_{mi}.

Table E.4. Mass parameters from (5.4) and their standard deviations estimated from the simulations which assumed a normal distribution.

Constants	# 12	# 13	# 19	# 21	# 28	# 43
$\breve{k}_{fit}$ $\left(\frac{g^2}{hr}\right)$	2.01	2.58	0.50	1.22	0.71	0.05
$SE_{\breve{k}_{fit}}$	0.13	0.09	0.03	0.04	0.04	0.01
μ_m	-.000012	-.000007	0.000894	-0.001160	-0.000141	-0.000059
SE_{μ_m}	0.001668	0.000374	0.010387	0.010996	0.009915	0.009533
$\sigma^2_{\eta_m}$	-	-	0.0002	0.0002	0.0002	0.0002

Figures E.3(a) and E.3(b) are histograms of the mass parameters $\breve{k}$ and μ_m, respectively, estimated from the simulated data. By inspection, Figure E.3(b) resembles a normal distribution however Figure E.3(a) resembles a uniform distribution. Another approach to gain insight into the distributions of these parameters is to investigate the normal probability plots in Figures E.4(a) and E.4(b). Figures E.4(a) and E.4(b) are normal probability plots of $\breve{k}$ and μ_m respectively. In both plots, the tails of the data deviate from linearity, which does not imply whether these parameters follow a normal distribution or not.
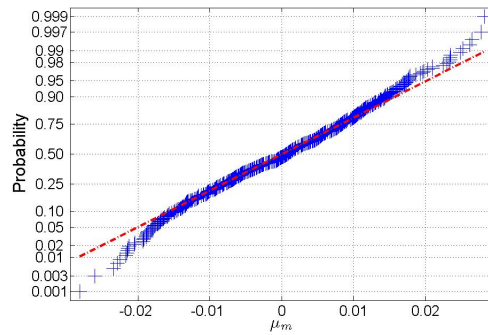
112
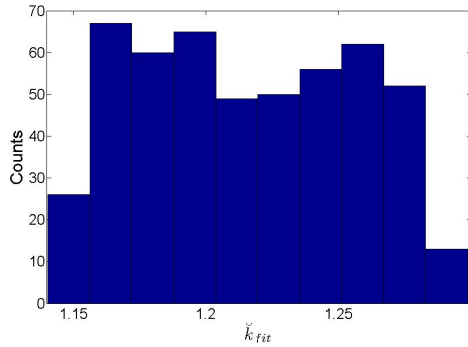
(a) Histogram of $\breve{k}$ for subject 21.
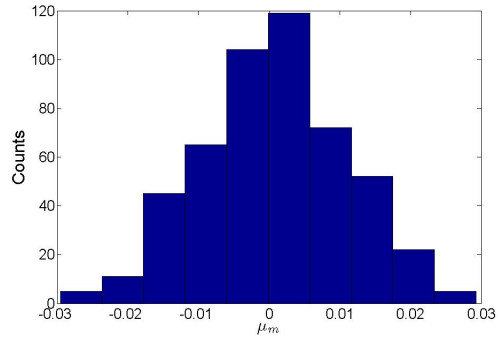
(b) Histogram of μ_m for subject 21.

Figure E.3. Histograms of the mass parameters from (5.4) assuming a normal error distribution for subject 21.
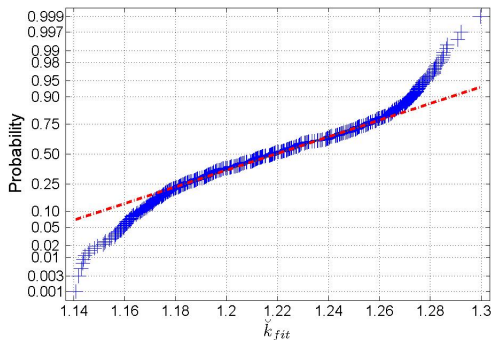
(a) Normal probability plot of $\breve{k}$ for subject 21. (b) Normal probability plot of μ_m for subject 21.

Figure E.4. Normal probability plots of the mass parameters from (5.4) assuming a normal error distribution for subject 21. The crosses represent the data points and the dotted line is used to help evaluate the linearity of the data.

$m(\infty)$ Calculated Using Parameters Estimated From Simulations Of The Normal Distribution

This section presents the results of the calculation of $m(\infty)$ as described in Section 4.3. It presents the calculation of $m(\infty)$ using parameters estimated from the normally distributed data. $m(\infty)$ will be calculated using 3 estimates of the mass parameter $\breve{k}$: 1) $\breve{k}$ found using

113

non-linear regression of mass data, $\breve{k}_{fit}$, 2) $\breve{k}$ calculated using (3.16), $\breve{k}_{pred}$, and 3) $\breve{k}$ calculated using (2.8), $\breve{k}_{calc}$. The 3 estimates of $\breve{k}$ are used to investigate the error in our new protocol when using a predictive equation to calculate $\breve{k}$.

Using the activity and mass parameters estimated from the data simulated assuming the $N(0, \frac{\varsigma^2}{9})$ distribution, D_T was calculated as described in Section 4.3. Here, $\breve{k}_{fit}$ was used to calculate D_T. With an estimate of D_T, $\bar{\alpha}_{subject}$ was found as described in Section 4.3. Table E.5 contains $\bar{\alpha}_{subject}$ and its respective variance for each subject. Using these values, a minimum variance estimate of α was calculated to be $\hat{\alpha}_{mv}$=0.0033 Gy^{-1} with $V(\hat{\alpha}_{mv})$=8.99E-10 Gy^{-2}.

Table E.5. For each subject an average α, $\bar{\alpha}_{subject}$ was calculated along with the variance in $\bar{\alpha}_{subject}$ as described in Section 4.3.

Constants	# 12	# 13	# 19	# 21	# 28	# 43
$\bar{\alpha}_{subject}$ (Gy^{-1})	0.0038	0.0038	0.0026	0.0035	0.0030	0.0041
$V(\bar{\alpha}_{subject})$ (Gy^{-2})	4.52E-9	5.60E-9	2.95E-9	9.13E-9	6.48E-9	9.13E-9

Using $\hat{\alpha}_{mv}$ for all subjects, $m(\infty)$ could be calculated as described in Section 4.3. To calculate $m(\infty)$, D_T and thus an estimate of $\breve{k}$ is required. Again, here we used $\breve{k}_{fit}$ to calculate D_T and $m(\infty)$. Table E.6 contains estimates of $\breve{k}_{fit}$, D_T and $m(\infty)$. The standard deviation of the parameters were found as described in Section 4.5. The confidence interval of $m(\infty)$, $CI_{m(\infty)}$, was calculated as described in Section 4.5 assuming a 95% confidence level

The statistical distributions of D_T and $m(\infty)$ were investigated with the use of histograms as described in Section 4.5. The histograms of D_T and $m(\infty)$ were similar to the histograms in Figure 5.4.1 and were not included in this thesis.

Table E.6. $\breve{k}_{fit}$, D_T, and $m(\infty)$ were calculated from parameters estimated from data simulated assuming the normal distribution. The standard deviation of the parameters were found as described in Section 4.5. The confidence interval of $m(\infty)$, $CI_{m(\infty)}$, was calculated as described in Section 4.5 assuming a 95% confidence level.

Constants	# 12	# 13	# 19	# 21	# 28	# 43
$\breve{k}_{fit}$ $(\frac{g^2}{hr})$	2.01	2.58	0.50	1.22	0.71	0.04
$SD_{\breve{k}_{fit}}$	0.13	0.08	0.03	0.04	0.04	0.01
D_T (Gy)	400	448	758	367	384	366
SD_{D_T}	4.25	5.59	9.58	4.74	4.53	4.24
$m(\infty)$ (g)	8.7	6.3	1.7	5.5	4.6	2.7
$SD_{m(\infty)}$	0.2	0.2	0.1	0.2	0.1	0.1
$CI_{m(\infty)}$	[8.3 9.1]	[6.0 6.6]	[1.6 1.9]	[5.2 5.8]	[4.4 4.8]	[2.6 2.9]

Table E.7 reports estimates of $\breve{k}_{pred}$, D_T, and $m(\infty)$ which were calculated from parameters that were estimated from data that was simulated assuming a normal distribution. Table E.8 reports estimates of $\breve{k}_{calc}$, D_T, and $m(\infty)$. The parameter estimates and their standard errors are very similar between Tables E.7, E.8, and E.6. For example, $m(\infty)$ =8.4, 8.2, and 1.5 grams for subjects 12, 13, and 19 from Table E.7. For the same subjects, $m(\infty)$ =8.7, 6.3, and 1.7 grams from Table E.6 and $m(\infty)$ =9.1, 8.2, and 1.1 grams from Table E.8. The $m(\infty)$ values for a particular subject are within 1.9 grams of each other between the three tables. This provides evidence that $\breve{k}_{pred}$ and $\breve{k}_{calc}$ provide a reasonable estimate of $\breve{k}_{fit}$ and produce similar estimates of $m(\infty)$. However, the confidence intervals are unrealistically narrow.

Table E.7. $\breve{k}_{pred}$, D_T, and $m(\infty)$ were calculated from parameters estimated from data simulated assuming the normal distribution. The standard deviation of the parameters were found as described in Section 4.5. The confidence interval of $m(\infty)$, $CI_{m(\infty)}$, was calculated as described in Section 4.5 assuming a 95% confidence level.

Constants	# 12	# 13	# 19	# 21	# 28	# 43
$\breve{k}_{pred}$ $\left(\frac{g^2}{hr}\right)$	2.22	1.74	0.62	0.88	0.92	0.25
$SD_{\breve{k}_{pred}}$	0.06	0.05	0.02	0.02	0.03	0.01
D_T (Gy)	410	368	795	320	407	430
SD_{D_T}	6.10	5.71	11.38	4.44	5.89	5.92
$m(\infty)$ (g)	8.4	8.2	1.5	6.4	4.3	2.2
$SD_{m(\infty)}$	0.3	0.3	0.1	0.2	0.1	0.1
$CI_{m(\infty)}$	[8.0 8.9]	[7.7 8.6]	[1.4 1.7]	[6.1 6.7]	[4.0 4.5]	[2.1 2.3]

Table E.8. $\breve{k}_{calc}$, D_T, and $m\left(\infty\right)$ were calculated from parameters estimated from data simulated assuming the normal distribution. The standard deviation of the parameters were found as described in Section 4.5. The confidence interval of $m(\infty)$, $CI_{m(\infty)}$, was calculated as described in Section 4.5 assuming a 95% confidence level.

Constants	# 12	# 13	# 19	# 21	# 28	# 43
$\breve{k}_{calc}$ $\left(\frac{g^2}{hr}\right)$	1.71	1.73	0.83	0.63	0.92	0.29
$SD_{\breve{k}_{calc}}$	0.05	0.05	0.02	0.02	0.03	0.01
D_T (Gy)	387	368	893	298	407	447
SD_{D_T}	5.70	5.48	13.15	4.30	6.15	6.40
$m\left(\infty\right)$ (g)	9.1	8.2	1.1	6.9	4.3	2.1
$SD_{m(\infty)}$	0.3	0.3	0.1	0.2	0.1	0.1
$CI_{m(\infty)}$	[8.6 9.6]	[7.8 8.6]	[1.0 1.2]	[6.6 7.2]	[4.0 4.5]	[2.0 2.2]

BIBLIOGRAPHY

[1] FS Greenspan and DG Garder. *Basic & Clinical Endocrinology.* McGraw-HIll, New York, 7th edition, 2004.

[2] LJ DeGroot, GF Cahill Jr., WD Odell, L Martini, JT Potts Jr., DH Nelson, E Steinberger, and AI Winegrad, editors. *Endocrinology. Volume 1.* Grune & Stratton, New York, 1979.

[3] JM Links. *Werner & Inbar's The Thyroid: A Fundamental and Clinical Text.* Lippincott Williams & Wilkins, New York, 8th edition, 2000.

[4] H Jönsson and S Mattsson. Excess radiation absorbed doses from non-optimised radioiodine treatment of hyperthyroidism. *Radiation Protection Dosimetry*, 108:107–114, 2003.

[5] B Solomon, D Glinoer, R Lagasse, and LN Warofsky. Current trends in the management of Graves' disease. *Journal of Clinical Endocrinology and Metabolism*, 70:1518–1524, 1990.

[6] B Shapiro. Optimization of radioiodine therapy of thyrotoxicosis: What have we learned after 50 years? *Journal of Nuclear Medicine*, 34:1638–1641, 1993.

[7] W Muhammad, S Faaruq, A Hussain, MB Kakakhail, S Fatmi, and Matiullah. Quantitative analysis of the factors responsible for over or under dose of ^{131}I therapy patients of hyperthyroidism. *Radiation Protection Dosimetry*, 128:90–97, 2008.

[8] RA Nordyke and FI Gilbert Jr. Optimal iodine-131 dose for eliminating hyperthyroidism in Graves' disease. *Journal of Nuclear Medicine*, 32:411–416, 1991.

[9] WD Leslie, L Ward, EA Salamon, S Ludwig, RC Rowe, and EA Cowden. A randomized comparison of radioiodine doses in Graves' hyperhtyroidism. *Journal of Clinical Endocrinology and Metabolism*, 3:978–983, 2003.

[10] LD Marinelli, EH Quimby, and GJ Hine. Dosage determination with radioactive isotopes. ii practical considerations in therapy and protection. *American Journal of Roentgenology and Radium Therapy*, 59:260–281, 1948.

[11] T Kita, K Yokoyama, S Kinuya, J Taki, T Michigishi, and N Tonami. Single dose planning for radioiodine-131 therapy of Graves' disease. *Annals of Nuclear Medicine*, 2:151–155, 2004.

[12] B Catargi, F Leprat, M Guyot, N Valli, D Ducassou, and A Tabarin. Optimized radioiodine therapy of Graves' disease: analysis of the delivered dose and of other possible factors affecting outcome. *European Journal of Endocrinology*, 141:117–121, 1999.

[13] H Peters, C Fischer, U Bogner, C Reiners, and H Schleusener. Radioiodine therapy of Graves' hyperthyroidism: standard vs. calculated [131]iodine activity. results from a prospective, randomized, multicentre study. *European Jounal of Clinical Investigation*, 25:186–193, 1995.

[14] UF Willemsen, P Knesewitsch, T Kreisig, CR Pickardt, and CM Kirsch. Functional results of radioiodine therapy with a 300-Gy absorbed dose in Graves' disease. *European Jounal of Nuclear Medicine*, 20:1051–1055, 1993.

[15] T Carlier, P Salaun, M Cavarec, F Valette, A Turzo, M Baries, Y Bizais, and O Couturier. Optimized radioiodine therapy for Graves' disease: Two MIRD-based models for the computation of patient-specific therapeutic ^{131}I activity. *Nuclear Medicine Communications*, 27:559–566, 2006.

[16] AC Traino, F DiMartino, M Lazzeri, and MG Stabin. Influence of thyroid volume reduction on calculated dose in radioiodine therapy of Graves' hyperthyroidism. *Physics In Medicine and Biology*, 45:121–129, 2000.

[17] AC Traino, F DiMartino, M Lazzeri, and MG Stabin. Study of the correlation between administered activity and radiation committed dose to the thyroid in ^{131}I therapy of Graves' disease. *Radiation Protection Dosimetry*, 95:117–124, 2001.

[18] AC Traino, F DiMartino, M Grosso, F Monzani, A Dardano, N Caraccio, G Mariani, and M Lazzeri. A predictive mathematical model for the calculation of the final mass of Graves' disease thyroids treated with [131]I. *Physics In Medicine and Biology*, 50:2181–2191, 2005.

[19] AC Traino and F DiMartino. A dosimetric algorithm for patient-specific ^{131}I therapy of thyroid cancer based on a prescribed target-mass reduction. *Physics in Medicine and Biology*, 51:6449–6456, 2006.

[20] AC Traino, F DiMartino, and M Lazzeri. A dosimetric approach to patient-specificc radioiodine treatment of Graves' disease with incorporation of treatment-induced changes in thyroid mass. *Medical Physics*, 31:2121–2127, 2004.

[21] EJ Hall. *Radiobiology for the Radiologist.* Lippincott Williams & Wilkins, Philidelphia, 5th edition, 2000.

[22] HE Johns and JR Cunningham. *The Physics of Radiology.* Charles C Thomas, Springfield,Illinois, 4th edition, 1983.

[23] AM Kellerer and HH Rossi. The theory of dual radiation action. *Current Topics in Radiation Research Quarterly*, 8:85–158, 1978.

[24] KH Chadwick and HP Leenhouts. A molecular theory of cell survival. *Physics in Medicine and Biology*, 18:78–87, 1973.

[25] RG Dale. Dose-rate effects in targeted radiotherapy. *Physics In Medicine and Biology*, 41:1871–1884, 1996.

[26] RG Dale. The application of the linear-quadratic dose-effect equation to fractionated and protracted radiotherapy. *British Journal of Radiology*, 58:515–528, 1985.

[27] RE Toohey, MG Stabin, and EE Watson. The AAPM/RSNA physics tutorial for residents. internal radiation dosimetry: Principles and applications. *RadioGraphics*, 20:533–546, 2000.

[28] MG Stabin. MIRDose:personal computer software for use in internal dose assessment in nuclear medicine. *Journal of Nuclear Medicine*, 37:538–546, 1996.

[29] F DiMartino, AC Traino, AB Brill, MG Stabin, and M Lazzeri. A theoretical model for prescription of the patient-specific therapeutic activity for radioiodine therapy of Graves' disease. *Physics in Medicine and Biology*, 47:1493–1499, 2002.

[30] RS Figliola and DE Beasley. *Theory and Design for Mechanical Measurements.* John Wiley & Sons,Inc., New Jersey, 3rd edition, 2000.

[31] AJ Wheeler and AR Ganji. *Introduction To Engineering Experimentation.* Prentice-Hall, New Jersey, 1996.

[32] M Degon, SR Chipkin, CV Hollot, TR Zoeller, , and Y Chait. A computational model of the human thyroid. *Mathematical biosciences*, 212:22–53, 2008.

[33] B Efron and RJ Tibshirani. *An Introcuction To The Bootstrap.* Chapman & Hall/CRC, New York, 1993.

[34] AC Davison and DV Hinkley. *Bootstrap Methods and Their Application.* Cambridge University Press, New York, 1st edition, 1997.

[35] MR Chernick. *Bootstrap Methods: A Guide for Practitioners and Researchers.* John Wiley & Sons,Inc., New Jersey, 2nd edition, 2008.

[36] W Mendenall and T Sincich. *Statistics For Engineering And The Sciences.* Prentice-Hall, New Jersey, 5th edition, 2007.

[37] MJ Schervish. *Theory of Statistics.* Springer-Verlag, New York, 1995.

120

[38] H Motulsky and A Christopoulos. *Fitting Models to Biological Data Using Linear and Nonlinear Regression: A Practical Guide To Curve Fitting.* Oxford University Press, New York, 2004.